Modified Nafion Membranes for Hydrogen Production in Cu-Cl Thermochemical Cycle

By

Naser Abdo

A THESIS SUBMITTED IN PARTIAL FULFILLMENT OF
THE REQUIREMENTS FOR THE DEGREE OF
MASTER OF SCIENCE
in
THE FACULTY OF SCIENCE
MATERIALS SCIENCE

UNIVERSITY OF ONTARIO INSTITUTE OF TECHNOLOGY
July 2015

Abstract

The decomposition of water by a thermochemical cycle is a promising green method of producing hydrogen on a large scale. A thermochemical cycle is a combination of thermal and chemical reactions that ultimately leads to splitting water into hydrogen and oxygen. The Cu-Cl cycle, which is one of the most promising hybrid cycles, has many potential advantages. First, all the copper chloride compounds used in the cycle are recyclable. Second, the copper chlorine cycle has relatively low operating temperatures (500-600 °C) compared to other thermochemical cycles. Third, it can have high energy efficiency by utilizing low-grade waste heat. One step in the Cu- Cl cycle employs an electrochemical process where Cu(I) is oxidized to Cu(II) at the anode and hydrogen is generated at the cathode. The electrochemical cell used is similar to a water electrolysis cell and employs a membrane electrode assembly (MEA) that utilizes a proton exchange membrane (PEM). Nafion, the most widely used PEM, is permeable to cations and neutral species. Because of this, Cu can permeate the membrane and enter the cathode where it is readily oxidized to metallic copper and deposited on Pt catalytic sites. This drastically reduces cathode efficiency as well as the whole cell.

In this research, we have modified Nafion membranes, with different thicknesses, by *in situ* polymerization with pyrrole and aniline compounds. *Ex situ* permeation experiments were performed along with impedance spectroscopy to investigate the rate of the copper crossover and the proton conductivity of the composite membranes, respectively. The electrochemical behavior of the composite membranes was investigated using a full copper chlorine electrolytic cell. The efficiency of both copper conversion and hydrogen production were used as indicators of the membrane performance.

Acknowledgements

I would like to express my sincere gratitude to my supervisor, Dr. Brad Easton, for the opportunity to work under his supervision on my Master's thesis. Your patience, motivation, enthusiasm, and knowledge have been a tremendous help to me during my research and writing my thesis.

I am also grateful to the members of my supervisory committee, Dr. Olena Zenkena, Dr. Igor Svishchev and Dr. Isaac Tamblyn for enriching this thesis with their insightful and constructive comments.

I would like to acknowledge funding from the Ontario Research Fund through the Research Excellence program and Atomic Energy of Canada Limited (AECL). Additional funding was also provided by the Natural Sciences and Engineering Research Council (NSERC) of Canada through the Discovery Grant program, and UOIT. I am also grateful for scholarship support from the Ontario Graduate Scholarship (OGS) program during my study.

I would also like to thank all members of the Easton group: Farhana, Reza, Ranga, Jennie, Patrick, Stefanie, Mohammadreza, Jessie, O'Rian and Chris for their support and fruitful discussions.

Special thanks to Richard Bartholomew, Michael Allison, and Clayton Jakins for the technical and logistic support. I am also very grateful for Catherine Lee from the Student Learning Centre for her tedious work of reading my thesis and correcting my writing.

I owe my gratitude to the fond memory of my parents, who I cannot thank enough; God bless them.

I would like to express my deepest gratitude and love to Raghad, my wife and best friend. For her patience and words of encouragement through challenging times. I will be always grateful. Thanks to my sons: Mohannad, Ibrahim, Yousef, and Yassine for their patience while I was busy working away from them.

I am grateful for all the support I received from my extended family and friends. I would like to thank you for your overwhelming love and support over the years.

Table of Contents

List of Tables

List of Figures

List of Abbreviations and Symbols

A – Ampere

AAS – Atomic absorption spectroscopy

AC – Alternating current

Ag/AgCl – Silver/Silver chloride electrode

APS – Ammonium persulfate

ASR – Area specific resistance

ATR FT-IR – Attenuated total reflectance Fourier transform infrared spectroscopy

CEM – Cation exchange membrane

CFP – Carbon fiber paper

Cu-Cl – Cupper chlorine cycle

CV – Cyclic voltammetry

DC – Direct current

DI – Deionized water

dl – Double layer

DMFC – Direct methanol fuel cell

DPASV – Differential pulse anodic stripping voltammetry

DTG – Differential thermogravimetry

E^0 – Standard electrode potential

EIS – Electrochemical impedance spectroscopy

EW – Equivalent weight

F – Faraday's constant

FID – Flame ionization detector

GC – Gas chromatograph

HCL – Hollow cathode lamp

HyS – Hybrid sulfur cycle

IEC – Ion exchange capacity

LSV – Linear sweep voltammetry

M – Moles L^{-1}

MEA – Membrane electrode assembly

n – Number of moles of electrons

Ƞ – Overpotential

N115 – Nafion 115

N117 – Nafion 117

NRE 212 – Nafion NRE212

Ƞc – Current efficiency

NMR – Nuclear magnetic resonance

OCV/OCP – Open circuit voltage / Open circuit potential

PANI – Polyaniline

PBI – polybenzimidazole

PCD – Probe current detector

PEEK – Poly ether ether ketone

PEM – Proton exchange membrane / Polymer electrolyte membrane

PEMFC – Polymer electrolyte membrane fuel cell

Ppy – Polypyrrole

PSU – Polysulfone

Pt/C – Platinum on carbon support

Py – Pyrrole

RHE – Reference hydrogen electrode

SEM – Scanning electron microscopy

SHE – Standard hydrogen electrode

S-I – Sulfur iodine cycle

SPEEK – sulfonated poly ether ether ketone

SPI – Sulfonated polyimide

TGA – Thermogravimetric analysis

TMA – Polysulfone tetramethyl ammonium cation in chloride form membrane

UME – Ultramicroelectrode

V – Voltage

YSZ – Yttrium –stabilized zirconium

Z’ – Real impedance

Z” – Imaginary impedance

ZeSe – Zinc selenide

α – Selectivity

ΔG^0 – Standard free energy change

ΔH^0 – Standard enthalpy of reaction

σ – Proton conductivity

Chapter 1

Introduction to Hydrogen Production

1.1 H_2 Production Methods

Hydrogen is a colorless, odorless and non-poisonous gas. It is also the lightest element on earth as air is 15 times heavier than hydrogen gas [1]. Moreover, molecular hydrogen does not exist naturally on earth but is confined in compounds such as water and hydrocarbons. In recent years, H_2 has received much attention due to its usage in a wide range of applications such as a coolant, and as a clean fuel. A fuel can be defined as a material that can release energy when it is converted from one form to another. Therefore, wood, coal, gasoline and H_2 are considered as fuels. Ideal fuels should have a high energy density (amount of energy released per volume of fuel). Commonly, fuels are described by their "fuel value", which is defined as the ratio of the amount of energy released by burning a specific fuel to its mass (i.e. its mass-specific energy density). Hydrogen has an exceptionally high fuel value compared to many common fuels, as shown in Table 1.1. The fuel value of hydrogen is three times higher than that of gasoline. The high fuel value and the zero emission of the combustion of H_2 make it an ideal fuel.

Table 1.1: Fuel values of different chemicals [1].

Chemical	Types of bonds	Fuel value (kJ/g)
Hydrogen	H-H	141.4
Gasoline	C-H	48
Coal	C-H, C-O	15-27
Wood	C-H, C-O	15
Ethanol	C-H, O-H	29.7
Butanol	C-H, O-H	36.0
Octane	C-H	48.0
Butane	C-H	49.5
Methane	C-H	55.5
Methanol	C-H, C-OH	22.7

While H_2 is not naturally occurring, we can produce it from the thermal splitting of water, reaction of specific chemicals with water, reforming of hydrocarbons, and the electrolysis of water. At present, most hydrogen is produced from non-renewable resources such as fossil fuels by methane steam reforming, oil naphtha reforming and coal gasification which will eventually cause devastating effects to our environment [2]. The following sections will describe the conventional methods of hydrogen production from fossil fuels and from water decomposition by thermolysis and electrolysis.

1.1.1 H_2 Production from Fossil Fuels

Most of the hydrogen these days is produced from fossil fuels through different physical and chemical processes. Fossil fuels such as coal, oil and natural gas are natural resources that contain hydrocarbons. They are used to produce hydrogen by heating with steam at elevated temperatures in the presence of a catalyst in a process known as steam reforming. For example, coke and methane react with steam at 1100-1300 °C and 700-925 °C, respectively, as in the following reactions to produce hydrogen gas and carbon monoxide.

$$C\ (coke) + H_2O\ (1100\text{-}1300\ ^\circ C) \longrightarrow CO + H_2 \qquad \text{Eq. 1.1}$$

$$CH_4 + H_2O\ (700\text{-}925\ ^\circ C) \longrightarrow CO + 3H_2 \qquad \text{Eq. 1.2}$$

Hydrogen can also be produced by the water gas shift reaction which includes passing the carbon monoxide and steam over a metal oxide catalyst at a temperature around 400 °C as in the following reaction.

$$CO + H_2O\ (400\ ^\circ C) \longrightarrow CO_2 + H_2 \qquad \text{Eq. 1.3}$$

Although steam reforming is considered a low-cost method of producing hydrogen, it has negative environmental effects since it produces CO, CO_2, SO_2 and NOx [3] . Petroleum, natural gas, and coal are non-renewable energy sources because the natural reserves will be depleted within hundreds of years. The high demand for energy world-wide has resulted in an immense consumption of these sources, which is having a detrimental effect on our environment. As such, there is an urgent need for a method of generating hydrogen that is cleaner and renewable. One of the candidate methods of producing hydrogen is from water through thermolysis and electrolysis which will be introduced by next sections.

1.1.2 H_2 Production from Water

Water splits to oxygen and hydrogen according to Eq. 1.4 which has positive standard free energy (ΔG^o) and enthalpy (ΔH^o).

$$H_2O\ (l) \longrightarrow \tfrac{1}{2}\ O_2\ (g) + H_2\ (g) \quad \Delta G^o = 237.1\ kJ/mol,\ \Delta H^0 = 285.8\ kJ/mol \qquad \text{Eq. 1.4}$$

The production of hydrogen gas from water has the potential to meet the energy demand in a clean and renewable manner, provided it can be generated efficiently. Water can decompose to H_2 and O_2 in different ways, but all require the input of energy to drive the reaction. Thermolysis and electrolysis are the most common methods of producing hydrogen gas from water. The next sections will describe these methods and focus on different types of electrolysis.

1.1.2.1 Thermolysis

If heat alone is used to split water to hydrogen and oxygen gas, the process is called thermolysis. It is one of the conventional methods to produce hydrogen from water. However,

temperatures around 2500 °C are required to thermally split water into hydrogen and oxygen [4]. In addition to being energy intensive, specialized advanced materials are required to withstand the extremely high temperatures. As such, this method is not practical for large scale hydrogen production.

1.1.2.2 Electrolysis

An alternative method to produce H_2 from water is through electrolysis. This is a process of water decomposition to hydrogen and oxygen by applying a potential across the cell to drive the reaction. A device, called an electrolyzer is used for this purpose and is composed of anode and cathode parts separated by an electrolyte. Commonly, a catalyst is used on both electrodes to reduce the potential required for hydrogen production. During this process and in an acidic medium, oxygen is produced at the anode, while H_2 is produced at the cathode, as shown in the following reactions:

Anode $H_2O \longrightarrow \frac{1}{2} O_2 + 2H^+ + 2e^-$ $E^o = -1.23$ V Eq. 1.5

Cathode $2H^+ + 2e^- \longrightarrow H_2$ $E^o = 0.0$ V Eq. 1.6

Overall $H_2O \longrightarrow H_2 + \frac{1}{2} O_2$ $E^o = -1.23$ V Eq. 1.7

The theoretical cell potential for this water electrolysis reaction is -1.23 V. Thus energy must be added in order for the reaction to proceed. Furthermore, the standard free energy (ΔG^o) for this reaction can be calculated from Eq. 1.8 and is equal to + 237.1 kJ/mol.

$$\Delta G^0 = - n F E^0 \quad \text{Eq. 1.8}$$

where, n is the number of moles of electrons and F is the Faraday constant. To produce H_2 from electrolysis of water, a potential equal to about 1.75 V is required. The additional electrical energy is required to overcome the overpotential resulting from activation and ohmic losses within the cell.

Electrolysis of water can be performed at very low temperatures ca. < 100 °C, while thermolysis needs extremely high temperatures for water decomposition. In addition, during the thermolysis and at very high temperatures the produced oxygen and hydrogen can recombine to form water again.

Different types of electrolyzers are classified according to the nature of the electrolyte. There are mainly three types of electrolyzers: alkaline, solid oxide and polymer electrolyte membrane (PEM). These different types of electrolyzers will be describes in details in the following sections.

1.1.2.2.1 Alkaline Water Electrolysis

Alkaline electrolysis is a well-established technology that utilizes an alkaline electrolyte such as 20-30 % sodium or potassium hydroxide solution. An alkaline electrolyzer consists of two electrodes immersed in a liquid electrolyte and separated by a diaphragm as shown in Fig. 1.1 (a). This diaphragm functions as a barrier to separate the produced gases from each other as well as to allow the hydroxide ions to permeate to the anode side. Although alkaline electrolysis does not employ expensive noble catalysts, it has long term stability issues.

There are many problems facing alkaline electrolysis. First, the water used in the electrolysis should be very pure, since the presence of any metals, such as naturally occurring

magnesium and calcium, can form scales which could clog the diaphragm [5]. Second, the diffusion of the produced gases through the diaphragm reduces the efficiency of the electrolyzer. Third, only low maximum current density can be obtained due to high ohmic losses from both the electrolyte and the diaphragm.

1.1.2.2.2 Polymer Electrolyte Membrane Electrolysis

The polymer electrolyte membrane (PEM) electrolyzer was first developed by General Electric in the 1960s [6]. It consists of an anode and a cathode separated by PEM as shown in Fig. 1.1 (b). As PEM functions as a solid acidic electrolyte, it allows the transport of protons from the anode to the cathode. The most widely used PEM is a Nafion, a perfluorosulfonic acid polymer developed by Dupont.

A PEM electrolyzer utilizes a very thin membrane *ca.* 200 μm or less with excellent proton conductivity and high current density. In addition, the compact design and high operational pressure are facile as the electrolyte is in the solid state.

1.1.2.2.3 Solid Oxide Electrolysis

A solid oxide electrolyzer attracts many researchers because it can generate hydrogen from electrical energy with high efficiency. It splits water as steam at high temperatures. Solid oxide electrolyzers utilize solid, nonporous metal oxides such as yttrium-stabilized zirconium (YSZ) as an electrolyte. At very high temperatures (1000-1300 K), such an electrolyte is conductive to oxygen ions.

The solid oxide electrolyzer cell consists of end plates, gas channels, anode, cathode and electrolyte. The electrolyte-electrode assembly is comprised of a thin layer of solid oxide

sandwiched between a porous cathode and anode. The Faradic efficiency can approach 100 % when the cell is operated at current density of 0.3 A cm^{-2} and a voltage of 1.07 V [7]. Although this technique has a promising future for mass production of hydrogen, its durability still under development.

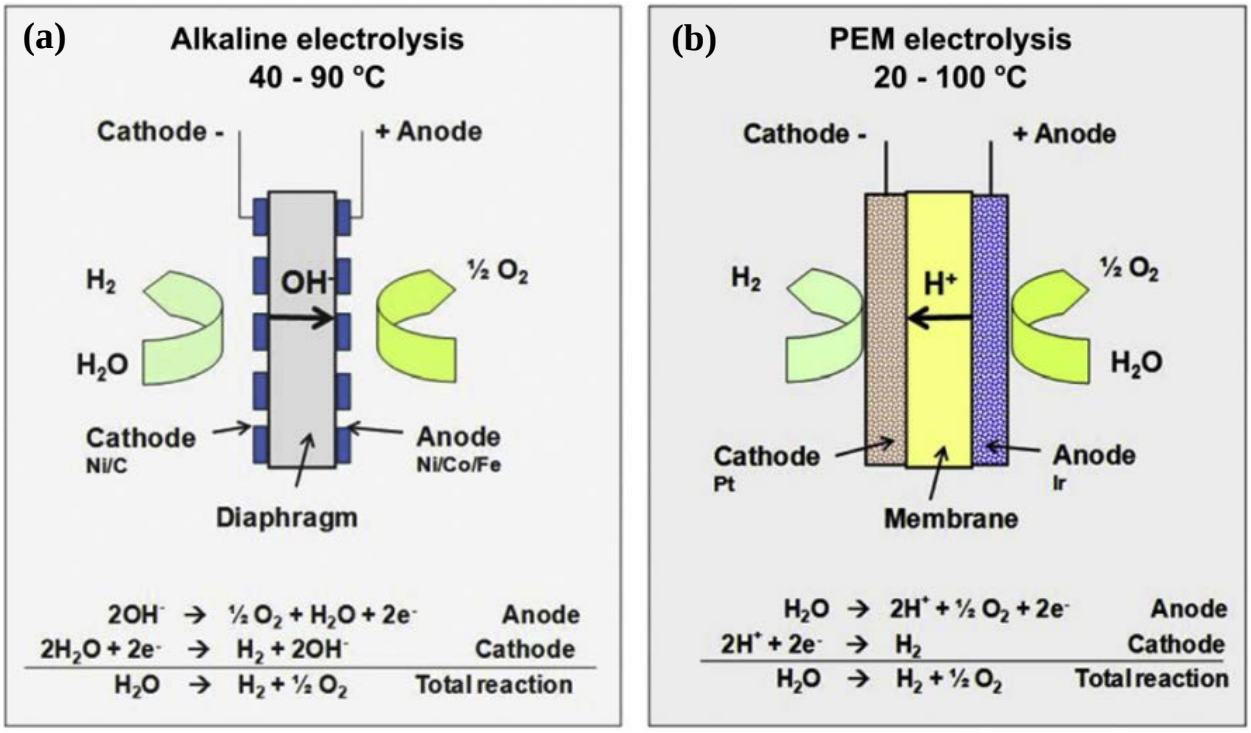

Fig. 1.1: Schematic diagram of (a) alkaline and (b) PEM water electrolysis cell. Reproduced with permission from [7].

Despite the potential advantages of electrolysis, only 4 % of the world's hydrogen is produced by electrolysis. This is because it is energy intensive, requiring both a voltage above 1.5 V to drive the reaction especially the PEM electrolysis, and also due to high overpotential losses resulting from the activation, ohmic resistance and mass transport limitations [2, 8]. In addition, water electrolysis consumes a considerable amount of electricity compared to the steam reforming method. Because of this, water electrolysis is an expensive method of producing hydrogen with very low efficiency (*ca*.18-24 %) [9].

1.2 Introduction to Thermochemical Cycles

Instead of producing hydrogen directly from water, one can also produce hydrogen indirectly through a catalytic cycle. In the thermochemical cycles, the energy consumption is significantly reduced compared to water electrolysis. Generally, a thermochemical cycle is comprised of a closed loop of thermally driven chemical reactions that decompose water to hydrogen and oxygen. A hybrid thermochemical cycle utilizes both thermochemical and electrochemical reactions in their cycles [10-14]. All the chemicals used in these cycles are regenerated and remain within the system. More than 200 potential thermochemical cycles have been identified, though only a few have been deemed to be practically feasible [15]. The availability of a potential waste heat source (e.g. a nuclear reactor) that matches the temperature requirements of a cycle is a major factor in the development of a particular cycle. Sulfur Iodine (S-I), hybrid-sulfur (HyS), and the copper-chlorine (Cu-Cl) cycles are three of the most promising and widely studied thermochemical cycles [15], and each will be discussed in more detail below.

1.2.1 Sulfur Iodine Cycle

The sulfur iodine (S-I) cycle, consisting of three chemical reactions, dissociates water to oxygen and hydrogen, with the maximum required temperature of 850-900 °C [16-18], as can be seen in Fig. 1.2. In this cycle, HI and sulfuric acid are produced by a reaction known as Bunsen which includes a reaction of I_2 with SO_2 in the presence of H_2O. In the second step, HI is decomposed at 400 °C to produce hydrogen and I_2, while the thermal decomposition of sulfuric acid at 900 °C produces oxygen, SO_2 and water. The S-I cycle has been scaled up to a pilot plant stage and is continuously investigated by many international research teams [16, 19-21].

The S-I cycle is considered one of the most promising thermochemical cycles due to many advantages. One of these advantages is that all the reactants and products are either in a liquid or gas state as it is less convenient to deal with solid products. Furthermore, hydrogen does not need to be compressed in a separate energy intensive step since it is generated at high pressure [8]. However, some disadvantages do exist, such as the requirement of a high temperature *ca*. 900 °C for sulfuric acid decomposition. Subsequently, advanced construction materials are needed to endure the corrosion from compounds such as I_2, SO_2, HI, and sulfuric acid.

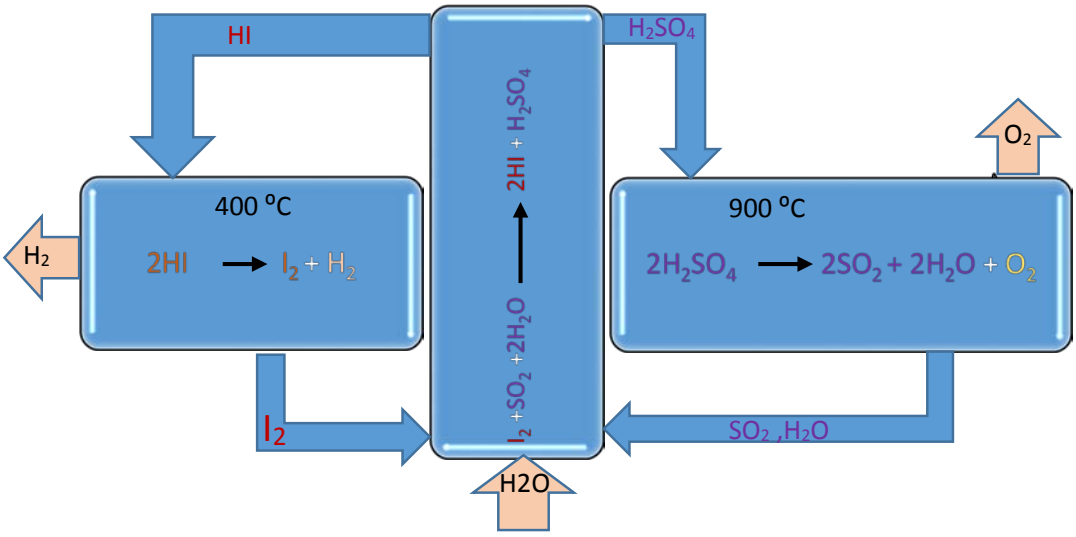

Fig. 1.2: Scheme of the thermochemical Sulfur-Iodine cycle.

1.2.2 Hybrid-Sulfur Cycle

The hybrid sulfur (HyS) cycle is a modification of the S-I cycle by including an electrolysis step and reducing the overall steps to two, as shown in Fig. 1.3. Westinghouse Electric Corporation was the first to propose and develop the HyS cycle in the 1970s [22]. The first step is the thermal decomposition of H_2SO_4 to SO_2, O_2, and H_2O at 850 °C. The second step is a low temperature (*ca.* 100 °C) electrolysis of SO_2 and H_2O to produce H_2 and regenerate H_2SO_4 [23], according to the following reactions:

$$H_2SO_4\,(g) \longrightarrow SO_2\,(g) + H_2O\,(g) + \tfrac{1}{2}\,O_2\,(g)\ (850\ ^{o}C\text{-thermochemical}) \quad \text{Eq.1.9}$$

$$SO_2\,(aq) + 2H_2O\,(l) \longrightarrow H_2SO_4\,(aq) + H_2\,(g)\ (100\ ^{o}C\text{-electrolysis}) \quad \text{Eq. 1.10}$$

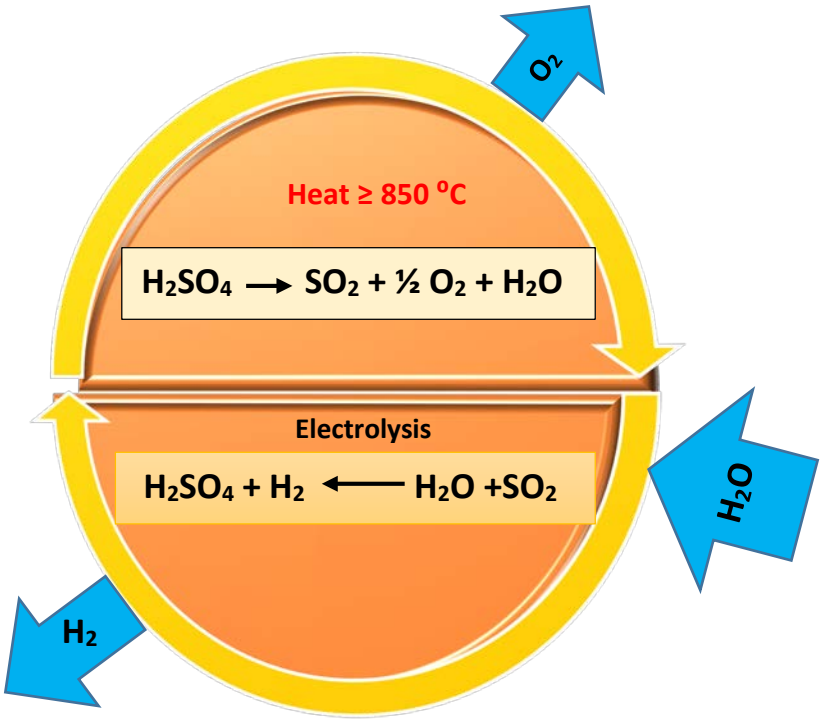

Fig. 1.3: Scheme illustrates the HyS thermochemical cycle.

One of the main advantages of this cycle is its simplicity – a 2-step cycle where all species in either the liquid and gaseous state. Both S-I and HyS cycles require a source of high temperature which could be supplied from gas cooled nuclear reactors [24, 25]. Some challenges facing the advancement of hybrid sulfur cycle include the extreme temperature requirement and the corrosion effects from the sulfuric acid. In addition, when a PEM is used in the electrolysis step, the production of sulfuric acid dehydrates the membrane and reduces the efficiency of the cycle [25].

1.2.3 Cu-Cl Cycle

The Cu-Cl cycle is another promising thermochemical cycle that can be used to produce H_2 gas. The Cu-Cl cycle consists of three chemical reactions, as can be seen in Table 1.2 and Fig. 1.4. One of the reactions of the Cu-Cl cycle is the CuCl/HCl electrolysis at temperatures less than 100 °C while the other two are hydrolysis and decomposition reactions which occur at around 400 and 500 °C, respectively. The Cu-Cl cycle is a promising hybrid cycle that has many potential advantages, including relatively low operating temperatures (500-600 °C), which enable the utilization of a low-grade waste heat source, and potentially more affordable materials. In addition, less energy is required to produce the same amount of hydrogen compared to water electrolysis due to the thermodynamics of the cycle. Many early efforts have been employed to investigate the feasibility and the efficiency of this cycle [9, 26, 27]. Furthermore, an international team is engaged in the development and improvement of the Cu-Cl cycle for H_2 production [13, 28-31].

Table 1.2: Reactions in the three step hybrid CuCl/HCl thermochemical cycle [12].

Step	Reaction	Temperature/^{o}C
Electrolysis	$2CuCl.nH_2O\ (aq) \longrightarrow 2CuCl_2.(n+m)H_2O\ (aq) + H_2\ (g)$	25-80
Hydrolysis	$2CuCl_2\ (s) + H_2O\ (g) \longrightarrow CuCl_2.CuO\ (s) + 2HCl\ (g)$	310-375
Decomposition	$CuCl_2.CuO\ (s) \longrightarrow 2\ CuCl\ (s) + ½\ O_2\ (g)$	450-530

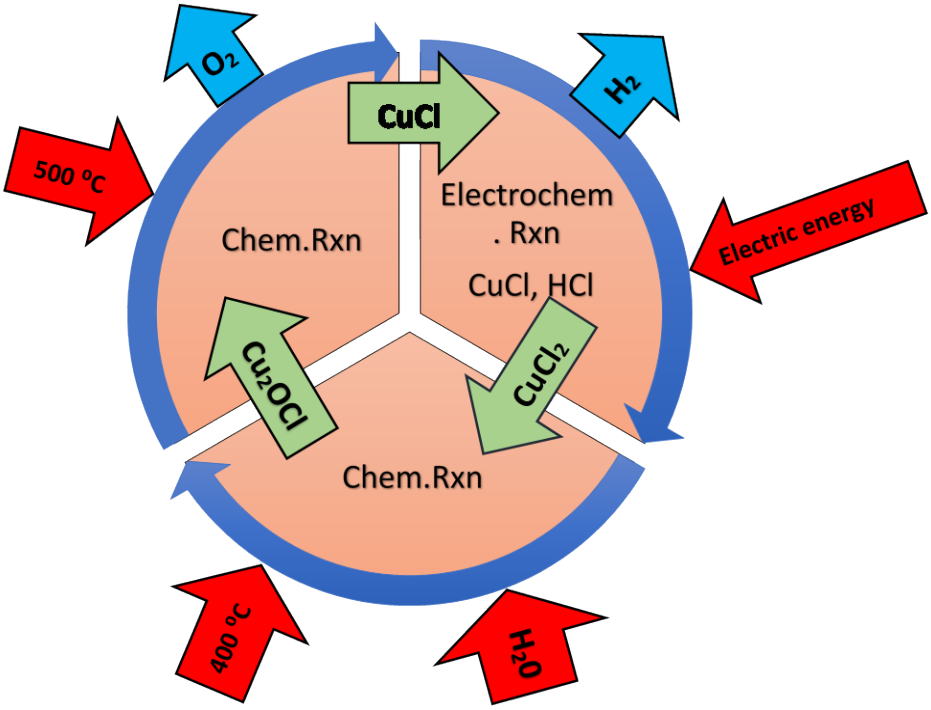

Fig. 1.4: The thermochemical Copper Chlorine cycle diagram.

One step in this cycle employs an electrochemical process where Cu(I) is converted to Cu(II), and hydrogen is evolved from an acidic solution. The electrochemical cell that is used similar to a water electrolysis cell and employs a membrane electrode assembly (MEA), that utilizes either an anion exchange membrane that is chloride conductive or a cation exchange membrane i.e. a proton exchange membrane (PEM) that is a proton conductive, as an electrolyte,

as shown in Fig. 1.5. The electrolysis cell in the Cu-Cl cycle with a cation exchange membrane as a proton conductive is the focus of this work. As such, it will be described in more detail below.

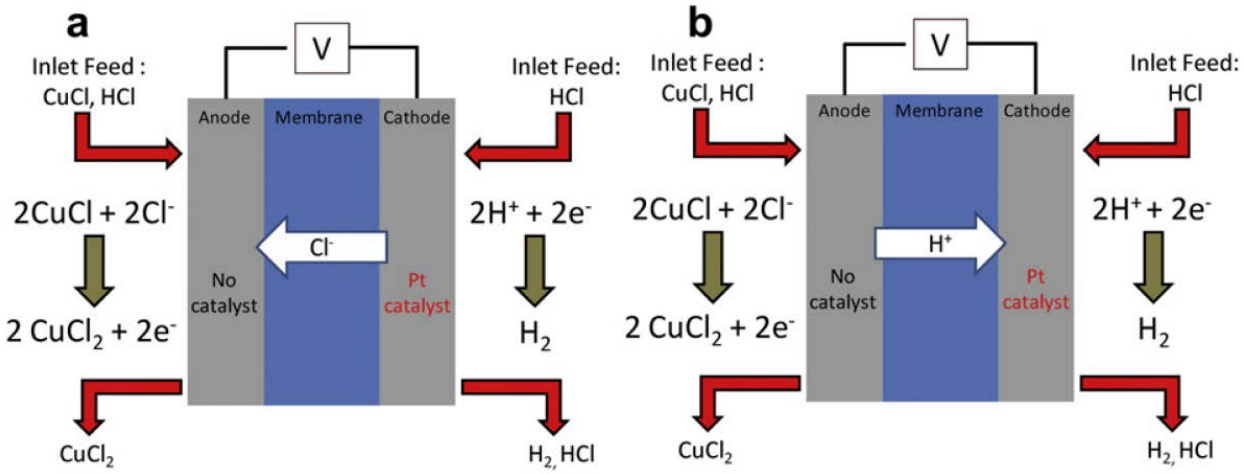

Fig. 1.5: Schematic diagram of the electrolysis cell used in the three step Cu-Cl thermochemical cycle. The cell can employ either (a) an anion exchange membrane or (b) a proton exchange membrane. Reproduced with permission from [10, 32].

1.3 Proton Exchange Membranes

A proton exchange membrane or a polymer electrolyte membrane is a membrane made from ionomers to conduct protons in the PEM fuel cell or the electrolyzer. An ionomer is a polymer composed of neutral and ionized parts. The PEM can function either as a cation or as an anion exchange membrane according to the connected ions on the membrane backbone. For example, a cation exchange membrane would have a negatively charged group such as $–SO_3^-$ or $–PO_3^{2-}$ attached to the membrane's backbone. This group permeates positively charged ions and blocks those negatively charged. On the contrary, an anion exchange membrane would have a

positively charged group such as $–NH_3^+$ connected on the membrane's backbone. This positively charged group permeates anions and blocks cations to pass through the membrane [32].

There are two main types of PEMs according to whether the structure of the membranes is associated with fluorinated backbones. Nafion is an example of a PEM that contains fluorinated backbones while hydrocarbon based polymers do not have fluorine in their backbone structure.

1.3.1 Perfluorosulfonic Acid (PFSA) Membranes

A Nafion membrane is a solid polymer electrolyte that conducts protons. It is developed and produced by Dupont, the most common membrane used in MEA because of the superior chemical and mechanical stability, high proton conductivity and excellent electronic insulation [33]. Nafion is, an aliphatic perfluorocarbon sulfonic acid, produced by a copolymerization of tetrafluoroethylene with a perfluorinated vinyl ether. It contains sulfonic acid groups as a hydrophilic part and $-CF_2-CF_2-$ as a hydrophobic backbone of the polymer, as shown in Fig. 1.6 (a). The hydrophobic part is responsible for the strength of the membrane while the hydrophilic part is essential for the proton conductivity.

The morphology of Nafion was examined by many researchers using different techniques. According to Fig. 1.6 (b), clusters of sulfonate-ended perfluoroalkyl ether groups that are arranged as inverted micelles have a diameter around 40 Å and are connected by channels of 10 Å. These channels are responsible for intercluster proton hopping [34].

(a)

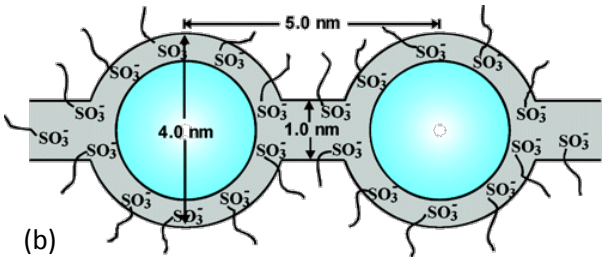

(b)

Fig. 1.6: (a) Schematic structure of Nafion (b) Cluster-network model of Nafion. Reproduced with permission from [35].

The mass of the polymer repeating units per mole of a sulfonic acid group is known as equivalent weight (EW). Nafion membranes are commercially available in different EW and thickness. For example, Nafion 115 has an EW of 1100 as indicated by the first two digits and a thickness of 5 mils (1mil=1/1000 of an inch=25.4 μm) as indicated by the third digit [35].

Nafion has many advantages over other PEMs due to its profound physical properties, such as chemical and mechanical stability. In addition, proton conductivity is one of the most characteristic of Nafion membrane. Although Nafion has many advantages, it suffers from sharp decrease in proton conductivity above 100 °C due to loss of water molecules. Moreover, high prices of Nafion membranes restricted them from being implemented in a wide range of applications.

On the other side, there are other non-fluorinated PEMs that can be used in electrolyzers and fuel cells applications due to their cheap prices and easy preparation. The chemical structures of such membranes and their characteristics will be explained in the next section.

1.3.2 Non-Fluorinated PEM

Non-fluorinated PEMs are widely used in large scale applications because of their low prices. An example of a non-fluorinated PEM is sulfonated polysulfones, as can be seen in Fig. 1.7 (a) which is characterized by its availability and low cost of production. It has been prepared and tested as a promising membrane in PEMFCs [36].

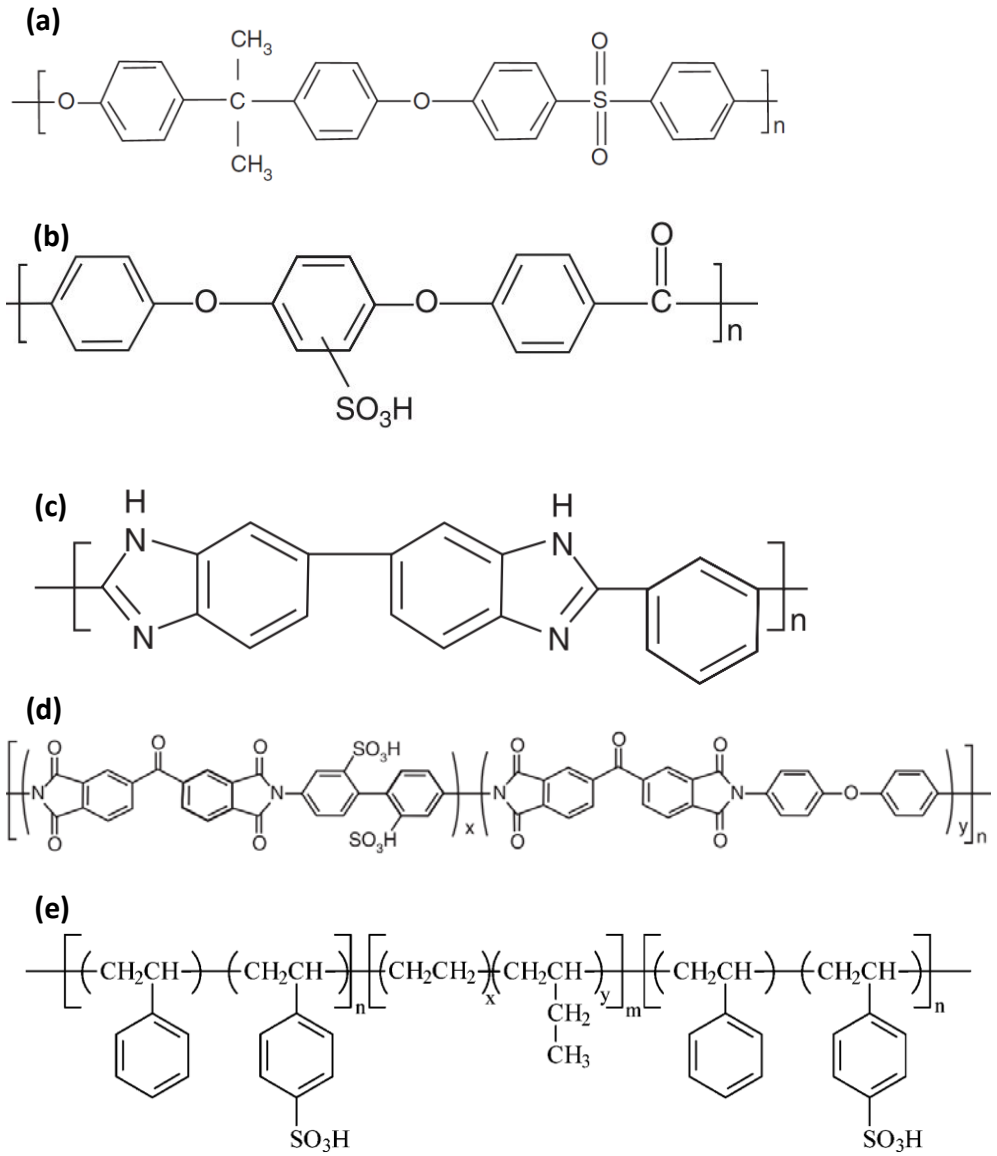

Fig. 1.7: The chemical Structure of (a) Polysulfone (PSU) (b) SPEEK (c) Poly (benzimidazole) (PBI) (d) Sulfonated polyimide (SPI) (e) Styrene-ethylene/butylene styrene.

The structure of sulfonated poly(ether ketone) (SPEEK) as shown in Fig. 1.7 (b) is another non-fluorinated aromatic PEM that has application for hydrogen fuel cells because of high conductivity and thermal stability. It is prepared from poly (ether ether ketone) PEEK by sulfonation to improve the conductivity [37, 38].

Polybenzimidazole (PBI) is synthesized from aromatic tetramine and dicaboxylate. Fig. 1.7 (c) shows the structure of commercially available PBI that is characterized by its chemical and thermal stability. PBI is used in many applications such as a membrane in the HyS cycle for hydrogen production [23].

Sulfonated polyimides as shown in Fig. 1.7 (d) are potential polymer candidates as membranes in DMFCs as their structure controls the methanol permeability and the sulfonic acid groups enhance proton conductivity. For example, sulfonated polyimide membranes have been reviewed by Marestine et al. [39] to be used as membranes in fuel cells. They investigated different methods of synthesis, and characterization as well as the behavior of these membranes in fuel cells.

Another commercial PEM is the block copolymer which consists of blocks of different polymerized monomers. The styrene ethylene/butylene styrene family is one type of this polymer with a structure as appears in Fig. 1.7 (e). The styrene content is about 20-35 wt % of the triblock copolymer. This type of PEM is characterized by its low production cost compared to Nafion, but suffers from poor oxidative stability due to its partially aliphatic character [40].

We can conclude that non-fluorinated PEMs are chemically easy to be prepared and their prices are affordable for large scale applications. However, the lack of viability and short life time are disadvantages that restricting them from improvement.

1.4 Methanol and Cu Crossover

The configuration of the electrochemical Cu-Cl electrolysis cell using a proton-conducting membrane is shown in Fig. 1.8. The cell consists of a positively charged anode and a negatively charged cathode separated by a membrane that conducts protons. The introduced reagent on the anode side (anolyte) is CuCl(s) dissolved in an aqueous solution of HCl, whereas on the cathode side, either pure water or an aqueous solution of HCl is used as a catholyte. Applying enough potential, the Cu(I) is oxidized to Cu(II) and the produced protons permeate through the membrane to the cathode side. Hydrogen gas is produced in the cathode side by the reduction of protons.

The electrochemical cell in the Cu-Cl cycle has one major drawback - copper crossover. The copper species (cationic and neutral) present at the anolyte can easily diffuse through the Nafion membrane (cation exchange membrane) and reach the cathode where it can be easily reduced to metallic copper at the Pt sites, as shown in Fig. 1.8. The presence of Cu on Pt effectively acts as a poison, drastically reducing the efficiency of the cathode and, in turn, that of the cell [10, 13, 31, 41].

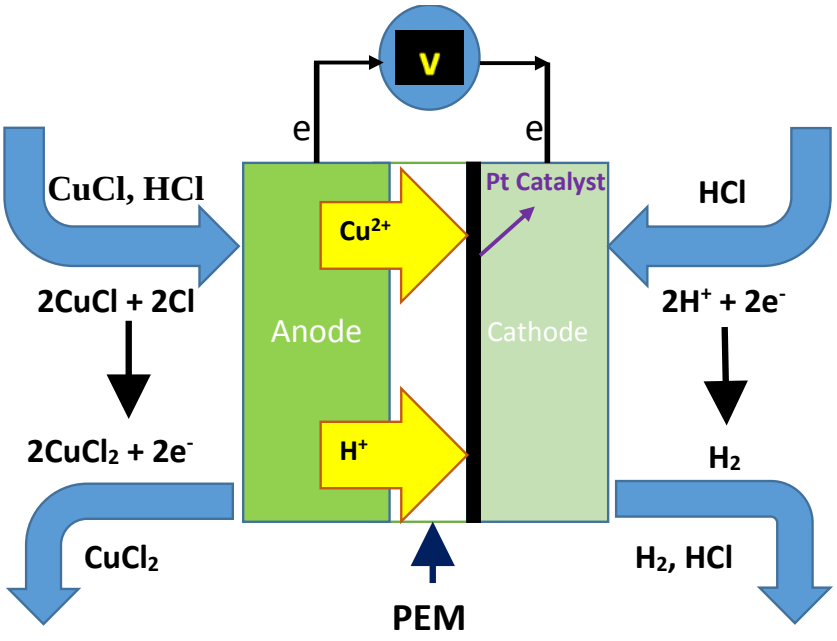

Fig. 1.8: Schematic diagram of a CuCl/ HCl electrolyzer illustrating copper crossover.

The copper crossover is somewhat similar to the methanol crossover in direct methanol fuel cells DMFC, as illustrated in Fig. 1.9. In general, a fuel cell has a similar structure as water electrolyzer. It is a device that converts chemical energy (fuel) into electrical energy. Therefore, in DMFC, methanol is used as a fuel which is directly oxidized at the anode with the aid of a catalyst to protons and electrons. Protons permeate to the cathode through a polymer electrolyte membrane such as Nafion, which is the most widely used in DMFC. The diffused protons combine with electrons and oxygen to produce water and electricity. However, methanol can also permeate through the membrane from the anode to the cathode which is known as methanol crossover. This methanol crossover decreases the lifetime and the overall cell efficiency [42].

Therefore, we have hypothesized that the same strategy used to reduce methanol crossover would work for Cu crossover. To examine this hypothesis, we have prepared Nafion

composite membranes via modifying the Nafion membranes by *in situ* polymerization with some promising heterocyclic aromatic monomers such as pyrrole. The formed polymer, conjugated heterocyclic polypyrrole (Ppy), was intensively investigated because of its stability and higher conductivity [43]. It has been shown that polymerization reduces the porosity of the membrane in such a way that it allows the passage of protons but prevents or reduces the permeation of methanol. Such membrane materials have been shown to be effective in reducing the rate of methanol crossover in DMFC [44-49]. Thus our hypothesis is that membrane materials that have been shown to have higher selectivity of protons over methanol (and thus promising for DMFC application) will also have higher selectivity of protons over Cu species.

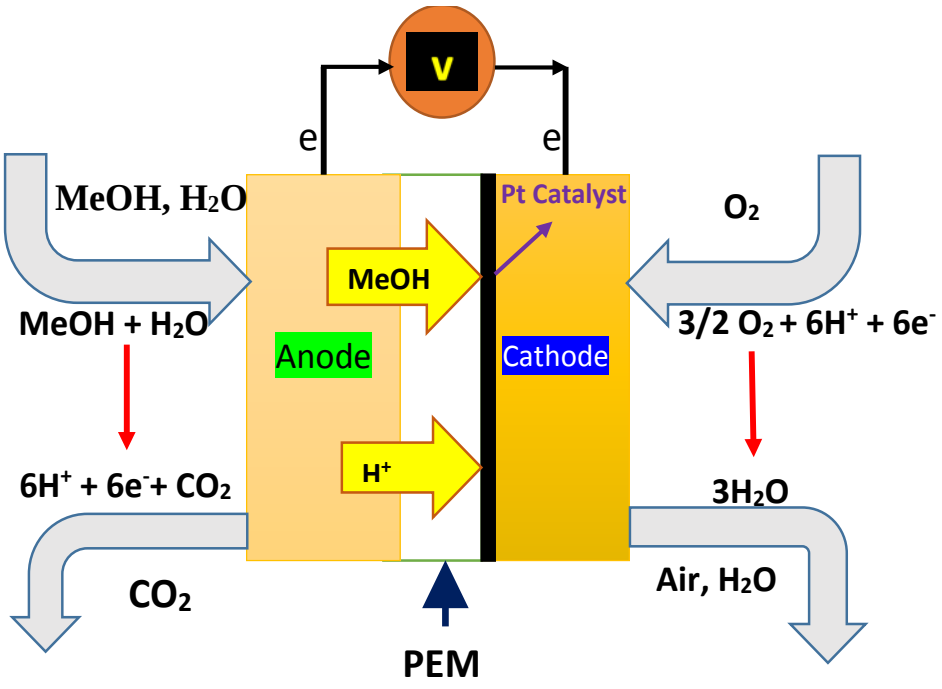

Fig. 1.9: Schematic diagram of DMFC illustrating methanol crossover.

1.4.1 Composite Membranes

The word *composite* is from Latin origin and means made up of separate parts. Here *composite membranes* means incorporation of a conductive polymer such as Ppy or PANI into an appropriate matrix such as Nafion membranes. In our research, Ppy and PANI have been chosen due to their high conductivity, stability in the oxidized state, availability and stability of their monomers and the facile synthesis procedure [50]. Preparation of composite membranes can be achieved either by chemical or electrochemical polymerization.

1.4.1.1 Electrochemical Polymerization

Electropolymerization of monomers occurs at the surface of conducting materials. Therefore electropolymerization is not possible on insulating materials. Few studies have focused on the electropolymerization of pyrrole and /or aniline [51-53]. Bhadra et al. prepared PANI by electrochemical and chemical methods and compared between the two prepared polymers. They concluded that the electrochemically prepared PANI has lower conductivity and higher solubility than that prepared chemically [52]. Fig. 1.10 shows the mechanism of electropolymerization of aniline according to kinetic studies. The oxidation of the aniline monomer is the slowest step in the polymerization. Once the aniline is oxidized to form the dimer, it is rapidly oxidized to form the oligomers and finally the PANI polymer [54].

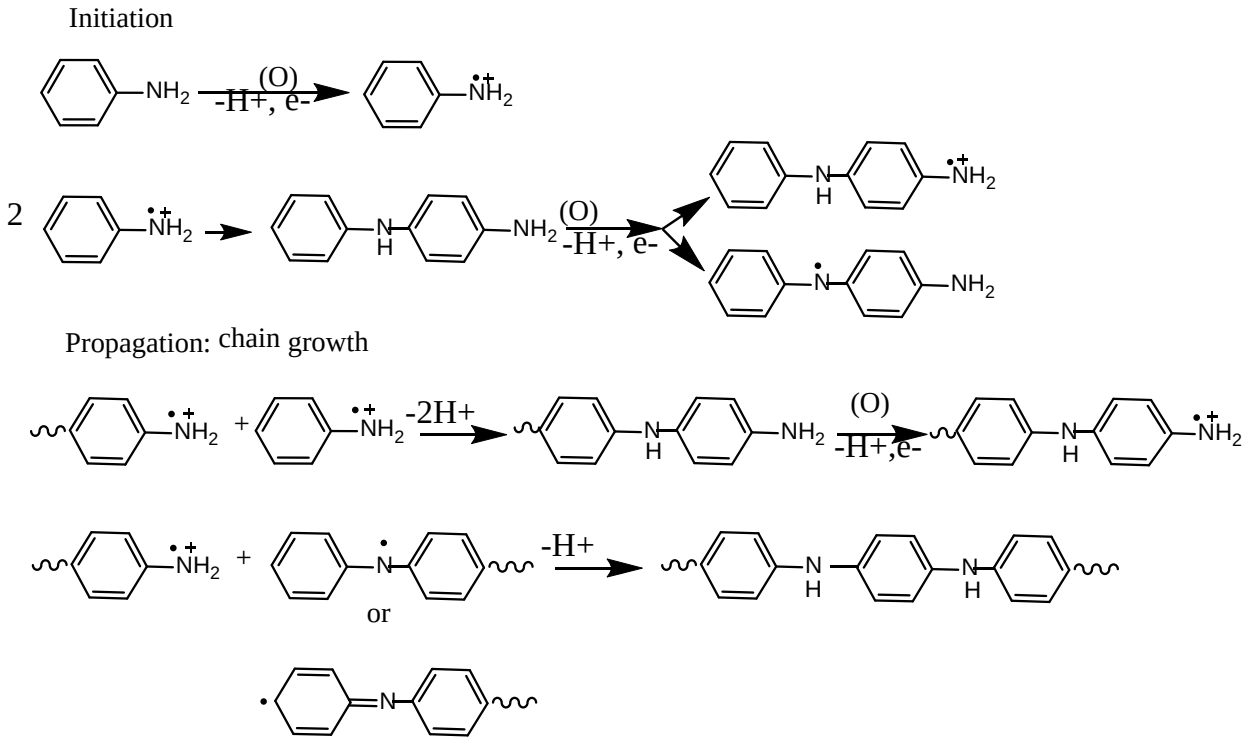

Fig. 1.10: The mechanism of aniline polymerization.

1.4.1.2 Chemical Polymerization

Most of the published papers dealing with modifying Nafion membranes with either Ppy or PANI utilized chemical polymerization. Chemical polymerization can be performed by two approaches. The first approach is to mix a monomer such as pyrrole or aniline with an oxidizing agent such as ferric chloride, ammonium persulphate (APS) or hydrogen peroxide solutions in the presence of a membrane. In this case, a bulk polymerization would be produced on the membrane and in the solution in the form of an insoluble solid. Therefore, the resulting membrane might have a rough surface. The second approach is to soak the membrane in a monomer solution then treat the membrane with an oxidizing agent. In this method, the monomer

is diffused into the pores of the membrane and then the polymerization occurs inside the pores by an oxidizing agent. This avenue allows the pores to be filled with the formed polymer. This membrane's modification can block undesired species from permeating through the membranes while maintaining its conductivity. In our study, we will focus on the second approach of the chemical polymerization.

Polymerization of Ppy is easy and rapid, as this method can be performed by either using hydrogen peroxide or a ferric chloride solution. The mechanism is well known in the literature as oxidative coupling of monomer molecules. As can be seen in Fig. 1.11, the first step is the oxidation of the pyrrole monomer to form radical cations which are highly active. The radical cations then dimerise by eliminating two protons and this process continues to form the polymer [55].

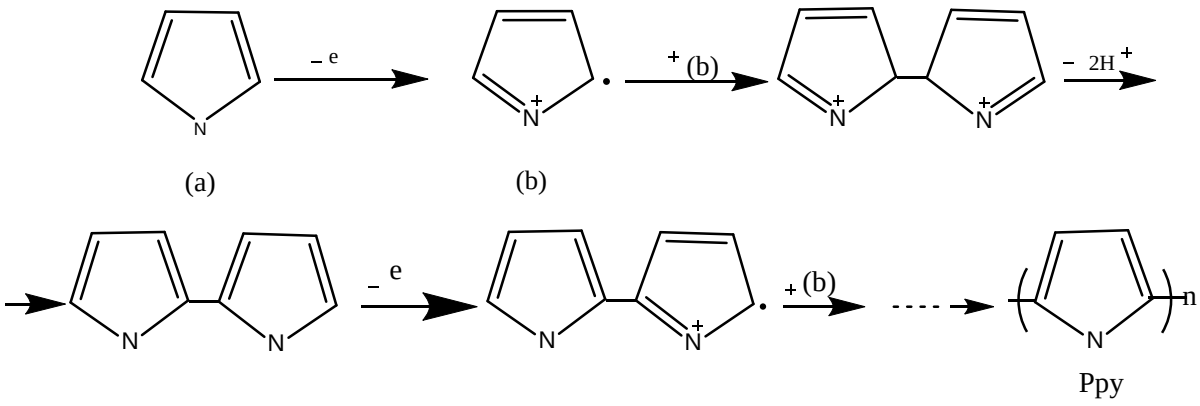

Fig. 1.11: The mechanism of pyrrole's polymerization.

Many researchers modified Nafion membranes by Ppy to overcome the methanol crossover. For example, Easton et al. modified the Nafions N112 and N115 by Ppy using either hydrogen peroxide or Fe(III) as an oxidant [44]. They found that the modified membranes

reduced the methanol crossover in DMFC. However, Fe(III) modified membranes showed higher ionic resistivity. Pickup et al. examined the neutral and acid forms of Nafions modified by Ppy using Fe(III) as an oxidizing agent [46]. These modified membranes were tested in DMFC and showed that the use of neutral Nafion for the preparation of Ppy modified membranes has superior performance over the use of the acid form. In another study, Pickup et al. showed that using Nafion in its tetrabutylammonium form has a significant methanol reduction in DMFC [56]. They also found that as the concentration of pyrrole increases in the Nafion modification, the methanol permeation and the exchangeable protons significantly decrease. This could be explained by an ionic association between Ppy and the sulfonate groups of Nafion which leads to contractions of the Nafion pores. Bouzek et al. examined different methods of modifying the Nafion membrane by Ppy [57]. They concluded that by soaking the membrane in pyrrole first, then with an oxidizing agent such as sodium persulfate, or keeping the membrane between two separate reservoirs of monomer and an oxidizing agent, resulted in a promising modified membrane that can be used to reduce methanol permeation in DMFC. Sungpet investigated Nafion 117 modified by Ppy using a hydrogen peroxide solution [58]. He found that this composite membrane was able to decrease the percent sorption of methanol from 38 to 19 g/g membrane. Innocent et al. studied the modification of Nafion 115 with Ppy using hydrogen peroxide and ammonium persulfate solutions for fuel cell applications [48]. They concluded that the composite membrane has 30 % lower methanol crossover although it has lower proton conductivity by a factor 2-3.

PANI was also used to improve the electrochemical and physical properties of membranes. Different oxidizing agents, such as hydrogen peroxide, Fe(III) and APS, were used

to polymerize aniline. At high pH, oxidation of aniline forms oligomers, i.e. dimers to tetramers, whereas at acidic pH, PANI is formed according to Fig. 1.12 [59].

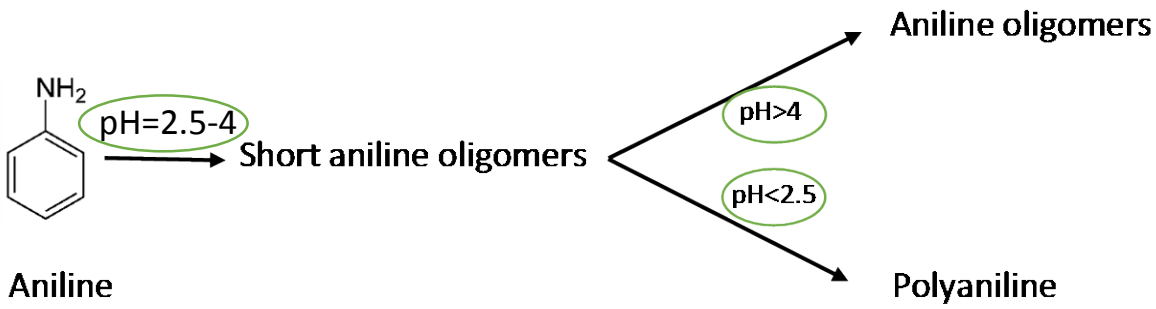

Fig. 1.12: Effect of pH on the polymerization of aniline.

In the same way, PANI was used by many researchers to modify membranes for methanol permeation reduction in DMFC. Bélanger et al. investigated the permselectivity of a cation exchange membrane (CEM) bearing sulfonate groups chemically modified by a thin PANI layer [60]. They observed that the permeation of Zn^{2+} and Cu^{2+} reduced from 10.1 to less than 1 % compared to the unmodified membrane. In another published paper, Bélanger et al. found that a long period of polymerization, with a high concentration of oxidizing agent APS, facilitates PANI degradation [61]. Furthermore, they concluded that a very thin and homogeneous layer of PANI on the membrane is required to block the transport of divalent cations such as Zn^{2+} [62]. Moreover, they indicated that when using 1 M of APS as an oxidant, PANI formed on the surface of the Nafion, while when using lower concentration such as 0.1 M, PANI formed inside the pores of the Nafion [63]. Nafion 112 was modified by PANI using APS as an oxidant [64, 65]. The composite membrane showed high ionic conductivity and superior performance when examined in a fuel cell compared to the unmodified membrane.

1.5 Membrane's Evaluation

Solid electrolyte membranes are the most widely used membranes in fuel cells and electrolyzers. Efficient membranes intended to be used in fuel cells and electrolyzers should have many requirements such as: physical separation of the anode and the cathode electrodes, efficient prevention of mixing the fuel and the oxidant, or the anolyte and the catholyte; high proton conductivity; and mechanical and thermal stability.

Potential candidate membranes should be examined before they can be applied in fuel cell and electrolysis applications. Permeability and proton conductivity are two major characteristics that should be examined and optimized for different applications. For example, to have an efficient and viable DMFC, the membranes should be modified to reduce methanol permeability and at the same time should maintain sufficient proton conductivity. In contrast, the Cu-Cl electrolyzer, the membranes should be modified to prevent the Cu species to permeate from the anode to the cathode side, as the diffused Cu species can deteriorate the cell efficiency.

1.5.1 Permeability

Permeability is one of the membrane characteristics that has a significant effect on the operation of an electrochemical cell. It has to be adjusted to reduce the movements of undesired species from the anode to the cathode and *vice versa*. Any permeation of the undesired species can result in mixed potentials and low efficiency as well as poisoning the catalyst layers.

1.5.2 Methanol Permeability

The most significant challenge in DMFC is the methanol crossover which is related to properties of the used membranes. This drawback in DMFC results from the transport of

methanol from the anode side of the fuel cell to the cathode side. The methanol crossover causes not only loss of fuel but also a mixed potential at the cathode which leads to lower voltage performance.

Methanol is permeated through the membrane by diffusion and moves through the ion-cluster pores and the connecting ion channels. Furthermore, the literature extensively examined this problem and tried to solve it. For example, methanol permeability was studied and determined by using diffusion cell-gas chromatography [58, 66-68], diffusion cell-Raman spectroscopy [48], pervaporation-gas chromatography [69-71] and fuel cell-electrochemical methods [44, 72].

1.5.3 Copper Permeability

The copper crossover in the Cu-Cl cycle is similar to the methanol crossover in DMFC as it can poison the cell and reduce its efficiency. Previous studies showed that the copper species permeating from the anode to the cathode reduced to solid copper and deposited on the membrane as well as on the cathodic catalyst layer [10, 12, 31]. To evaluate the copper crossover through a membrane we need an easy and simple method. Copper permeability can be measured by an *ex situ* diffusion cell similar to the methanol permeability method where copper diffused by time can be measured by atomic absorption spectroscopy (AAS). Another method to evaluate the copper crossover in the Cu-Cl electrolyzer was applied by Lvov [73]. The method includes determining the amount of Cu^{2+} by complexometric titration with an ethylenediaminetetraacetic acid standard solution using murexide as an indicator.

1.5.4 Membranes Conductivity

Membrane conductivity, which is the permeation of protons through the membrane, is one of the essential parameters required for high efficient fuel cells and electrolyzers. The capability of a membrane to conduct protons depends on the water content, acid content, chemical structure, morphology and the temperature. For example, a saturated Nafion membrane has very high conductivity as water molecules facilitate the proton movement. In fact, protons can pass from one water molecule to another neighbouring molecule which leads to high proton conductivity.

Nafion has hydrophilic sulfonic groups which are attached to the hydrophobic backbone part of the polymer. As expected, protons move through the hydrophilic part of the polymer which consists of channels and spherical domains. The protons which are very close to the sulfonic groups cannot freely move as they attract each other. Furthermore, extra water molecules allow the hydrophilic channels spherical domains to swell. Therefore protons can easily move through the hydrophilic parts and the conductivity increases. In the contrary, when there are fewer water molecules, these channels and spherical domains shrink and become disconnected through the membrane. Hence, protons cannot freely move and the conductivity decreases.

There are many methods available to measure proton conductivity such as electrochemical impedance spectroscopy (EIS), current interruption, and nuclear magnetic resonance (NMR) [74]. EIS is the most popular and the easiest technique that is utilized to measure proton conductivity. Proton conductivity can be measured by two-probe and four-probe methods. The four-probe method is usually used to measure the resistivity of membranes with

low resistance, whereas the two-probe method is used to measure the resistivity of membranes with high resistivity [75]. The proton conductivity of a membrane can be easily determined by measuring the resistance of the membrane using an electrochemical impedance spectroscopy (EIS) [76]. The proton conductivity of a membrane can be measured either in-plane or through-plane (perpendicular). With in-plane measurement, a membrane is set on the edge of two electrodes, while with through-plane measurement a membrane is sandwiched between two Pt electrodes, as shown in Fig. 1.13. It is believed that the in-plane conductivity measurements are conducted easily with high accuracy due to greater cell constant, whereas in the through-plane setup, the cell constant is small [77].

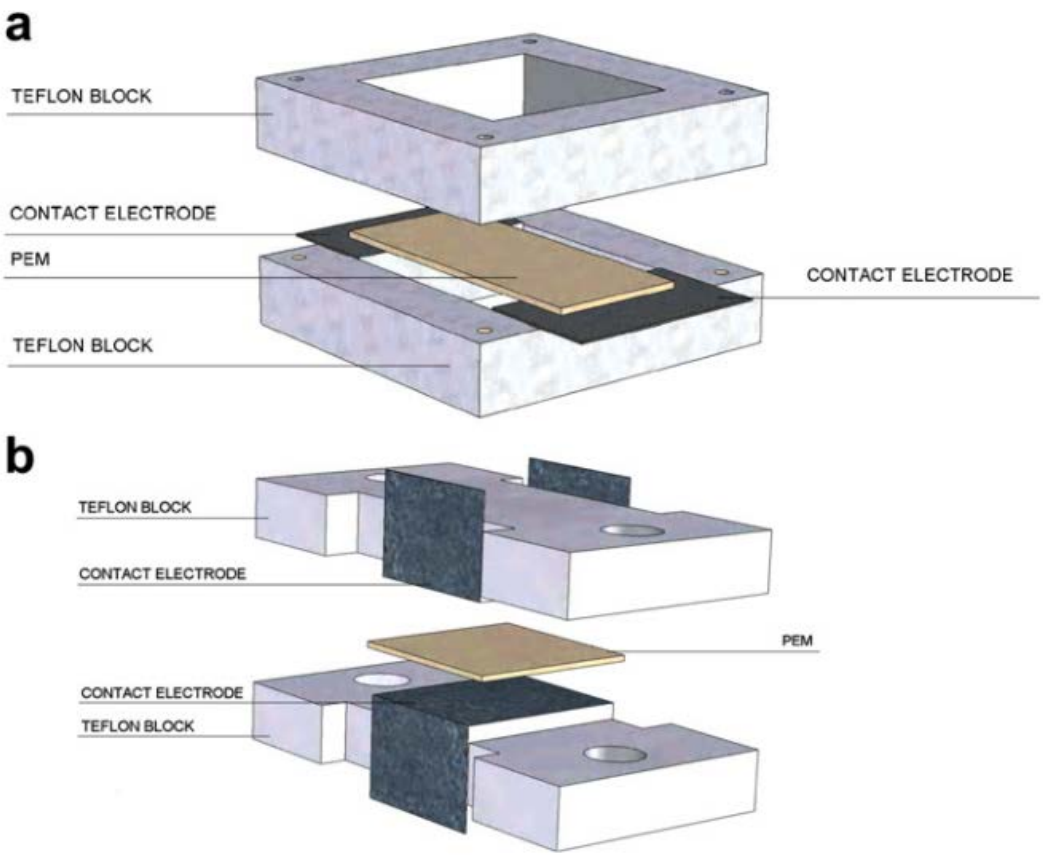

Fig. 1.13: (a) In-plane and (b) through-plane impedance cells showing the probe arrangement. Reproduced with permission from [77].

1.6 Electrochemical Assessment Techniques

Electrochemical reaction is a type of reaction associated with electron transfer between an electronic conductor (electrode) and an electrolyte. The reaction that occurs at the anode is called anodic where the electroactive species is oxidized, whereas a reaction occurs at the cathode is called cathodic where the electroactive species is reduced. An electrolytic cell is composed of two electrodes separated by an electrolyte. It is an electrochemical cell where oxidation and reduction (redox) occur when electrical energy is applied. In fact, the electrochemical reactions in the electrolytic cell are controlled by Faraday's law which states that there is a stoichiometric relation between the number of reactant molecules involved in an electrode reaction and the number of electrons flowing in the circuit.

The cell voltage can be determined from Eq. 1.11

$$E^e_{cell} = E^e_c - E^e_a \qquad \text{Eq.1.11}$$

where E_c, E_a are the equilibrium potentials of the cathodic and anodic reactions, respectively. Practically, additional potential is required to drive a reaction at a specific rate which is called overpotential η, so it is important to implement this overpotential for both electrodes to increase the rate of electron transfer and also to move the ions through the membrane. Hence, to have an electrolysis current, extra voltage is required according to Eq.1.12

$$E_{cell} = E^e_{cell} - |\eta_c| - |\eta_a| - |IR_{soln}| - |IR_{mem}| \qquad \text{Eq.1.12}$$

Fig. 1.14 shows the overpotentials in regular polarization curves. At the beginning, the charge transfer overpotential, which is the loss associated with the activation barrier, is required to overcome by the reactants. Ohmic losses then result from the membrane or the electrolyte

resistivity. Eventually, there is mass transfer overpotential, which is due to gradient concentration.

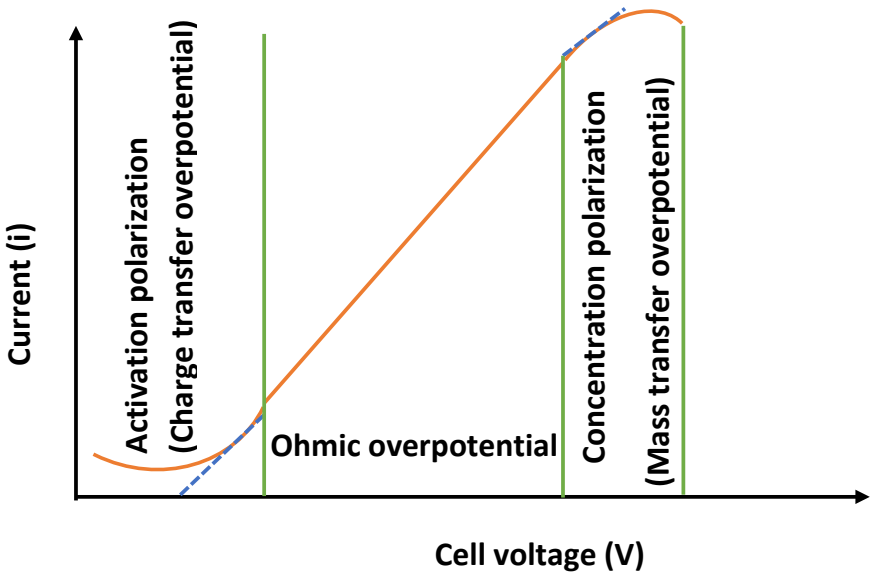

Fig. 1.14: Types of overpotentials in a polarization curve.

Fig. 1.15 shows the onset potential of the water electrolysis at around 1.8 V, while for the CuCl electolyzer the onset potential is around 0.4 V. Thus, the CuCl/HCl electrolysis requires a significantly lower voltage to produce hydrogen gas from dissociation of water compared to water electrolysis. Thus, a difference of 1.4 V is the saving in the potential.

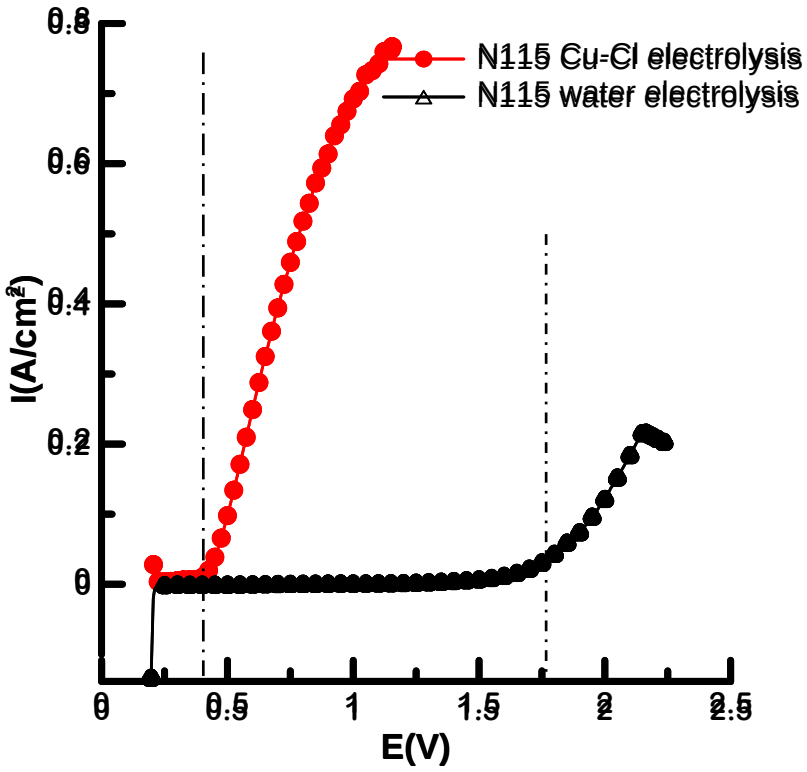

Fig. 1.15: Comparison of CuCl and H_2O electrolysis. CuCl electrolysis collected using 0.2 M CuCl in 2.0 M HCl as anolyte and DI water as catholyte with a flow rate of 60 mL min^{-1} under nitrogen atmosphere.

The three electrode-cell consists of working, reference and auxiliary electrodes. The working electrode is where the electroactive species reactions occur therefore the surface should be clean and conductive, whereas the reference electrode should always hold a fixed potential so its value can be referenced by the working electrode. One of the common reference electrodes is the standard hydrogen electrode (SHE) which has a potential of zero by default. In addition the auxiliary (counter) electrode should provide an equal magnitude current to the working electrode with an opposite sign. Inert atmosphere such as nitrogen is required to prevent any oxidation from the atmospheric gases.

Electrochemical techniques are used to study electroactive species, qualitatively and quantitatively. By applying these techniques, we can study the behavior of the electrodes and the

membrane in any electrolysis cell. In addition, we can determine the onset potential and the current response at varying potentials and *vice versa*. Furthermore, we can detect the copper deposition on the membrane, as well as any copper crossover in the catholyte. Current efficiency of different membranes can also be evaluated by electrochemical methods.

1.6.1 DC Voltammetry Techniques

Voltammetry is based on the measurement of the current developed due to concentration polarization and can be conducted by varying the working electrode potential. There are many voltammetric techniques that can be applied for any electrochemical study. In potential step voltammetry, the applied potential is jumped from $V_{initial}$ to V_{final} stepwise, then the resulting current is measured as a function of time. Since the potential is also changed with time, the output plot regularly comes as current *vs*. potential. The onset potential and the overall current can be determined from such a technique.

The potentiostatic method is based on applying a fixed potential to the electrode and measuring the variation of current. The result of this method is a plot of current *vs*. time. At the beginning, a large current flows which is ascribed to the charging current of the electrode double layer (dl), whereas in the galvanostatic method a fixed current density is applied, and the potential is measured as a function of time. The applied current should be at least equals to the summation of Faradic and charging current to obtain potential representing the electrode reactions.

Cyclic voltammetry (CV) is another electrochemical technique which measures the current that develops under conditions where voltage is in excess of that required according to

the Nernst equation (Eq. 1.13). CV is obtained by cycling the potential of a working electrode, and measuring the resulting current.

$$E = E^{o} + (RT / n F) \text{ Ln } C_O/C_R \qquad \text{Eq. 1.13}$$

1.6.2 AC Electrochemical Impedance Spectroscopy (EIS)

EIS is a powerful technique for characterizing the electrical properties of electrodes and interfaces. An electrode-solution interface system can be represented by an equivalent circuit where elements such as resistors and capacitors can be used to describe the elementary process.

A Randles circuit is one of the circuits that describe the behavior of the electrode interface process by charge transfer resistance and Warburg impedance in parallel with the double layer capacitance, all of which are connected in serial with the uncompensated resistance, as shown in Fig. 1.16.

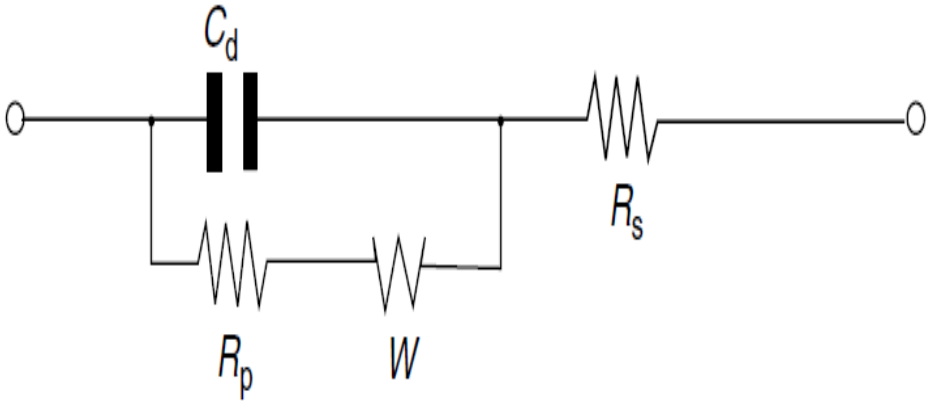

Fig. 1.16: Randles circuit.

Practically, electrochemical impedance is measured by applying a small sinusoidal potential to an electrochemical cell and then measuring the current response. The response to this

potential is a sinusoidal current signal with the same frequency but with a phase shift according to Equations (1.14, 1.15).

$$E = \Delta E \sin 2\pi f t \qquad \text{Eq. 1.14}$$

$$I = \Delta I \sin (2\pi f t + \phi) \qquad \text{Eq. 1.15}$$

The impedance (Z), which is a complex quantity, can then be calculated from the following equation:

$$Z = E / I = Z_{\circ} (\cos \phi + j \sin \phi) \qquad \text{Eq. 1.16}$$

The data output from the impedance spectroscopy is obtained by plotting the imaginary component of the impedance versus the real component as a function of frequency. Such a plot, known as a Nyquist, can be seen in Fig. 1.17. The R_{ct} can be determined from the diameter of the semi-circle. The double layer capacitance can also be found from the frequency of the maximum height of the semi-circle according to the following equation:

$$f = \frac{1}{2 \pi R_{ct} C_{dl}} \qquad \text{Eq.1.17}$$

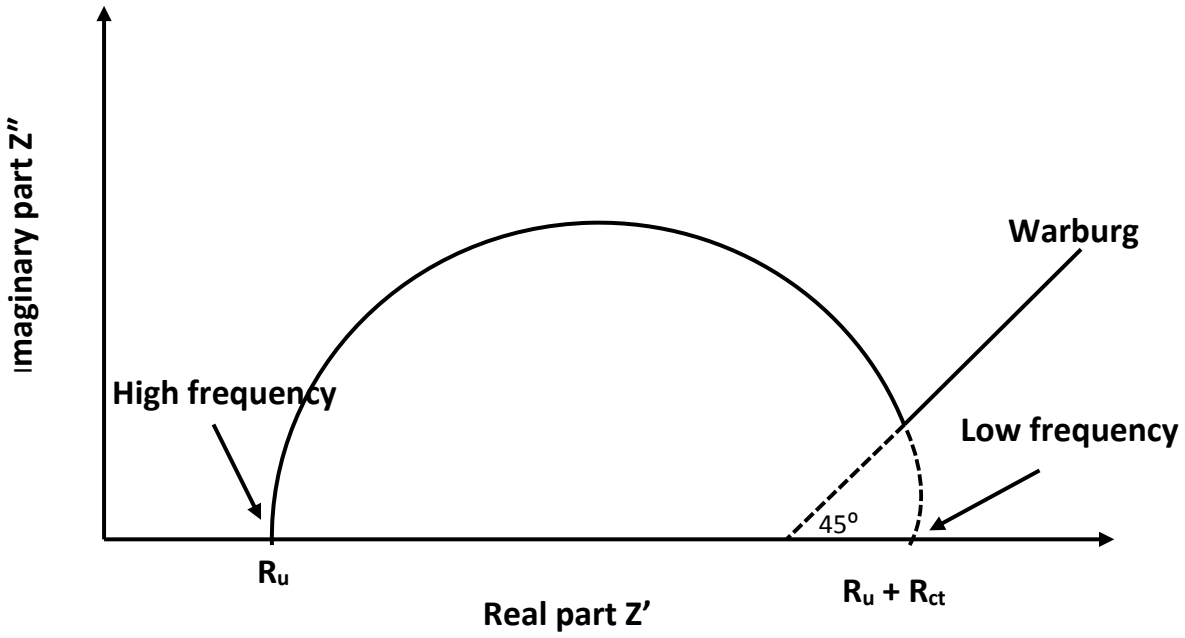

Fig. 1.17: Nyquist plot showing Warburg region.

1.7 Thesis Objectives

In this research, Ppy and PANI composite membranes of NRE212, N115 and N117 will be prepared by *in situ* polymerization using different oxidizing agents such as hydrogen peroxide, iron (III) chloride, and APS. The modified membranes will be characterized by different techniques such as ATR FT-IR, UV spectroscopy, TG and SEM. The physical properties of the modified composite membranes, such as water uptake and ion exchange capacity (IEC), will be studied. The proton conductivity (σ) of the modified and unmodified membranes will be determined by using EIS.

The diffusion of methanol and Cu for the modified and unmodified membranes will be investigated by an *ex situ* diffusion cell. The permeated methanol and Cu samples will be analyzed using gas chromatography and AAS, respectively. A relationship between methanol

and Cu permeability will be studied and evaluated for all membranes. Furthermore, the selectivity and relative selectivity of the modified and unmodified membranes will be determined.

MEAs of the modified and unmodified membranes will be assessed in the full cell of the Cu-Cl electolyzer. Many electrochemical techniques will be used to study the behavior of these membranes. For example, EIS, potential stair steps, potentiostatic, galvanostatic and CV techniques will be used to understand the electrochemical properties of these membranes as well as their capability to reduce the Cu crossover.

A modified setup of the Cu-Cl electrolyzer similar to Lvov setup [73] will be constructed to examine the current efficiency of these composite membranes through collecting the produced H_2 gas which evolved from the cathode side and compare them with the unmodified membranes.

Speciation of the Cu species in the anolyte solution after certain hours of Cu-Cl electrolysis will be examined using Ultramicroelectrode CV. A three-electrode cell will be utilized and a 25 μm Pt electrode will be used as a working electrode. This will give us a hint of the performance of the composite membranes compared to unmodified membranes.

An anion exchange membrane will be eventually used in the MEA in the Cu-Cl electrolysis cell instead of Nafion cation exchange membranes. Full electrochemical testing will be conducted and compared with the pristine Nafions.

Chapter 2

Methodology and Instrumentation

2.1 Materials and Chemicals

Nafion NRE212, Nafion 115 and Nafion 117 (1100 EW) were purchased from Ion Power and are hereafter referred to as NRE212, N115, and N117, respectively. Anhydrous methanol and n-butanol were supplied from Sigma Aldrich with a purity of 99.8 %. In addition, 30 % hydrogen peroxide, 98 % copper (II) sulfate penta-hydrate, ammonium persulfate, ferric chloride hexahydrate, aniline and copper (I) chloride 97 % were sourced from Sigma Aldrich. 99.0 % extra pure pyrrole was purchased from Acros Organics. All chemicals were used as received without any further purification. The water used for all experiments was deionized Milli-Q water (Millipore) (18 MΩ cm).

2.2 Membrane Modification

All membranes were cleaned prior to examination using a common literature procedure [78]. Briefly, Nafion membranes were cut into 5.0 x 5.0 cm pieces and were consecutively boiled in the following solutions for one hour: first, deionized water, then, 5 % H_2O_2 solution, followed by deionized water; then, 0.5 M H_2SO_4, and a final time with deionized water before being stored in fresh deionized water for at least 24 h prior to further use. To be consistent, four pieces of the cleaned membranes were modified at the same time in different petri dishes. Two of these modified membranes were used for diffusion studies. The third was used for conductivity and other physical properties measurements, with the fourth membrane reserved for electrochemical studies.

2.2.1 Nafion/Polypyrrole Composite Membrane

The composite membranes of polypyrrole (Ppy) were prepared according to the method described by Pickup's group [44]. The process of membrane modification consists of two steps.

First, the cleaned membranes were immersed in an aqueous solution of pyrrole in glass covered petri dishes for 15 minutes on each side. The membranes were then removed from the pyrrole solution, rinsed with deionized water, and then reimmersed in an oxidizing agent solution for the same time on each side. Finally, the membranes were washed with 1.0 M sulphuric acid, followed by deionized water, in which they were stored for 24 h prior to use. Fig. 2.1 compares a photograph of a Nafion membrane before and after the modification. As can be seen, the Nafion membrane is clear colorless whereas the Ppy composite membrane is dark green or brown. This change in colour is a result of *in situ* polymerization of pyrrole within the pores of Nafion. The Ppy composite membranes are hereafter referred to as X/Ppy, where X represents the base membrane chosen for modification (e.g. N115/Ppy). A 30 % hydrogen peroxide solution was used as an oxidising agent to start the polymerization unless otherwise mentioned.

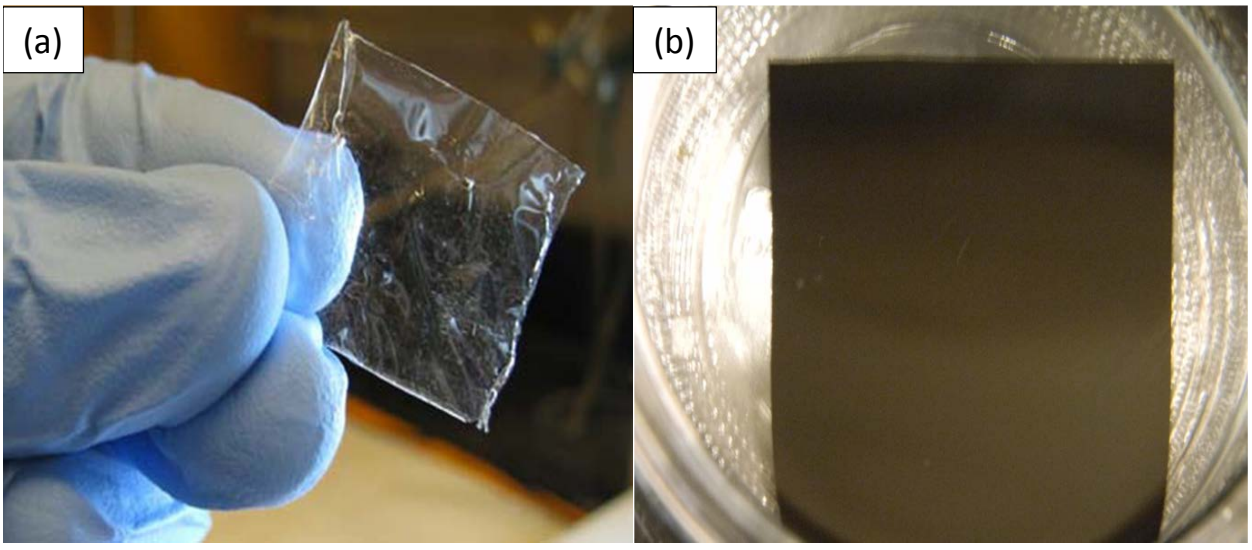

Fig. 2.1: (a) Photograph of the pristine Nafion and (b) Ppy composite membrane.

2.2.2 Nafion/Polyaniline Composite Membrane

The composite membranes of Nafion-polyaniline (PANI) were prepared by *in situ* chemical polymerization of aniline within Nafion membranes. Composite membranes were prepared using different polymerization times at ambient temperature and different oxidizing agents. Our synthetic method is similar to many others reported in the literature [79-81]. A solution of aniline dissolved in 1.0 M HCl was used to impregnate the cleaned Nafion membranes for 30 min on each side in a glass covered petri dish, after which they were rinsed with DI water. The membrane was subsequently immersed in one of the following solutions of oxidizing agents for polymerization; 30 % H_2O_2, 0.2 M ferric chloride in 1.0 M HCl or 0.2 M aqueous solution of ammonium persulfate (APS). The polymerization was allowed to proceed for 1, 5 and 24 h independently. The resulting composite membrane was then washed with DI water and coated by dipping it for few seconds in 5 % Nafion solution and hung to dry in a fume hood for *ca*. 3 hours. The coated membrane was washed with 1.0 M aqueous solution of sulfuric acid and stored in DI water for at least 24 h.

2.3 Materials Characterization

2.3.1 Water Uptake

The water uptake was measured for the pristine and composite membranes by measuring the mass difference of the totally hydrated and dried membranes. The mass of the hydrated membrane and the vacuum dried membrane were represented by m_{wet}, and m_{dry}, respectively. Initially, the water on the outer surface of the fully hydrated membrane was carefully blotted away with a Kim wipe and quickly weighed to determined m_{wet}. The membrane was then dried

in a vacuum oven at 60 °C for 24 h and subsequently weighed to determine m_{dry}, after which the water uptake was calculated using Eq. 2.1:

$$water\ uptake(\%) = \frac{m_{wet} - m_{dry}}{m_{dry}}\ X\ 100\ \% \qquad Eq.2.1$$

Membrane water content measurements were determined by Karl Fisher titration method using Mettler Toledo DL31 system. Approx. 0.1-0.2 g sample of a tissue-dried membrane was extracted by 1-2 mL of anhydrous methanol. A fraction of the extract was used to accomplish the water content analysis.

2.3.2 Ion Exchange Capacity (IEC)

The ion-exchange capacity (IEC) of the membranes was measured by titration with a dilute sodium hydroxide standard solution. Approx.0.1– 0.2 g of vacuum dried membranes were soaked in a 3.0 M NaCl aqueous solution for 24 h at an ambient temperature with occasional shaking. The solution was then titrated against a 0.005 M NaOH solution to neutralize the exchanged protons (H^+) using a phenolphthalein pH indicator. The IEC was calculated using Eq. 2.2:

$$IEC = \frac{\Delta V_{NaOH}\ C_{NaOH}}{m_s}\ \ (mol\ g^{-1}) \qquad Eq.2.2$$

where V_{NaOH} is the consumed volume of the NaOH solution, C_{NaOH} is the exact concentration of the NaOH standard solution, and m_s is the mass of the membrane sample in g.

2.3.3 Proton Conductivity

Membrane proton conductivity (σ) was evaluated via electrochemical impedance spectroscopy (EIS). Measurements were made using a Solartron 1260 frequency response analyzer controlled using Zplot software (Scribner) in "stand alone" mode. A 2 cm × 1 cm strip of hydrated membrane was placed into an in-plane conductivity cell containing two platinum electrodes separated by a distance of 1 cm. The cell also has 1 cm^2 window on both sides, allowing the membrane to be exposed to external conditions, as can be seen in Fig. 2.2. An illustration of the membrane dimensions and how they align with electrode contacts are shown in Fig. 2.3 (a,b). EIS measurements were made using a previously developed protocol [77, 78, 82] by applying a 100 mV sinusoidal voltage across the electrodes over a frequency range of 13 MHz to 100 Hz with zero bias voltage. All EIS data was fit to the simple equivalent circuit shown in Fig. 2.3 (c). The circuit consists of the membrane capacitance, C_m, connected in parallel to the membrane ionic resistance, R_m, all of which is connected in series with a contact resistance, R_c. The typical EIS response is a semi-circle Nyquist plot, as can be seen in Fig. 2.4, where the diameter of the semi-circle corresponds to R_m [78, 83, 84]. Proton conductivity (σ) was calculated from R_m using the following equation:

$$\sigma = \frac{L}{R_m W d} \qquad Eq. 2.3$$

where L, W and d are the length, width and height of the membrane samples, respectively.

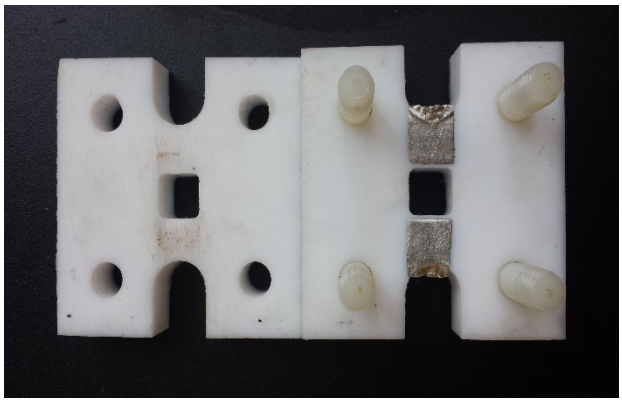

Fig. 2.2: In-plane conductivity cell.

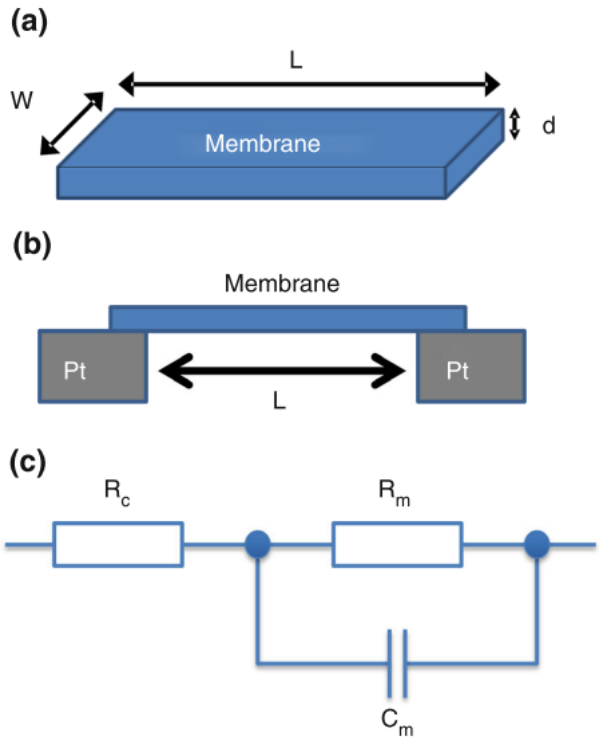

Fig. 2.3: Schematic diagram of (a) test membrane dimensions (b) cell geometry and (c) the equivalent circuit model used to determine membrane proton conductivity by EIS. Reproduced with permission from [84, 87].

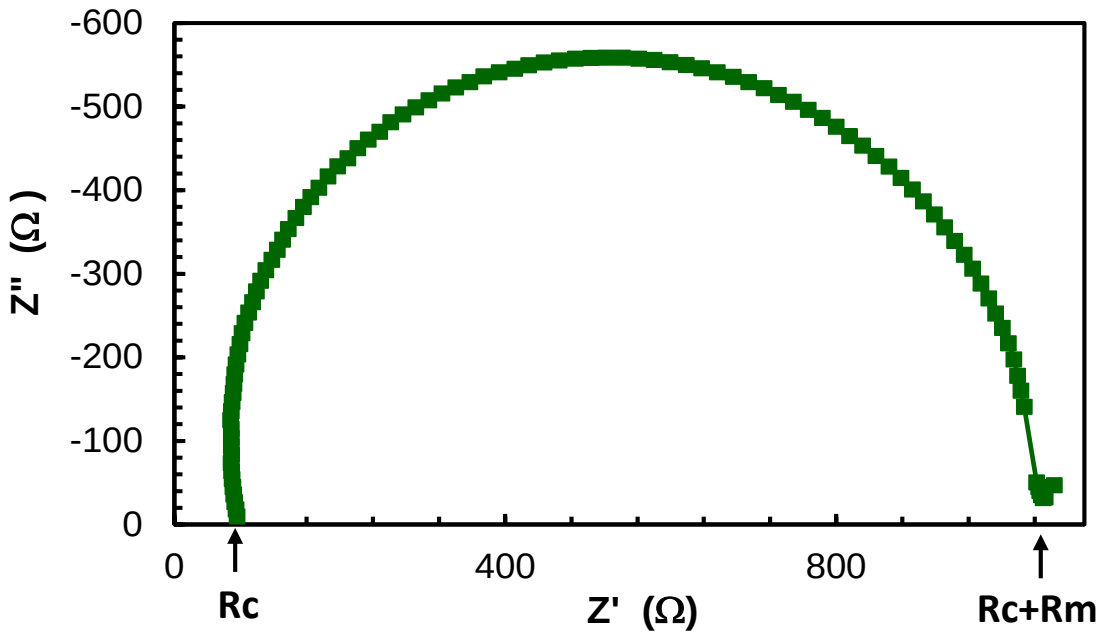

Fig. 2.4: Nyquist plot obtained for pure Nafion membrane.

2.3.4 Diffusion and Selectivity

Methanol permeability of the membranes was studied at room temperature using a glass diffusion cell [85, 86]. The diffusion cell consists of two 100 mL compartments, attached by a circular area of 4.5 cm^2. The membrane to be investigated was fixed between the two compartments by an O-ring and a thumb screw clamp. 100.0 mL of deionized water was kept in compartment B, while, 100.0 mL of a 1.0 M methanol aqueous solution was added into compartment A. A photograph of the cell is shown in Fig. 2.5. The solutions in the two compartments were stirred by magnetic bar stirrers with a moderate speed to maintain solution homogeneity. Compartment B was regularly sampled every ten minutes from the time of methanol addition for the first hour, then every hour for the next 2 hours and finally after an

additional 24 h. The samples were analyzed by a head space gas chromatograph using a Finnegan Ultra Trace (Thermo Fisher) equipped with a 30m TR-wax GC column, 0.53ID and 1µm film. A flame ionization detector (FID) was used to detect the analytes. In addition, n-butanol was utilized as an internal standard to overcome any inconsistency with the injection method.

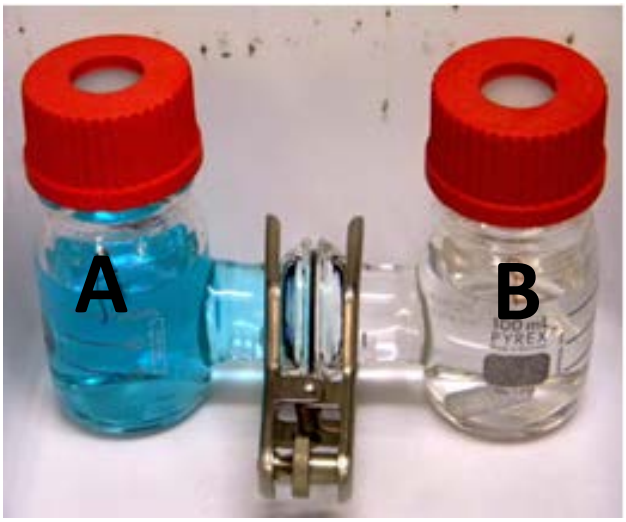

Fig. 2.5: Photograph of the diffusion cell used for both methanol and Cu permeability studies. In this case, Cu diffusion is being studied.

The diffusion of copper through pristine and Ppy composite membranes was investigated using the same glass diffusion cell. Compartment A was filled with 100.0 mL of a copper sulphate penta-hydrate solution dissolved in 1.0 M HCl, equivalent to 7100 ppm copper. Compartment B was only filled with 1.0 M HCl solution. Samples were taken from compartment B at 10 min, and then at time intervals of one, two, three, four and 24 hours and measured by a Flame Atomic Absorption Spectroscopy (AAS), Varian 240 FS.

The methanol and the copper concentration can be calculated from Eq. 2.4

$$C_B(t) = \frac{A\,D.K}{V_B\,L}\,C_A(t - t_0) \qquad Eq.2.4$$

where C is the methanol or copper concentration in compartment A or B and V_B is the volume in compartment B. A, L and t are the membrane area, the membrane's thickness and the time of the diffusion, respectively. DK represents the permeability which can be calculated from the slope of a straight line correlation between concentrations *vs.* time.

2.3.5 Thermogravimetric Analysis (TGA)

Thermogravimetric analysis (TGA) was performed using a TA Instruments Q600 SDT thermal analyzer. A sample, 10-20 mg, was heated from room temperature to 1000 °C in an alumina sample pan at a specific heat rate using either argon or air as the purging gas with a flow rate of 50.0 mL min^{-1}. TA Universal Analysis software was used to control and evaluate the data.

2.3.6 Scanning Electron Microscope (SEM)

SEM provides information about the surface topography and composition of samples. The membranes were completely dried in a vacuum oven as a requirement for SEM measurement. To reduce the charging current a small sample piece was coated with gold. The coated samples were later examined with SEM using a JEOL JSM-6400 (Japan). JEOL SEM is furnished with a tungsten hair pin filament as a cathode and equipped with a two-inch airlock and has a probe current detector (PCD).

2.3.7 Fourier Transform-Infrared Spectrophotometry Horizontal Attenuated Total Reflector (FT-IR HATR)

FT-IR spectra measurements were performed on a Perkin Elmer, spectrum 100 FT-IR spectrometer by using Horizontal Attenuated Total Reflection (HATR) with a zinc selenide (ZnSe) window, controlled using Spectrum 1 software.

2.4 Full Cell Production and Design

2.4.1 Catholyte/Anolyte Preparation

The anolyte solution was prepared by mixing approximately 335 mL of concentrated HCl with DI water and diluting it to 2.0 L to produce 2.0 M HCl. The solution was purged with N_2 gas for about 30 minutes to remove any dissolved O_2 gas. To this 2.0 M HCl solution, 39.6 g of 97 % CuCl solid was added slowly dissolved with continuous stirring under N_2 atmosphere for at least 20 min. DI water was used as a catholyte solution unless otherwise mentioned.

2.4.2 Membrane Electrode Assembly Fabrication

MEAs were constructed from in house materials. The cathode electrode was prepared by Patrick Edge (MSc student in Easton group) as a fuel cell electrode and consisted of a Pt-based catalysts deposited on carbon fiber paper (Pt loading=0.32 mg cm^{-2} with 30 wt. % Nafion, CFP thickness=280 µm). A 5 cm^2 section of cathode was hot-pressed onto a 5.0 × 5.0 cm section of a membrane, as shown in Fig. 2.6. Hot-pressing was performed as shown by the configuration, which consists of top and bottom flat metal plates that covered by aluminum foil. On the bottom side a Teflon sheet, a membrane and the cathode electrode with the coating part facing the membrane arranged consequently. The MEA was compressed under a load of 300 kg cm^{-2} at a

temperature of 140-150 °C for 75 s. The hot pressed membrane with the cathode electrode were then immediately placed onto a 5 cm^2 section of non-wet proof carbon paper (TGP-H-090 Toray paper) as an anode material in the full cell.

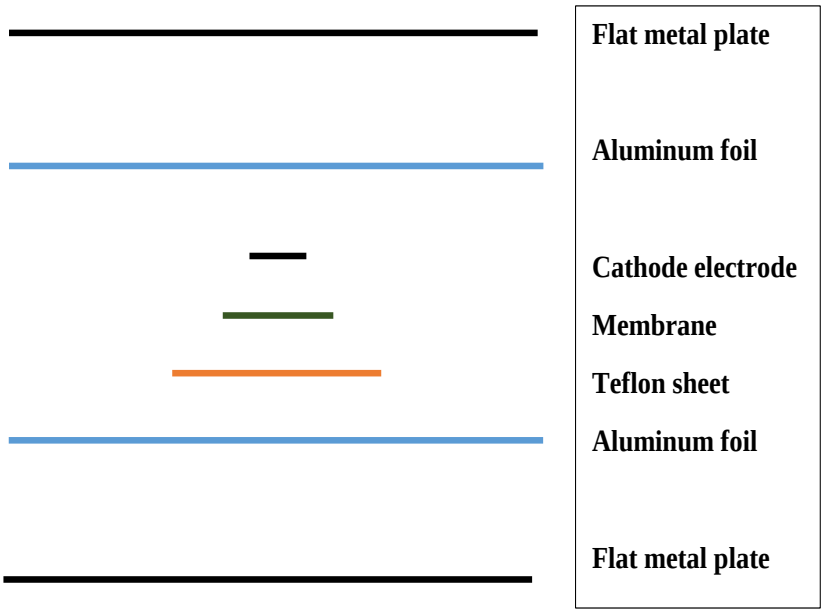

Fig. 2.6: Illustration of hot press configuration which consequently consists of a Teflon sheet, a membrane, and cathode electrode all of them sandwiched between two flat metal plates covered in with aluminum foil.

2.4.3 Full Cell Electrolysis System

Full cell electrolysis system was designed and constructed in-house by a previous student. A photograph of the system is shown in Fig. 2.7 [87]. A 5.0 cm^2 full graphite PEM electrolysis cell was used (FC-05-02 ElectroChem Hardware with Teflon fittings) with a dimension of (H x W x L) (11 x 9.5 x 4.5) cm. A 0.2 M CuCl in a 2.0 M HCl liquid electrolyte

was used as the anolyte solution and deionized water was used as the catholyte solution. The electrolyte solutions were stored in two 4 L Pyrex glass tanks with 1/4” OD Chemglass tubing adapters. Electrolyte flow was maintained using a Materflex L/S digital drive peristaltic pump (RK-07523-80) with variable flow rate capability of 4.8-480 mL min^{-1}. The pump was configured with two Masterflex L/S Easy-Load 3 roller pump heads. A standard platinum cured silicone L/S-16 tubing was used in the pump head and hard 1/4” OD PTFE tubing was used to transport the liquid electrolytes. 1/4” PTFE Swagelok connectors were used to connect the PTFE tubing to the electrolysis cell. A series of valves in the system enables the selection of alternate cell feeds. For example, HCl 2.0 M and H_2 gas were used for impedance and cyclic voltammetry (CV) investigations instead of CuCl/HCl solution, as can be seen in Table 2.1.

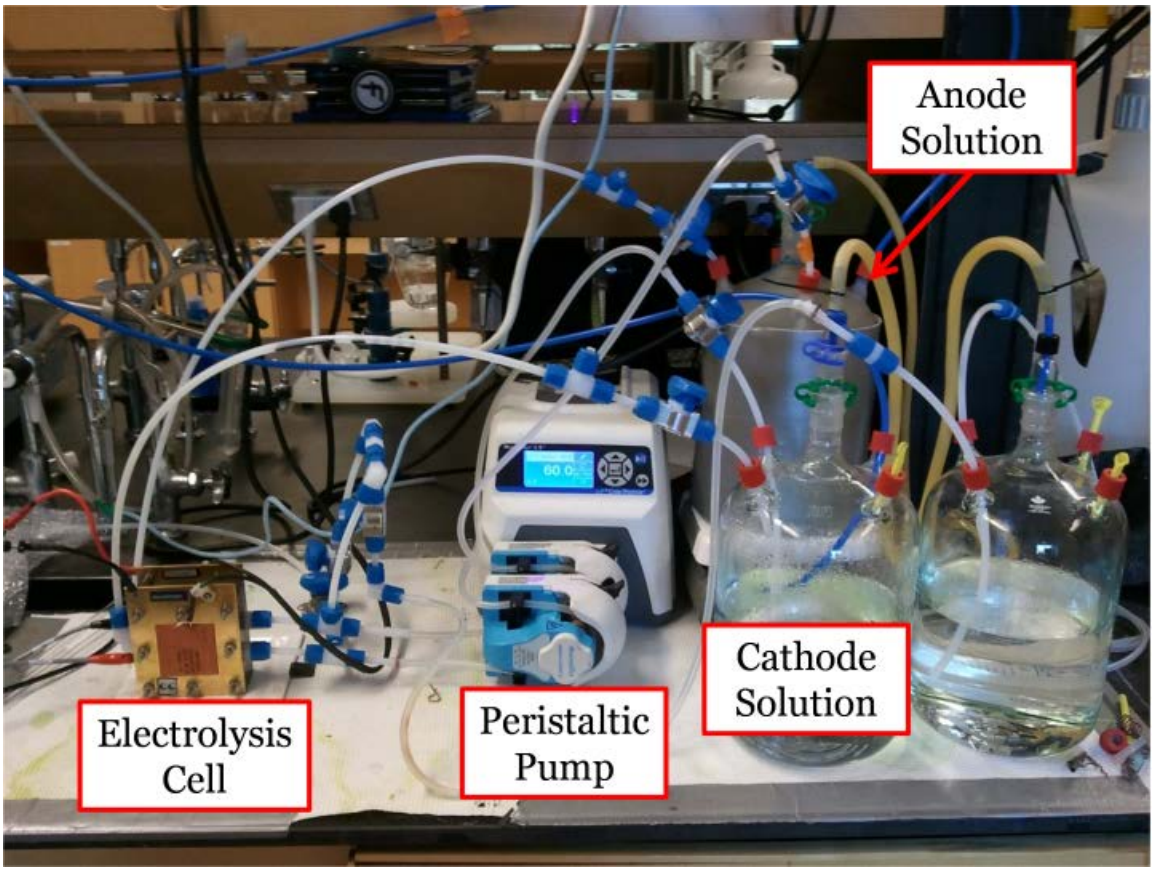

Fig. 2.7: Full electrolytic cell with recyclable catholyte and anolyte.

Table 2.1: The electrolyte of electrolysis and diagnostic modes.

Electrolyte	CuCl electrolysis mode	Electrochemical diagnostic mode
Anolyte	0.2 M CuCl in 2.0 M HCl (60 mL min^{-1})	2.0 M HCl (60 mL min^{-1})
Catholyte	DI Water (60 mL min^{-1})	H_2 (g) (25 mL min^{-1})

A programmable PID controller (Omega), a K-type thermocouple (Omega), and the existing heating pads on the cell's current collector plates were employed to observe and regulate the electrolysis cell at a constant temperature of 25.0 ± 0.5°C.

The complete MEA was placed between a layer of silicon gasket followed by graphite plates and the electrolysis cell bolts were tightened to 30 in lb (3.4 N m) of torque using a torque wrench. This compression ensures the gaskets seal properly, and result in intimate contact between the electrodes and the membranes.

For selected experiment, H_2 production efficiency measurements were performed using a method similar to that reported by Lvov et al. [12]. To do this, modification was made on the catholyte container in order to collect the produced H_2 as shown in Fig. 2.8. A glass container filled with deionized water was carefully connected to the catholyte container through a short combined hard PTFE and Tygon tube above water level. Inside this container, a glass tube was inserted to the bottom of the container. The upper part of the glass tube was connected to a Tygon tube into a 500 mL graduated measuring cylinder. Therefore, the produced H_2 that reached the catholyte container transferred to the water container and displaced the same volume of water to the measuring cylinder. The mass of displaced water was subsequently measured from the volume and density of the collected water. To validate the hydrogen production performance apparatus, water electrolysis was performed using H_2SO_4 0.5 M solution as

electrolyte for both the catholyte and anolyte. N115 was employed as a membrane and Pt/C was utilized as an electrode for both the cathode and anode. Current efficiency was measured to be 99.1 ± 0.5 % for water electrolysis, which confirms this configuration is highly accurate for hydrogen efficiency measurements.

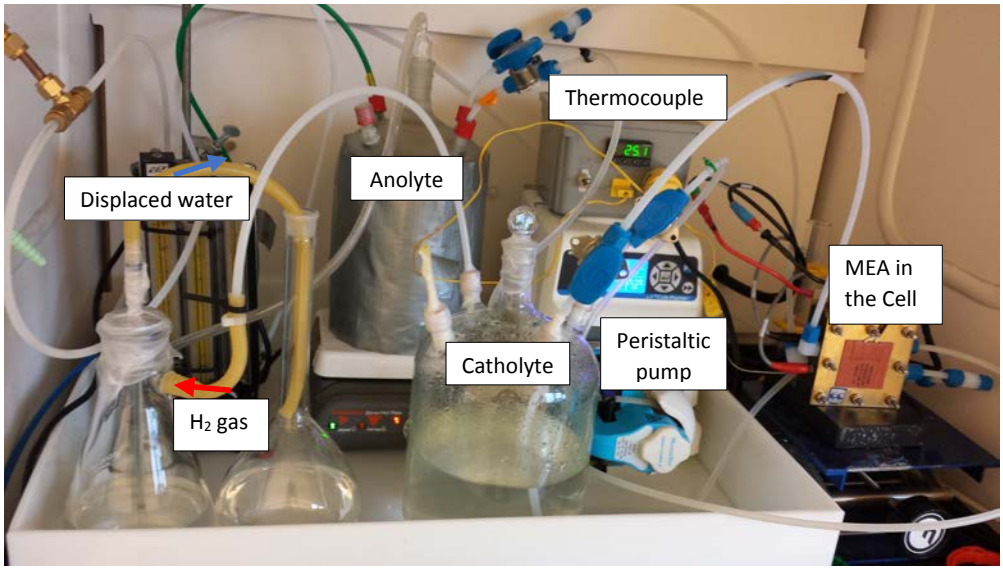

Fig. 2.8: Efficiency measurement of H_2 production setup using Cu-Cl electrolyzer with a modification that includes outlet from the catholyte container to move the produced H_2 to another flask that contains water which can be equivalently displaced by H_2 gas.

2.5 Electrochemical Characterization

2.5.1 Full Cell Electrochemical Techniques

Electrochemical measurements were performed using a Solartron 1470 E multichannel potentiostat and a Solartron SI 1260 Impedance Analyzer and were controlled by using Multi-Stat software. Capacitive CV and impedance measurements were measured under electrochemical diagnostic mode at a constant flow rate of 60 mL min^{-1} of 2.0 M HCl at the

working electrode side and 25 mL min $^{-1}$ of H_2 gas at the other side. CV measurements were taken between 0.0 and 1.0 V vs. RHE at scan rates of 50 and 100 mV s^{-1}. Impedance measurements were obtained over a frequency range of 100 kHz to 0.1 Hz using a DC bias potential of 0 V vs open circuit voltage (OCV).

Potential stair step measurements were taken from 0.2 to 1.2 V vs. RHE with stair steps of 5 mV and a dwell time of 0.5 s. Unless otherwise noted, potentiostatic and galvanostatic holds were taken at a cell potential of 0.7 V and/or 0.5 A, respectively for a specific time. A 0.2 M CuCl in a 2.0 M HCl liquid electrolyte was used as the anolyte solution and deionized water was used as the catholyte solution. Both the anolyte and catholyte were continuously purged with N_2 at a flow rate of 60 mL min^{-1} during the electrochemical measurements.

2.6 Copper Analysis

2.6.1 Spectroscopic Method-Atomic Absorption Spectroscopy (AAS)

Copper diffusion samples were examined by a fast sequential multi elements flame atomic absorption spectroscopy (FAAS) featured with 4 lamps positions and auto selection of the lamp, Varian FS 240. For the flame, acetylene and air were used as a fuel and oxidant, respectively. A single element copper Hollow Cathode lamp (HCL) was used as a light source. In addition the FAAS was fully controlled by SpectraAA software.

2.6.2 Electrochemical Methods

Electrochemical methods were used to analyze and evaluate the copper in the catholyte and anolyte solutions. These methods were used because of their availability and simplicity. The

catholyte and anolyte solutions were sampled and measured before the beginning and after finishing the Cu-Cl full cell electrolysis.

2.6.2.1 Ultramicroelectrode Measurements

UME CV measurements were recorded using Pine Instruments Wave Driver potentiostat which was controlled by using Aftermath software in 2.0 M HCl with a silver/silver chloride (Ag/AgCl) reference electrode with porous Teflon tip (CHI 111), a Pt wire as a counter electrode (CHI115), and a 25 μm Pt disc working electrode (CHI 108), all from CH Instruments, as shown in Fig. 2.9. Calibration measurements were first performed with solutions consisting of total concentration of 0.2 M of CuCl and $CuCl_2$. The weight percentage of both CuCl and $CuCl_2$ was varying from 0 to 100. CV measurements were recorded from -0.18 to 1.0 V vs. Ag/AgCl at 25 mV s^{-1} at an ambient temperature and under nitrogen gas. The working electrode was polished by 0.05 μm alumina powder. The values of anodic and cathodic current were used to construct a calibration curves for Cu(I) and Cu(II), respectively. The catholyte solution was then measured using the same procedure and the result was evaluated by comparing the anodic and cathodic current with the standard calibration curves.

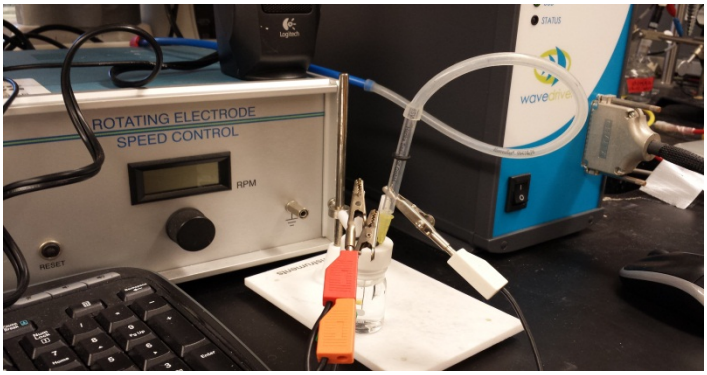

Fig. 2.9: Three-electrode cell set up using UMEs and Pine Instruments Wave Driver potentiostat under N_2 and at ambient temperature using 25 µm Pt disc working electrode, a silver/silver chloride (Ag/AgCl) reference electrode, and a Pt wire as a counter electrode.

2.6.2.2 Differential Pulse Anodic Stripping Voltammetry (DPASV)

DPASV measurements were recorded using a three-electrode technique with the same set up as in the UMEs CV and the same equipment. The applied deposition potential was -1.0 V vs. Ag/AgCl (E° = 0.197 V vs. SHE) for 3 min., after which a stripping potential sweep was performed from -500 to +500 mV. In addition, a differential pulse of 100 ms was used with 1 mV increment and the value of pre-pulse width and poste-pulse width was 1 ms. Different concentrations of copper solution were prepared as standard solutions. Concentrations of 1, 2, 5, and 10 ppm of Cu were prepared in 2.0 M HCl solution and measured by DPASV. A calibration curve was constructed between the current versus the copper's concentration. The catholyte solutions were then evaluated by the same technique and their Cu values were found from the calibration curve.

Chapter 3

Study of PolyPyrrole Composite Membranes

This chapter focuses on the characterization of prepared Ppy composite membranes and compares them with the pristine Nafion membranes. The characterization includes FTIR spectroscopy and thermogravimetric analysis (TGA). A solution of 0.2 M pyrrole in DI and a 30 % solution H_2O_2 were used as a monomer and an oxidizing agent, respectively, in the preparation unless otherwise stated.

The physical properties of the membranes such as water uptake and ion exchange capacity (IEC) were examined. Furthermore, the proton conductivity and methanol and copper diffusion were determined. In addition, the effect of different concentrations of pyrrole and different oxidizing agents on the Cu diffusion were investigated. The selectivity and relative selectivity of the methanol and Cu permeability were calculated and a relationship between them was constructed.

A Cu-Cl electrolyzer cell was constructed and used to investigate the electrochemical behavior and the performance of the Ppy composite membranes. Furthermore, the influence of membrane physical properties on electrochemical cell performance was investigated.

3.1 FT-IR Characterization

FT-IR spectroscopy was used to confirm the formation of polypyrrole (Ppy) in the composite membranes. Fig. 3.1 shows the spectra of Ppy powder, N115 and the composite membrane N115/Ppy. The two peaks at 793 cm^{-1} and 930 cm^{-1} are related to C-H wagging. The Ppy powder showed a peak at 1300 cm^{-1} attributed to C-N stretching, which was absent in the N115 spectrum. Furthermore, the Ppy powder and composite membrane displayed new characteristic peaks at 1560 and 1708 cm^{-1} corresponding to C=C and C=N, respectively. The presence of a small peak at 3520 cm^{-1} can be interpreted as the N-H stretching peak [88]. The

pristine Nafion membranes had asymmetric and symmetric C-F stretching vibration bands at 1211 and 1153 cm^{-1}, which were present in both samples. A broad band between 3200 and 3600 cm^{-1} and a band at 1630 cm^{-1} can be interpreted by absorbed water. A band for the sulfonate appeared at 1056 cm^{-1} while it was missed in the spectrum of the Ppy powder. Because FTIR-ATR analysis is restricted to the surface of the membranes, we cannot see a noticeable difference between the spectrum of the pristine membrane and the composite [56]. The peaks in the spectrum of the Ppy powder confirmed the formation of the Ppy polymer. Moreover, the data obtained from the ATR FT-IR to characterize the pristine Nafion, the Ppy powder and the composite membrane is in good agreement with the literature findings [48, 88-92].

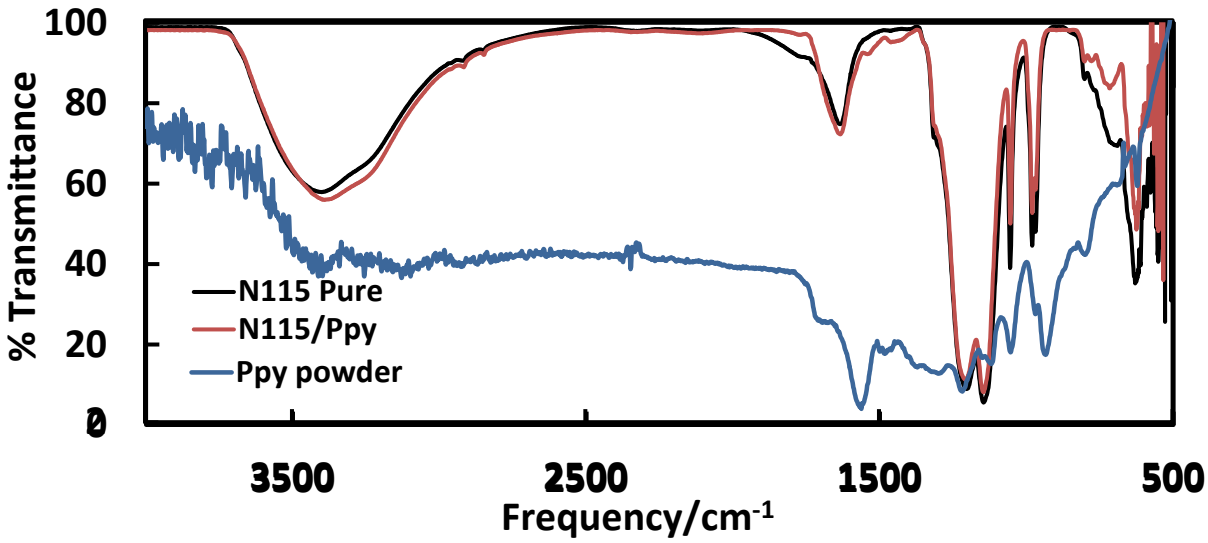

Fig. 3.1: Comparison of the FT-IR spectra obtained for a pure N115 membrane, N115/Ppy membrane, and Ppy powder.

3.2 TGA

Composition and stability of the membranes can be investigated by the TGA technique, as each material has its own specific thermal decomposition profile under a flow of air or inert

gas such as Ar. TGA and differential thermogravimetric (DTG) curves obtained for the Ppy powder, NRE212, N115, N117 and their Ppy composite membranes are shown in Fig. 3.2, to Fig. 3.6. The mass at 200 °C was set as the 100 wt. % values to account for water in the membrane. Fig. 3.2 (a) shows the thermal combustion of the Ppy polymer powder, which completely combusted under air between *ca.* 300-700 °C, whereas the same powder showed more stability under Ar. About 30 % of the mass residue remained when heated up to 1000 °C, as can be seen in Fig 3.3 (a). Acquiring the DTG of the Ppy polymer in argon showed one step decomposition at *ca.* 300 °C which could be attributed to the decomposition of the Ppy as can be seen in Fig. 3.3 (b). Under air, the DTG of the same sample showed two steps combustion at *ca.* 300 and 650 °C. Although the reason for this is not clearly understood, it can be likely explained by the combustion of the Ppy polymer and the monomer.

Fig. 3.4 (a,b) demonstrates that both the NRE212 prestine Nafion membrane and its composite Ppy membrane had a similar decomposition profile, with a loss of sulfonic acid at *ca.* 300 °C, followed by decomposition of the fluoropolymer side chain and backbone occurring above 400 °C into volatile components, leaving some residual mass in the pan above 550 °C. The composite membrane displayed a large decomposition process occurring around 300 °C that most likely originated from the decomposition of Ppy [93], though some contribution due to sulfonic acid decomposition is likely. All decomposition processes in the Nafion/Ppy concluded at 600 °C but a residual mass remained (*ca.* 8.2 – 9.3 wt. %) that is attributed to the carbonization of Ppy. Similar decomposition curves were also observed for both N115 and N117, and their composite membranes, although N115/Ppy showed more Ppy content with respect to the membrane's polymer than N117/Ppy at *ca.* 300 °C, as can be seen in Fig. 3.5 and Fig.3.6.

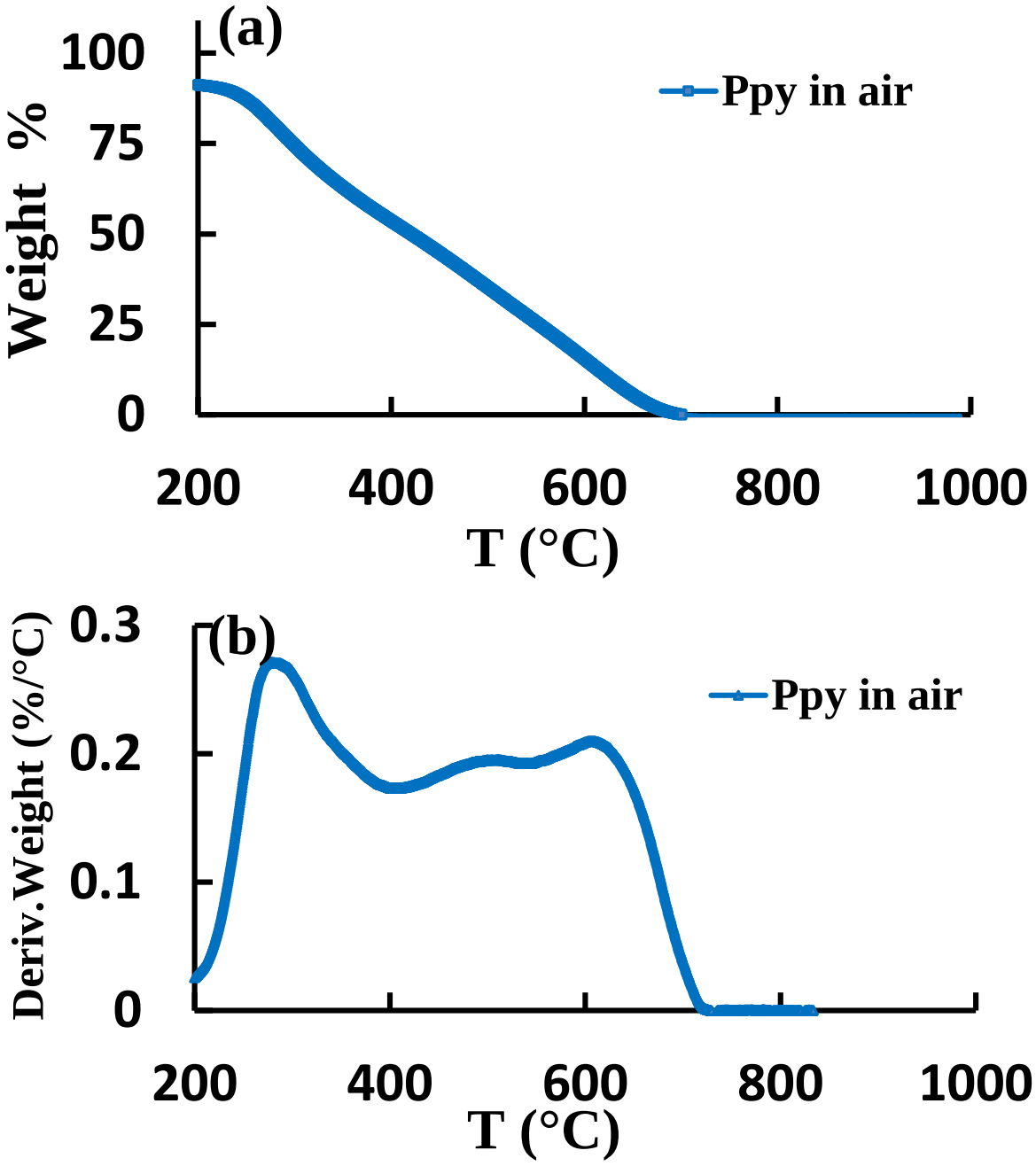

Fig. 3.2: Thermograms obtained for Ppy powder under flowing air. (a) TGA (b) DTG. Ppy sample was heated from room temperature to 1000 ^{0}C with rate 20 ^{0}C/min.

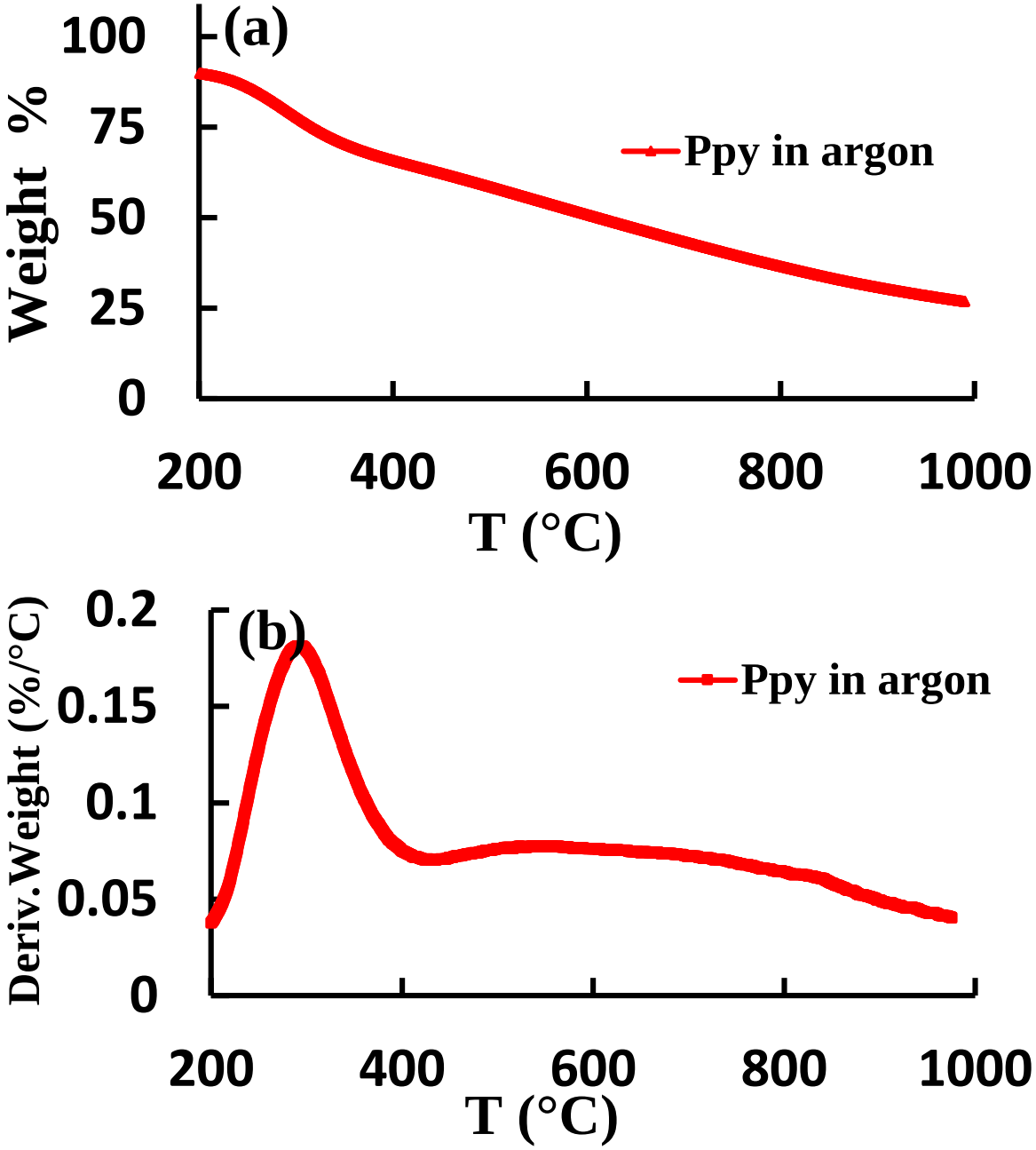

Fig. 3.3: Thermograms obtained for Ppy powder under flowing argon (a) TGA (b) DTG. Ppy sample was heated from room temperature to 1000 ^{0}C with rate 20 ^{0}C/min.

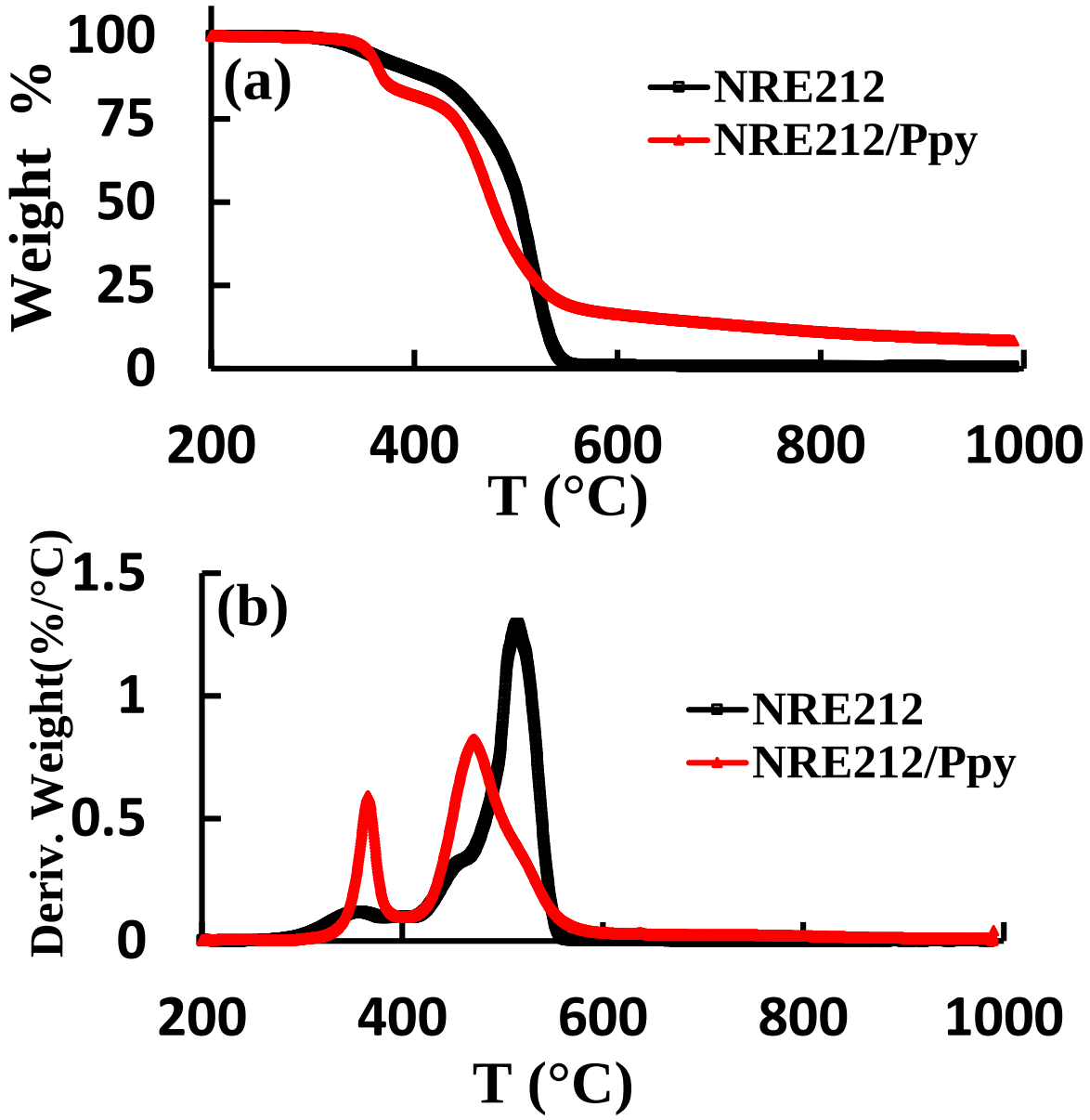

Fig. 3.4: Thermograms obtained for NRE212 and its Ppy composite membrane under flowing argon (a) TGA (b) DTG. Samples were heated from room temperature to 1000 ^{o}C with rate 20 ^{o}C/min.

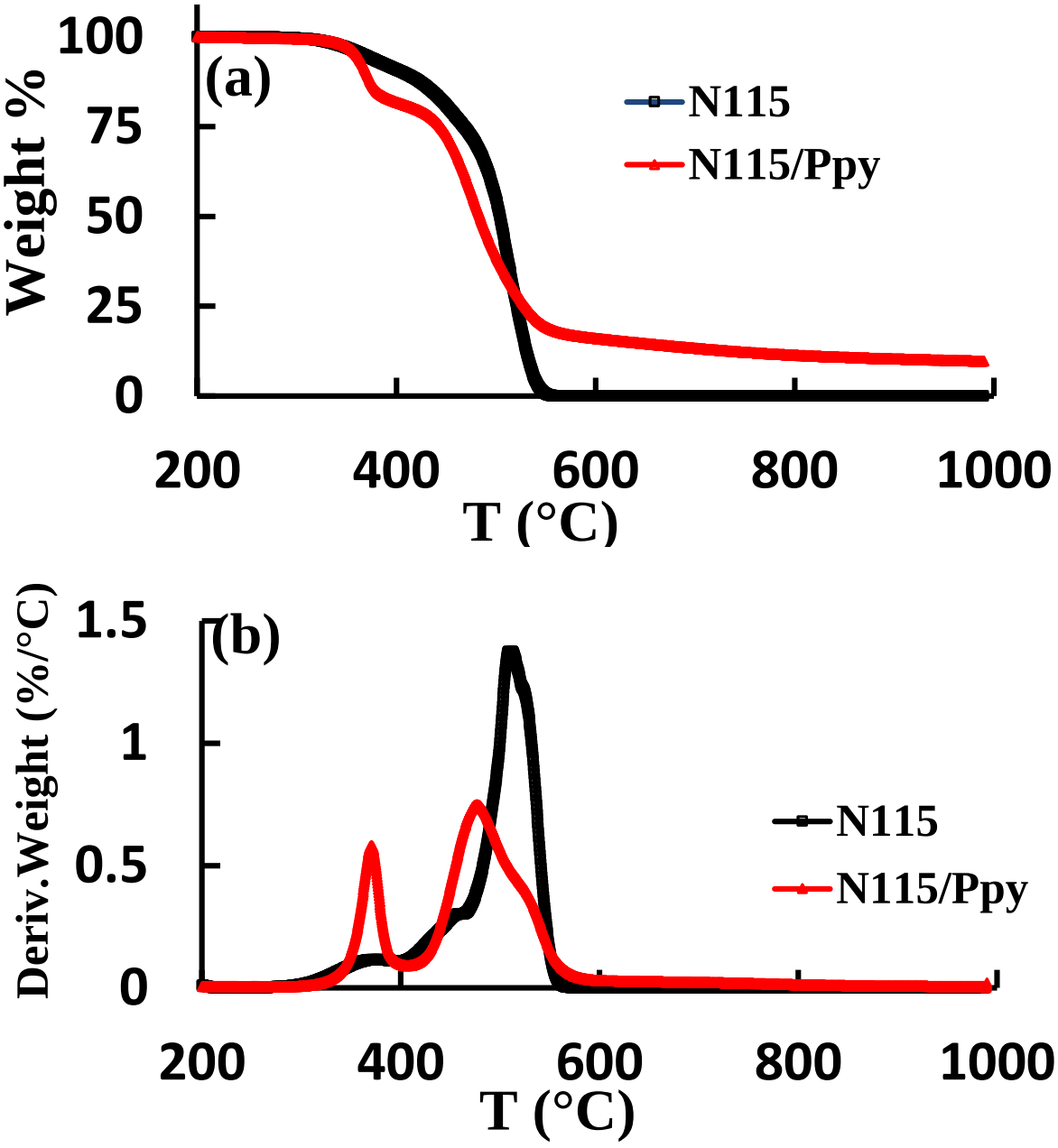

Fig. 3.5: Thermograms obtained for N115 and its Ppy composite membrane under flowing argon (a) TGA (b) DTG. Samples were heated from room temperature to 1000 ^{0}C with rate 20 ^{0}C/min.

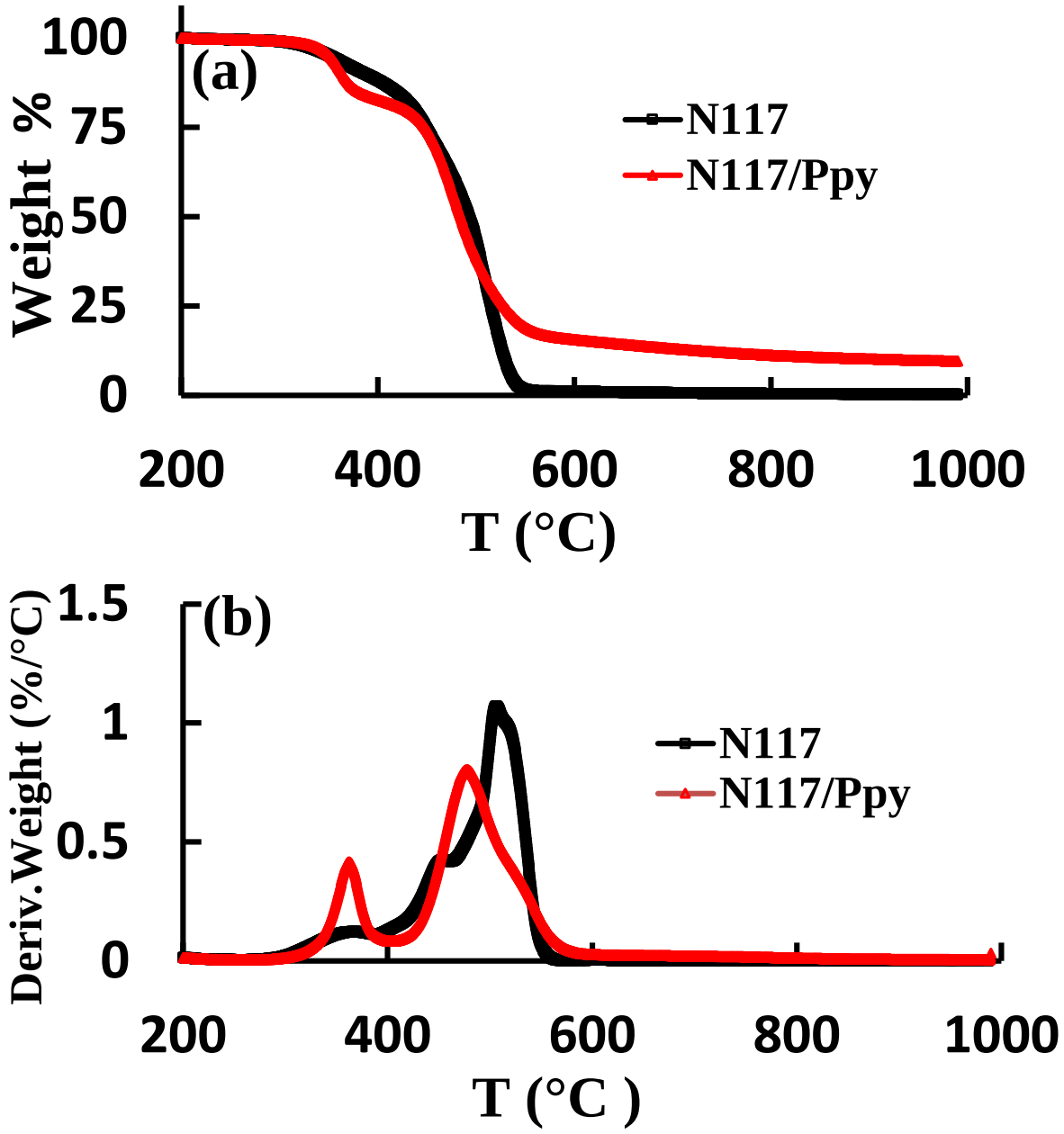

Fig. 3.6: Thermograms obtained for N117 and its Ppy composite membrane under flowing argon (a) TGA (b) DTG. Samples were heated from room temperature to 1000 ^{0}C with rate 20 ^{0}C/min.

3.3 Water Uptake

The water content of a membrane is an important criteria as there is a relationship between the water uptake and the conductivity of a membrane. The conductivity of a membrane increases, as the water uptake increases. The water uptake of the membranes was determined using a weight difference between a hydrated and a vacuum dried membrane according to Equation 2.1 and the values were listed in Table 3.1. The water uptake ranges from 31.53 to 26.80 % for pure Nafion membranes, and from 20.7 to 15.27 % for Nafion Ppy membranes. The *in situ* polymerization of pyrrole produced a significant reduction in water uptake over the unmodified membranes. This reduction in the water uptake is a result of a lower free pore volume available for water due to the presence of the Ppy. This finding is supported by prior reports that observed a decrease in the water uptake linked to decreased porosity in the composite membranes [44].

The water content of the membranes also was determined by Karl Fisher method. The water in the membranes was extracted by methanol and fraction of the extract is injected in the Karl Fisher vessel for analysis. The results showed that there was a water content reduction of ca. 35-72% for Ppy composite membrane compared to pristine membranes. Although the general trend is consistent with the water uptake experiments, the water content from Karl Fisher method had more error from extraction, small sample injection, and methanol volatility.

Table 3.1: The physical properties of different membrane

Membrane	σ_{H^+} S/cm	ASR Ωcm^2	P_{MeOH} (10^{-6}) cm^2/s	P_{Cu} (10^{-6}) cm^2/s	Selectivity $P_{MeOH}(10^6)$ $S.s/cm^3$	Selectivity $P_{cu}(10^6)$ $S.s/cm^3$	IEC(meq/g)	Water uptake %	Rel. Selectivity (Cu)	Rel. Selectivity (Meth.)
NRE212	0.103	0.050	0.953	0.637	0.108	0.161	0.87	31.53		
NRE212/Ppy	0.013	0.382	0.361	0.280	0.037	0.048	0.25	20.70	0.29	0.34
N115	0.091	0.140	1.520	0.686	0.060	0.132	0.88	26.80		
N115/Ppy	0.015	0.852	0.557	0.213	0.027	0.070	0.32	15.56	0.53	0.45
N117	0.097	0.188	1.693	1.050	0.057	0.093	0.89	27.72		
N117/Ppy	0.033	0.555	0.847	0.391	0.039	0.084	0.53	15.27	0.91	0.68

3.4 Ion Exchange Capacity

The sulfonic acid content in the membranes can be estimated by IEC titration. As listed in Table 3.1, the values of the IEC for the unmodified Nafion membranes ranged between 0.87 and 0.89 meq/g which are in good agreement with the literature values [58, 63, 94, 95]. The measured value of IEC for the composite membranes drastically dropped to 0.25, 0.32 and 0.53 meq/g for NRE212/Ppy, N115/Ppy and N117/Ppy, respectively. It is reasonable to assume that this drop in the IEC was due to the presence of positively charged Ppy within the pores, which reduces the number of exchangeable protons. Thicker composite membranes had higher IEC values, indicating a lower wt. % of Ppy in the composites. This conclusion is supported by Fig. 3.7 which shows the relationship between different Nafion composites with different thicknesses and the amount of Ppy extracted from the decomposition peak at *ca*. 370 °C in the TGA. This shows that the thickest membrane N117/Ppy had the lowest amount of Ppy.

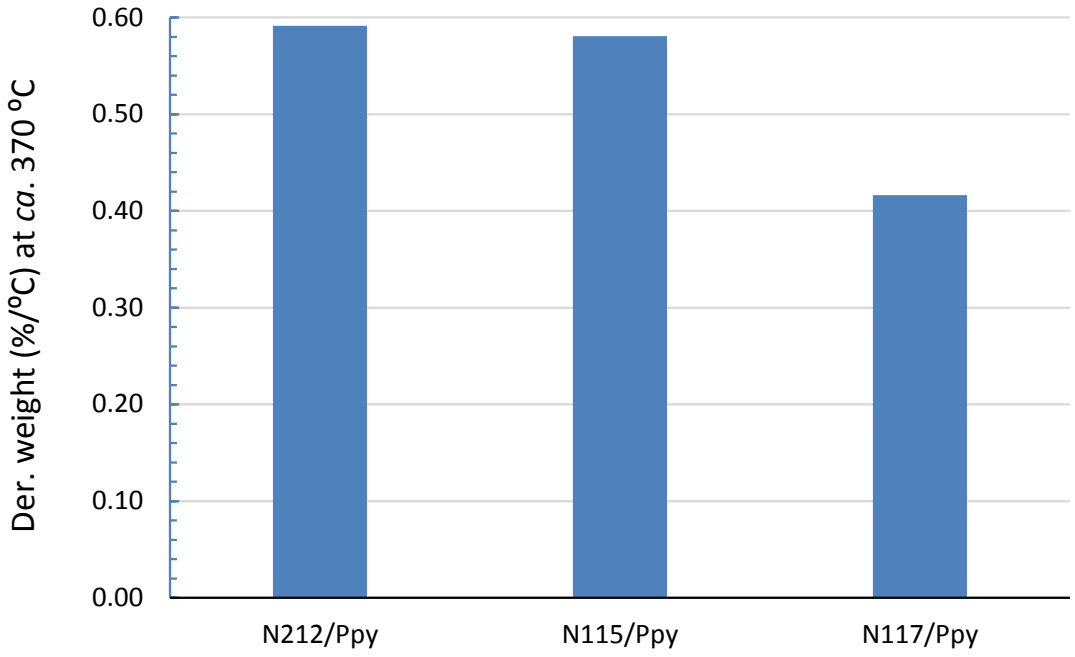

Fig. 3.7: The relationship between different Nafion composite membranes with different thicknesses and the derivative weight at ca. 370 ^{0}C.

3.5 Proton Conductivity

A high proton conductivity membrane is crucial for electrolyzer and fuel cell applications. The proton conductivity represents the free protons that can easily move from one side to another side of a membrane through the continuous nanochannels. Practically, the proton conductivity was measured by EIS for each fully hydrated membrane at 25 °C, which are listed in Table 3.1. The proton conductivity determined for Nafion membranes ranged between 0.091 and 0.103 S/cm which is in excellent agreement with the reports in the literature [32, 96-98]. In general, it is clear that proton conductivities were considerably decreased as the composites were formed. In fact, this could be explained because Ppy fills most of the membrane pores, leaving less volume for the water to present. In addition, much of the Ppy inside the membrane is in its doped (positively charged) form, which has an electrostatic interaction with sulfonic acid groups in the channels of the membrane. This interaction leads to lower proton conductivity since there are acidic sites [99]. The largest reduction occurs for NRE 212 from 0.103 to 0.013 S/cm which can be attributed to the very low thickness of the membrane and which likely contains the highest wt. % Ppy. However, the proton conductivities of the composite membranes measured here are still in a range suitable for full cell applications and are in similar to those reported for Nafion/Ppy composites used for DMFC application [44]. To verify this, the area specific resistance (ASR), which is defined in Eq. 3.1 as the thickness of the membrane over the proton conductivity, that would be predicted for each membrane when assembled in an MEA configuration (i.e. through plane), are listed in Table 3.1.

$$\text{ASR} = \frac{l}{\sigma_{H+}} \qquad \text{Eq. 3.1}$$

where l is the thickness of the membrane in cm and σ_{H+} is the proton conductivity in S/cm.

It is worth noting that thicker composite membranes have higher proton conductivities. This could be explained according to the deep pores available to hold more water which is expected to facilitate the proton conductivity. This can be supported by IEC values for the composite membranes which show a linear correlation with the proton conductivity over this range of study, as can be seen in Fig. 3.8. As expected, since the IEC exhibits the hydrophilic part of the Nafion membrane which is represented by the sulfonic acid groups that are associated with hydronium ions (H_3O^+). Therefore as the IEC increases, the proton conductivity increases accordingly.

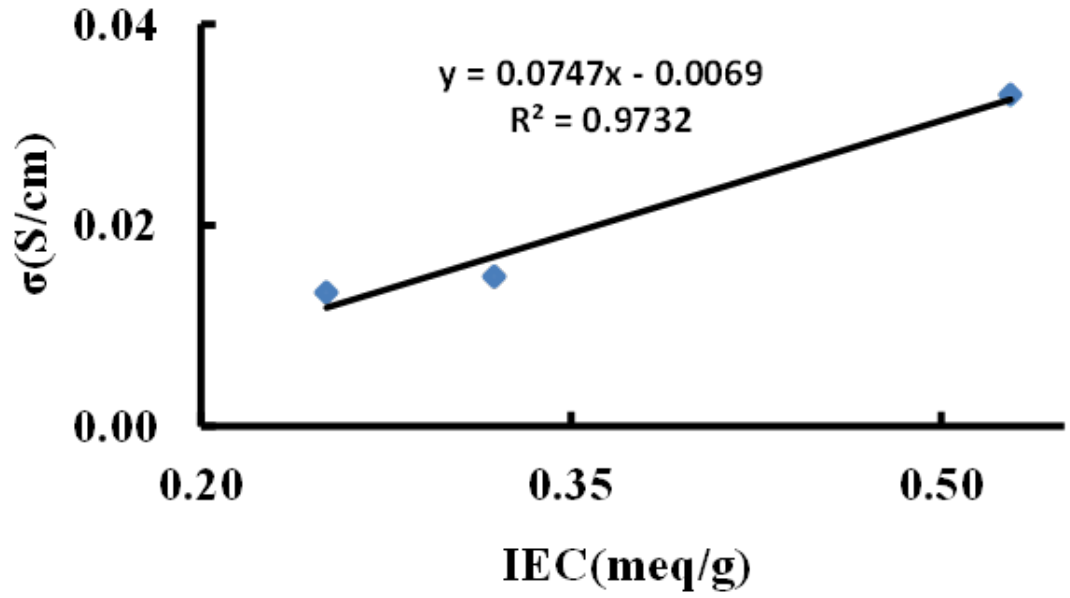

Fig. 3.8: Linear correlation between proton conductivity (σ) and IEC for Ppy composite membranes.

3.6 Methanol and Copper Diffusion

Methanol and Cu diffusion were examined by *ex situ* diffusion cell, which consists of two compartments A and B separated by a membrane. Compartment A contains a known concentration of methanol or Cu solution, while compartment B is known as the diffusion

receiving vessel which is regularly sampled. Fig. 3.9 (a,b) displays plots of methanol and copper concentration profiles in compartment B for two membranes: N115 and N115/Ppy. Similar measurements were obtained for all membranes. From this plot, the permeability of methanol and copper can be determined using Eq. 2.4. The methanol permeability values measured for Nafion membranes were in the range between (0.95-1.69) x 10^{-6} cm^2/s comparable with those reported in the literature [98, 100]. Fig. 3.9 (c,d) shows methanol permeability and copper permeability for all membranes, respectively. As predicted and seen in Fig. 3.9 (c), N115 and N117 had very similar methanol permeability values, since they were made by identical chemical process. However, NRE 212 had a lower methanol permeability as a consequence of the presence of capping groups in its structure to enhance stability [101]. The same trend was observed for the copper permeability, as shown in Fig. 3.9 (d). The composite membranes demonstrated a significant reduction in methanol and copper permeability over their unmodified counterpart *ca.* (50-63 %) and (56-69 %) reduction, respectively.

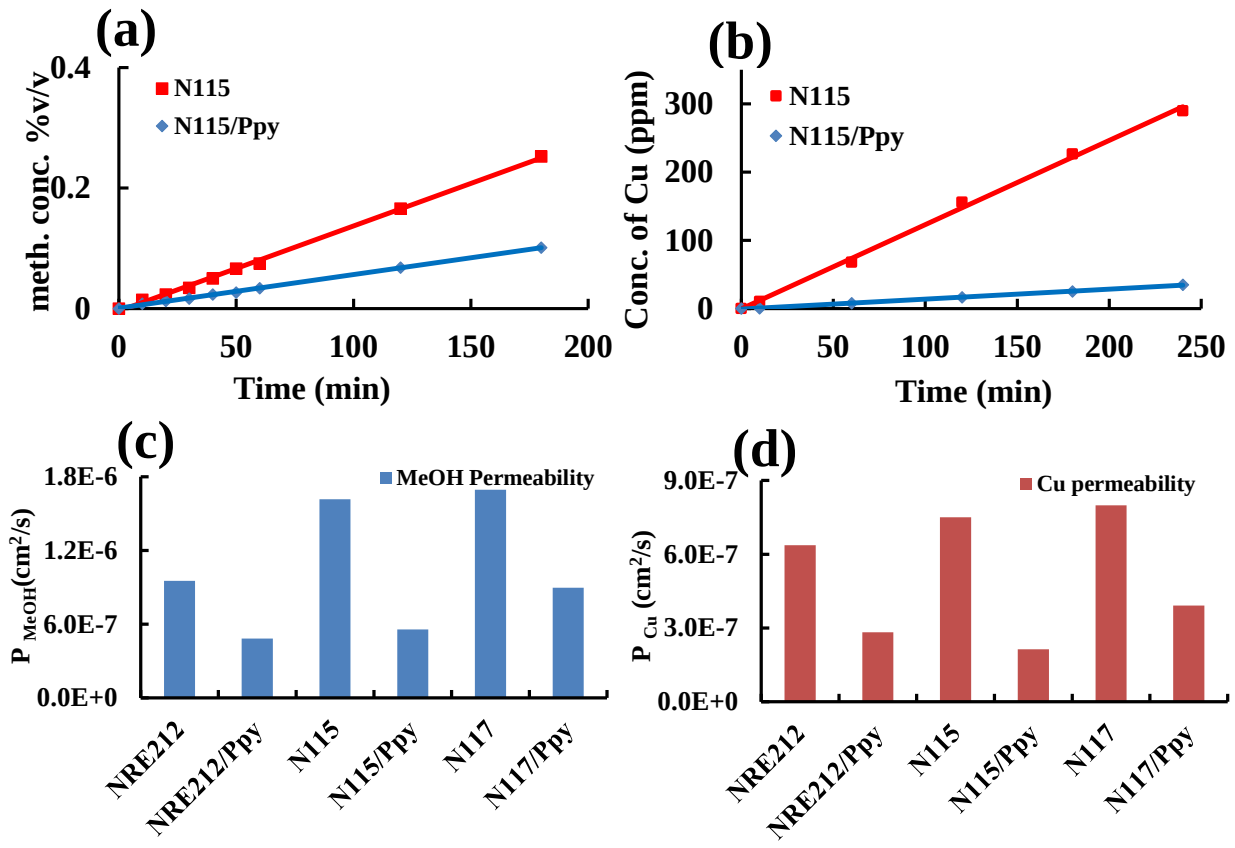

Fig. 3.9: The transport rate of (a) methanol and (b) Cu through pure Nafion N115 and N115/Ppy composite membranes. (c) and (d) are column graphs of the transport rate of methanol and Cu, respectively, for both pristine Nafion and composite membranes. This study has been conducted in an *ex situ* diffusion cell using 1.0 M methanol aqueous solution or acidic $CuSO_4$ aqueous solution in compartment A and deionized water or 1.0 M HCl in the other, at room temperature.

3.7 Influence of Ppy Concentration and Different Oxidizing Agents on Permeability

The synthetic conditions could have a significant influence on the amount of PPy incorporated into composite membranes. To examine this, composite membranes were prepared using different concentration of pyrrole and/or different oxidizing agents. Fig. 3.10 (a) displays the rate of Cu diffusion through a series of composite membranes prepared from solutions with different concentrations of pyrrole. As expected, the rate of copper diffusion decreased with

increasing pyrrole concentration. Furthermore, Fig. 3.10 (b) demonstrates that using either 30 % H_2O_2 or 0.1 M $FeCl_3$ solution as an oxidant in the preparation of Ppy produced almost the same reduction in the rate of copper diffusion. In addition, in a separate experiment, we found that changing the solvent of the diffusion solution in compartment A and B from 1.0 M HCl to DI water significantly reduced the copper diffusion rate for both pristine Nafion and composites membranes, as shown in Table 3.2. It is likely that the high Cu permeation in the HCl solution is due to the formation of neutral $CuCl_2$ (aq) species, which can easily permeate the membranes. In addition, the effect was more pronounced for the pristine membranes compared to the Ppy composite membranes. This finding can be explained by the fact that the pores of the composite membranes were filled with the Ppy polymer which was rigid compared to the pores of the pristine membrane which were filled with movable molecules of water.

Table 3.2: The effect of changing the solvent in the diffusion cell from 1.0 M HCl to DI water.

membrane	diffusion solvent	$P.Cu^{2+}(cm^2/s)x10^{-6}$
N115	1.0M HCl	0.75
N115	H_2O	0.25
N115/Ppy	1.0M HCl	0.21
N115/Ppy	H_2O	0.09
N117	1.0M HCl	0.80
N117	H_2O	0.24
N117/Ppy	1.0M HCl	0.39
N117/Ppy	H_2O	0.15

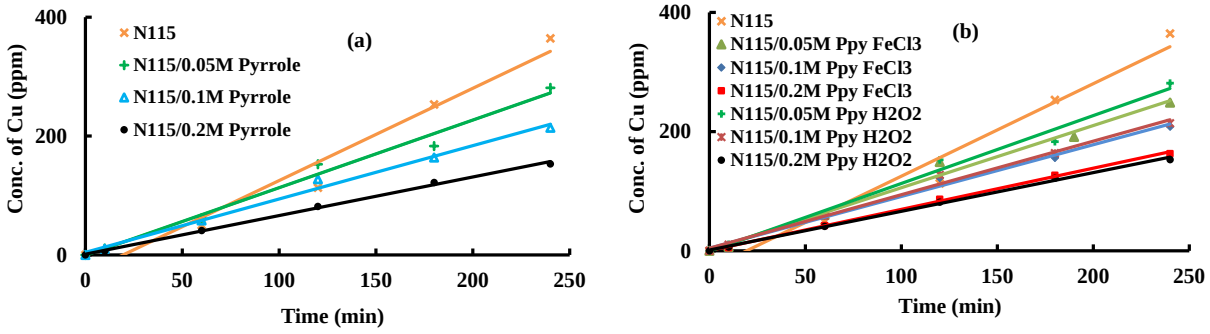

Fig. 3.10: (a) The rate of Cu transport through Nafion/Ppy composite membranes prepared using different pyrrole concentrations, (b) the impact of different oxidizing agents.

Selectivity (α) is defined as the ratio of fluxes of protons (proton conductivity-desired) to the fluxes of methanol (methanol permeability-undesired) or copper (Cu permeability - undesired) according to Eq. 3.2 [42, 98].

$$\alpha_{MeOH} = \frac{\sigma_{H+}}{P_{MeOH}} ; \qquad \alpha_{Cu} = \frac{\sigma_{H+}}{P_{Cu}} \qquad Eq. 3.2$$

where σ_{H+} is the proton conductivity and P_{MeOH} and P_{Cu} are methanol and Cu permeability, respectively.

A membrane with high selectivity is required for an efficient PEMFC and Cu-Cl electrolysis cell. This can be achieved by maintaining high proton conductivity and low permeability of methanol and/or Cu. The proton conductivity of the membrane and the permeability are affected by many factors which are not easy to control. These factors include the diffusion coefficient and the concentration of protons, the diffusion coefficient and the concentration of methanol, and the partition coefficient of methanol in the membrane.

Table 3.1 shows that the selectivity, of both methanol and Cu, was the highest for pristine membranes compared to the composite membranes and this can be attributed to the lower proton conductivity of the composite membranes. NRE212 shows the highest methanol and Cu selectivity compared to N115 and N117 due to low methanol and Cu permeability. However, N117/Ppy demonstrates the highest methanol and Cu selectivity values compared to other composite membranes. This can be explained by the high proton conductivity of N117/Ppy. It is worth noting that N115/Ppy had the lowest Cu permeability amongst modified and unmodified membranes.

Relative selectivity is defined as the ratio of the selectivity of the composite membrane to the pristine membrane according to Eq. 3.3 [102].

$$Relative\ Selectivity = \frac{\alpha_{composite}}{\alpha_{pristine}} \qquad Eq. 3.3$$

where $\alpha_{composite}$ and $\alpha_{pristine}$ are the relative selectivity of the composite and pristine membrane, respectively. Values for each membrane are listed in Table 3.1. It can be concluded that the relative methanol selectivity increases as the thickness of the membrane increases. It is likely that a membrane with high relative selectivity ensures superior performance. As expected, the same is true for the copper relative selectivity.

The relationship between the relative selectivity of copper and the relative selectivity of methanol for each composite membrane is shown in Fig. 3.11 (a,b). The relative selectivity, of both methanol and Cu, linearly increased from the thinnest, NRE/Ppy, to the thickest, N117/Ppy, membrane. There is a clear linear relationship between both relative selectivities which means that relative methanol permeability is an excellent predictor of relative Cu permeability. Thus, it may be reasonable to assume that the same relationship should hold true for the numerous membranes reported in the literature with reduced methanol permeability targeted at DMFC operation. Thus, any further promising DMFC membrane materials could also be evaluated for CuCl/HCl electrolysis.

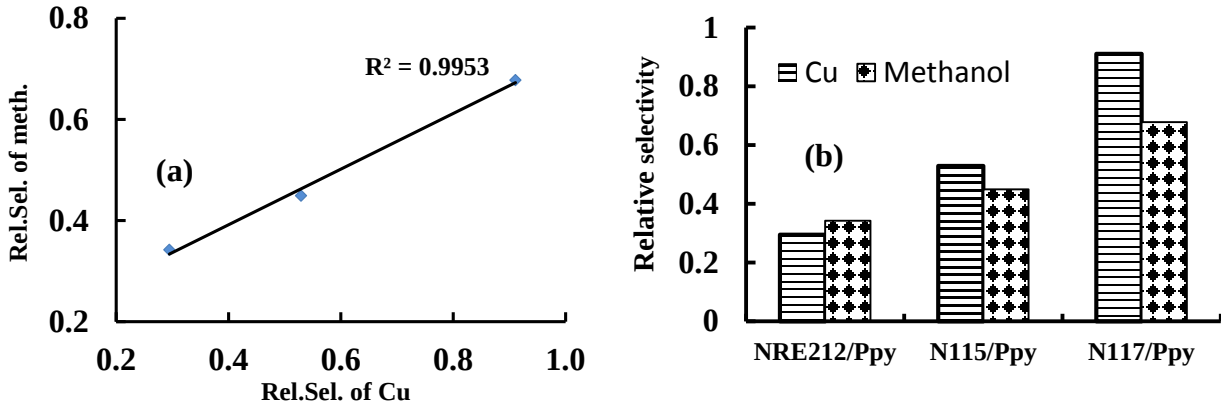

Fig. 3.11: (a) The relationship between relative selectivity of methanol to the relative selectivity of Cu, (b) Relationship between the relative selectivity of methanol and Cu as a function of composite membranes to pure Nafion.

3.8 Full Cell Electrochemical Characterization Results

Since both N115/Ppy and N117/Ppy membranes showed high Cu and methanol relative selectivity compared to NRE212/Ppy membrane, we have chosen to further test them in full cell Cu-Cl electrolyzer. During this test, cyclic voltammetry (CV), electrochemical impedance spectroscopy (EIS), Stair step polarization, potentiostatic and galvanostatic electrolysis testing were performed. The polarization curve, allow us to evaluate the performance of the membrane in the full cell. Fig. 3.12 shows typical polarization curves of the full cell electrolysis obtained with a pure N115 membrane and its composites for day 1 and 3 at a potential range from 0 to 1.2 V. The data is shown using the cell potential, E, and also the IR-corrected cell potential, $E_{corrected}$. IR-correction was performed so that the effect of ohmic resistance within cell is not present. Fig. 3.12 (b) shows that the response current of the composite membrane N115 was less than the pristine membrane. The onset polarization potential typically occurred around 0.4-0.5 V with no mass transport limitation. Fig. 3.12 shows that the polarization curves for the Nafion N115/Ppy composite were more stable during the three working days of testing the membranes, while the polarization curves for the pure Nafion N115 membrane showed a sizable shift in the onset potential on the 3rd day. Although the polarization curve of the pristine Nafion showed a higher current response and a steeper increase in the current compared to the Ppy composite membrane even after IR correction of the data, the Ppy composite not surprisingly showed lower Cu permeability, as shown in the CV experiment and as visually proved by inspecting the MEA as shown in the photos in the Fig. 3.15.

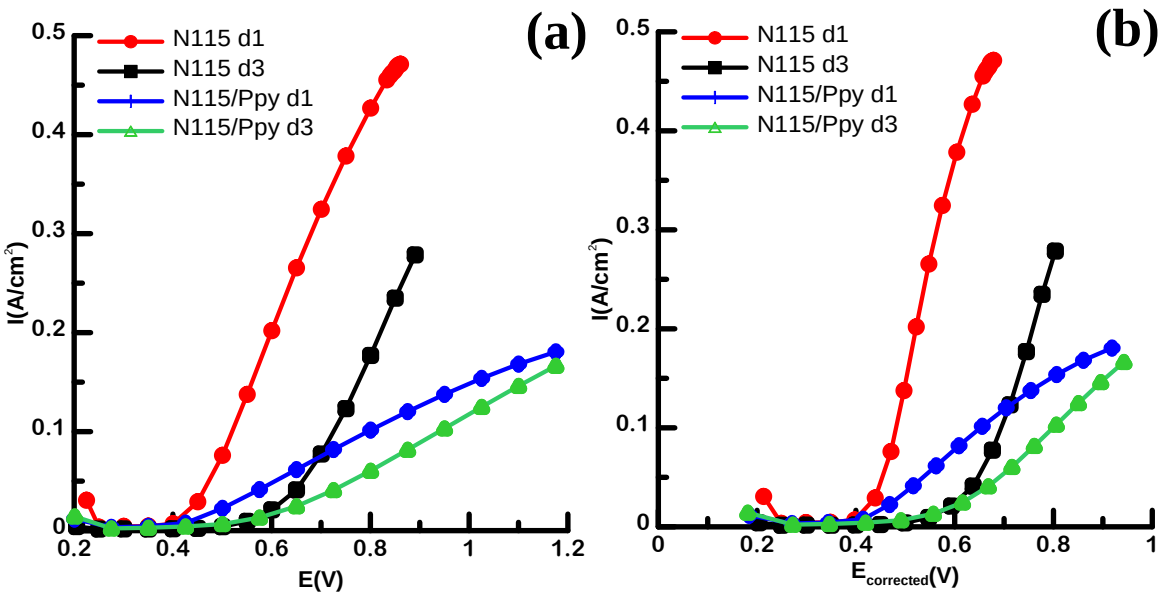

Fig. 3.12: Full cell polarization curves for the electrolysis of CuCl/HCl solution for pure Nafion membrane N115 and its Ppy composite membrane after certain working days (abbreviated d). Measurements were performed at 25.0 ^{0}C with 0.2 M CuCl in 2.0 M HCl flowing at the anode, and deionized water flowing at the cathode under nitrogen atmosphere.

One unique feature of our test station is the ability to quickly purge the anolyte and catholyte with water and a 2 M HCl solution consecutively. In our case, HCl 2.0 M was used to flow in the anode side and H_2 gas in the cathode side. This enables the diagnostic electrochemical measurements such as CV and EIS to be made so that we can assess the health of the MEA. In CV measurements, the working electrode potential is increased linearly versus time. As soon as the potential reaches the maximum set point, the potential of the working electrode is reversed again to reach the initial potential. A standard voltammogram includes the current at the working electrode versus the applied potential. We employed this technique to trace any copper deposition during the Cu-Cl electrolysis. Fig. 3.13 (a,b) displays the CVs obtained using MEAs made with pure Nafion membranes and their composites. The CVs showed that when pure Nafion 115 membrane was used, an oxidation peak appeared at *ca.* 0.4 V on the

2nd and 3rd day, likely due to copper deposits in the MEA. These peaks were absent for MEAs made with the Ppy composite membranes, even after seven days of operation. The same result was observed for N117 and its Ppy composite membrane, as can be seen in Fig. 3.14 (a,b). The deposition of copper on the pure membranes was also confirmed through visual inspection of the MEA, as shown in Fig. 3.15 (a,b). In contrast, the photographs of the composite membranes verify the absence of any Cu deposition, as shown in Fig. 3.15 (c,d).

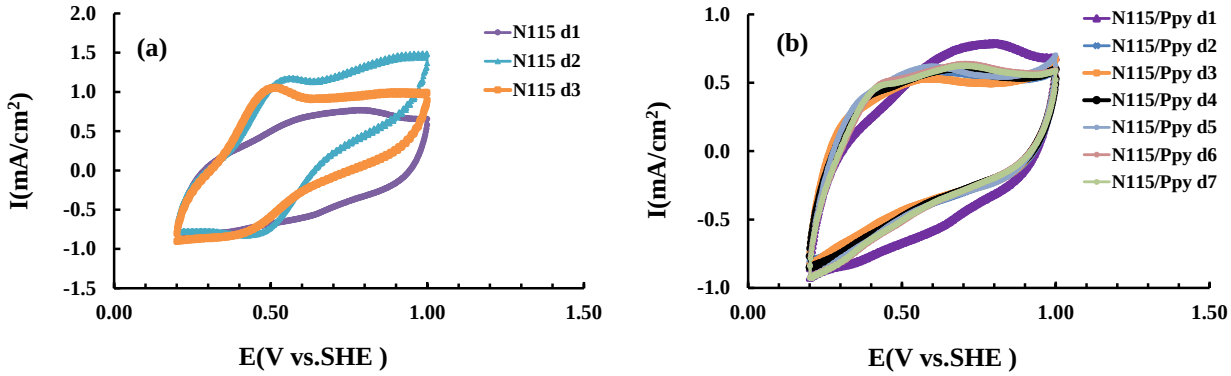

Fig. 3.13: Diagnostic mode full cell CV for pure Nafion N115 membrane and its Ppy composite membrane after certain working days (abbreviated d). Measurements were taken at a sweep rate of 50 mV s^{-1} at 25.0 °C with 2.0 M HCl flowing in the left side of the cell at 60 mL min^{-1} and H_2 flowing in the right side at 25 mL min^{-1}.

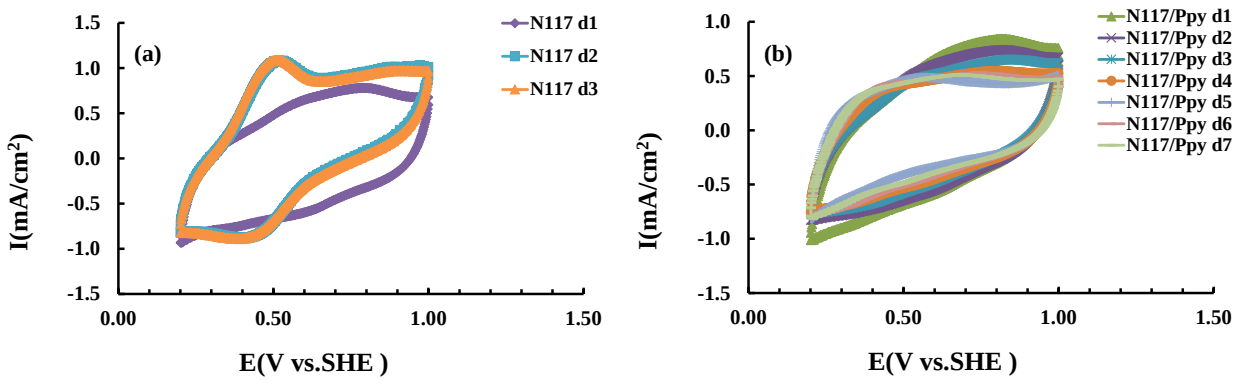

Fig. 3.14: Diagnostic mode full cell CV for pure Nafion N117 membrane and its Ppy composite membrane after certain working days (abbreviated d). Measurements were taken at a sweep rate of 50 mV s^{-1} at 25.0 °C with 2.0 M HCl flowing in the left side of the cell at 60 mL min^{-1} and H_2 flowing in the right side at 25 mL min^{-1}.

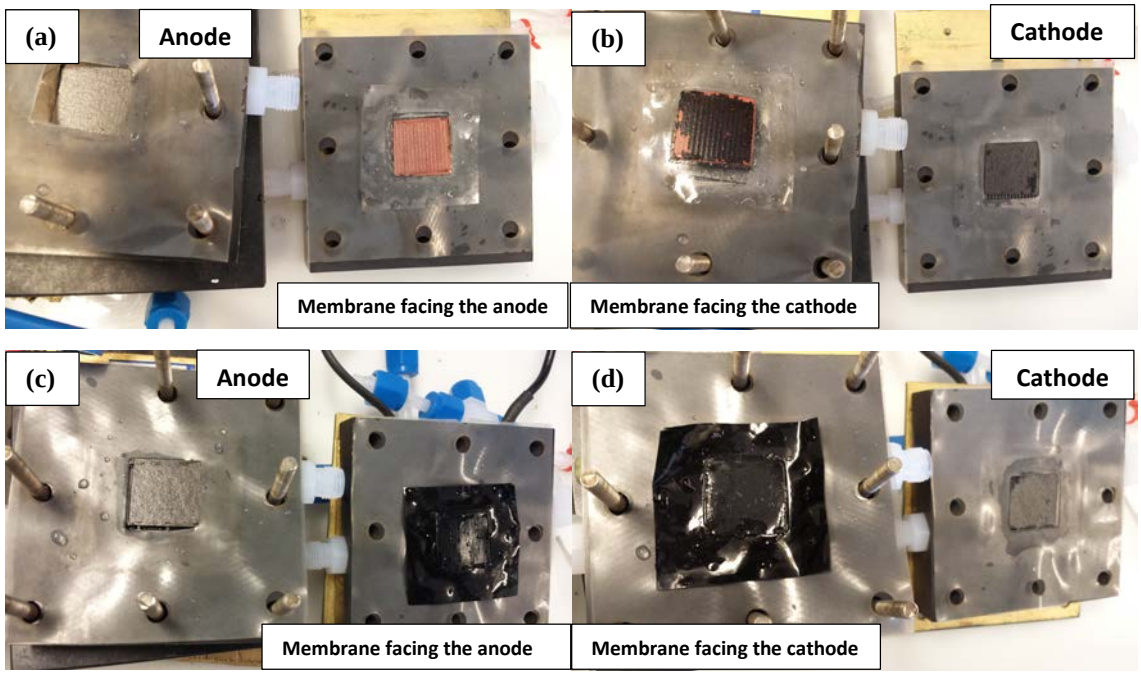

Fig. 3.15: Pictures of the Cu deposition after a few days of Cu-Cl electrolysis. (a,b) the anode and cathode sides for the Nafion 115 membrane after three working days. (c,d) The anode and cathode side for N115/Ppy membrane after seven working days.

3.9 Summary

The *in situ* polymerization of pyrrole changed the physical properties of the Nafion membranes. The Ppy filled the pores of the Nafion membranes and this affected the physical properties such as water uptake, IEC and conductivity. A Large reduction in water content was observed for the composite membranes as the Ppy occupied the void volume, expelling the water molecules. As a result, the proton conductivity was also reduced as fewer water molecules were available in the pores to transport the protons. Moreover, the IEC of the composites was reduced because of the positively charged Ppy chains were attracted to the negatively charged sulfonate groups leaving them with less exchangeable protons. Our aim was focused on blocking the Cu species from passing through the membranes by filling the pores with Ppy polymer. However, all these negative side effects of reducing the values of water content, IEC and conductivity were unavoidable to achieve our target.

The permeability of methanol and Cu was determined by an *ex situ* diffusion cell. The produced Ppy Nafion composite membranes showed lower methanol and Cu permeability compared to the pristine Nafion membranes. Furthermore, we found that there was a relationship between the methanol and Cu permeability. Therefore, as the methanol permeability decreased, the Cu permeability also decreased. In addition, there was a linear relationship between the relative selectivity of methanol and Cu which allows us to predict the Cu permeability from the methanol permeability.

Examining the MEAs that contain these membranes in the CuCl/HCl electrolyzer surprisingly showed that the Ppy composite membranes had lower performance. For example, the polarization curves of the Ppy composite membranes showed a lower current response even after the data was IR-corrected. However, the CV and the visual pictures of the MEAs for Ppy

membranes showed no sign of Cu deposition. These discrepancies in the results will be investigated later in chapter 4, by measuring the Faradic current efficiency of these membranes.

Chapter 4

Study of Polyaniline Composite Membranes

This chapter focuses on the characterization of prepared polyaniline (PANI) composite membranes and compares them with the pristine Nafion membranes. The characterization includes FTIR and UV-Vis spectroscopy. Thermogravimetric analysis (TGA) and scanning electron microscopy (SEM) will be used to examine the degradation and morphology of the modified membranes. Different concentrations of aniline solutions from 0.01-2.0 M were used as monomer's concentration. While three oxidizing agents: Ferric chloride, ammonium persulphate (APS), and hydrogen peroxide solutions were used for polymerization.

The physical properties of the membranes such as water uptake and ion exchange capacity (IEC) were examined. Furthermore, the proton conductivity and copper diffusion were determined and the selectivity of Cu permeability was calculated. High selectivity was pursued as it could represent a highly efficient membrane for CuCl/HCl electrolysis.

A Cu-Cl electrolyzer was utilized to investigate the electrochemical behavior and the performance of the PANI composite membranes. Many electrochemical methods were used for this purpose but polarization, potentiostatic, and cyclic voltammograms (CVs) are discussed in detail here.

Faradic current efficiency was measured for some promising modified membranes and compared with pristine Nafion membranes. In this method, the hydrogen produced at the cathode in the electrolysis cell, is collected and measured under the influence of a fixed current.

4.1 Characterization

The *in situ* chemical polymerization of aniline with Nafion membranes formed green to dark violet colored membranes. This change in colour indicates modification of the Nafion membranes. Different methods of characterization were used to identify the new composite membranes. UV-visible, FT-IR and TGA were used to indicate the presence of PANI in the composite membranes by comparing them with the pristine membranes.

4.1.1 FT-IR Spectroscopy

Fig. 4.1 (a,b) shows the FT-IR spectra of the N115, N115 PANI APS 24 c, N115 PANI H_2O_2 24 c and N115 PANI $FeCl_3$ 24 c. The composite membranes spectra differ from the pristine membrane due to the formation of the PANI polymer. Although the peaks were weak due to the location of the polymerization either within the membrane or on the surface, a peak corresponding to the N-H stretching bond was observed around 3300 cm^{-1}. The most characteristic peaks of the PANI actually appeared at 1530 and 1580 cm^{-1} which corresponds to benzenoid and quinoid stretching modes, respectively. The PANI composite membranes spectra show that the peak ratio of quinoid to benzenoid is almost 1 to 1 which suggests the formation of an emeraldine structure [63, 64, 103]. Since the peak at *ca.* 1700 cm^{-1} is due to the hydronium ions, it is clearly present in the unmodified Nafion membrane while it is absent or very weak in the composite membranes due to exchanging protons with the positive anilinium ions [63]. Fig. 4.1 (b) shows the enlargement spectra from 900-1100 cm^{-1}. The interactions between the sulfonate groups and the positively charged groups in PANI can be predicted from the symmetric stretching band of the sulfonate at around 1057 cm^{-1} for the pristine Nafion membrane. A shift in the sulfonate band towards lower values can be observed when there is a change in the ionic

environment. As can be seen from Fig. 4.1 (b), the sulfonate band shifts from 1057 to 1054 cm^{-1} for the PANI composite membranes. This shift could be explained by the interactions between the large groups of anilinium ion with the sulfonate groups, which caused the frequency of the S-O bond in the composite membranes to be shifted to a lower value compared to the pristine Nafion membrane [63].

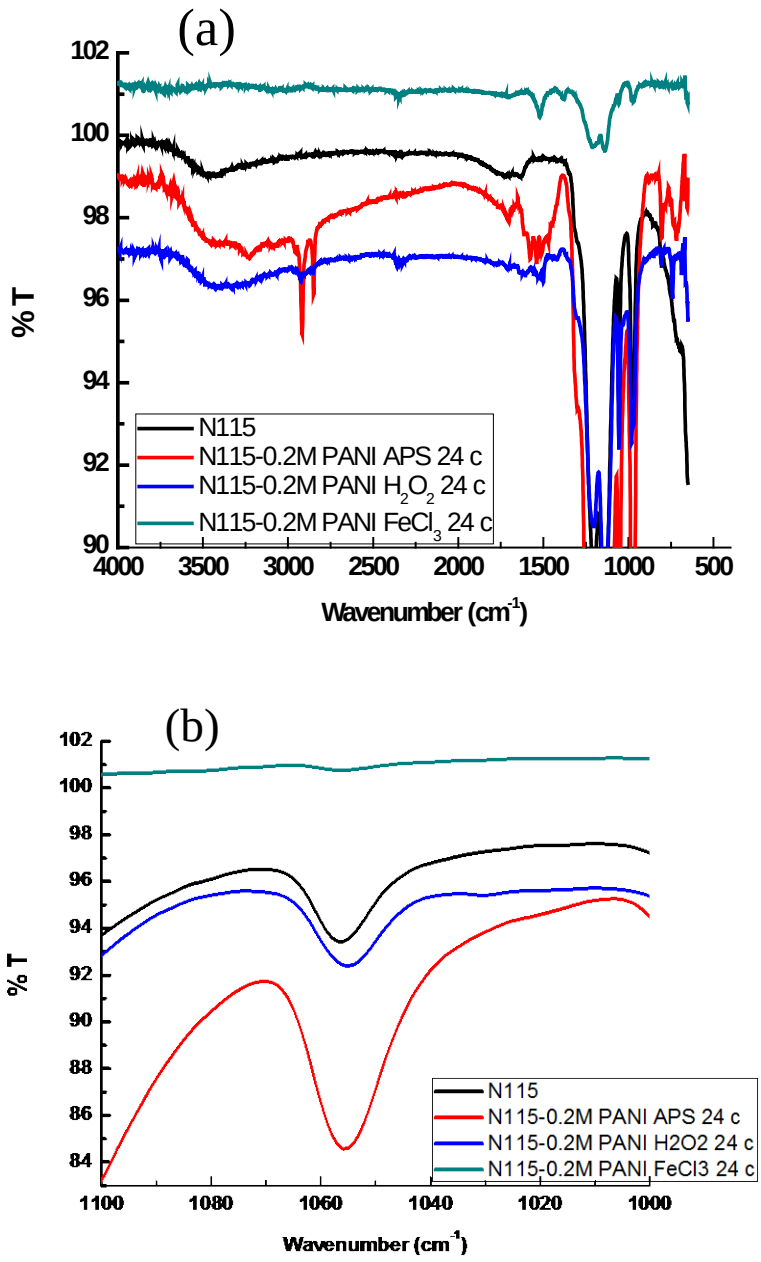

Fig. 4.1: ATR FTIR spectra of N115, N115 PANI APS 24 c, N115 PANI H_2O_2 24 c and N115 PANI $FeCl_3$ 24 c (a) spectral range 400-4000 cm^{-1} (b) spectral range 900-1100 cm^{-1}.

4.1.2 UV-Vis Spectroscopy

UV-Vis spectroscopy was used to identify the formation of PANI and its different oxidation forms. As can be seen from Fig. 4.2, there are three structural forms for the PANI; fully reduced-leucomeraldine, 50 % oxidized-emeraldine and fully oxidized-pernigraniline. Many literature reports has shown that each form of PANI has a characteristic UV-Vis spectra [51, 52, 79, 104, 105]. Fig. 4.3 shows the UV-Vis spectra of N115 PANI APS, N115 PANI H_2O_2, and N115 PANI $FeCl_3$. Peaks appeared in the ranges 380-390 nm and 720-830 nm. Furthermore, the peak at *ca.* 380-390 nm can be attributed to the π-π* transition in the benzene rings. The peak at around 720-830 nm is ascribed to π-polaron transition formed at the nitrogen oxidized atoms of PANI. This peak for both N115 PANI H_2O_2, and N115 PANI $FeCl_3$ membranes was red shifted (800-830 nm) compared to N115 PANI APS (730 nm) which means lower energy bands for both N115 PANI H_2O_2, and N115 PANI $FeCl_3$. These lower energy bands could represent higher conductivity which supports the formation of the 50 % oxidized-emeraldine structure. On the contrary, N115 PANI APS showed a peak at around 720 nm which has higher energy and lower conductivity than the other two composite membranes. It can be concluded that N115 PANI APS has a fully reduced form of PANI or a mixture of oxidation forms of PANI.

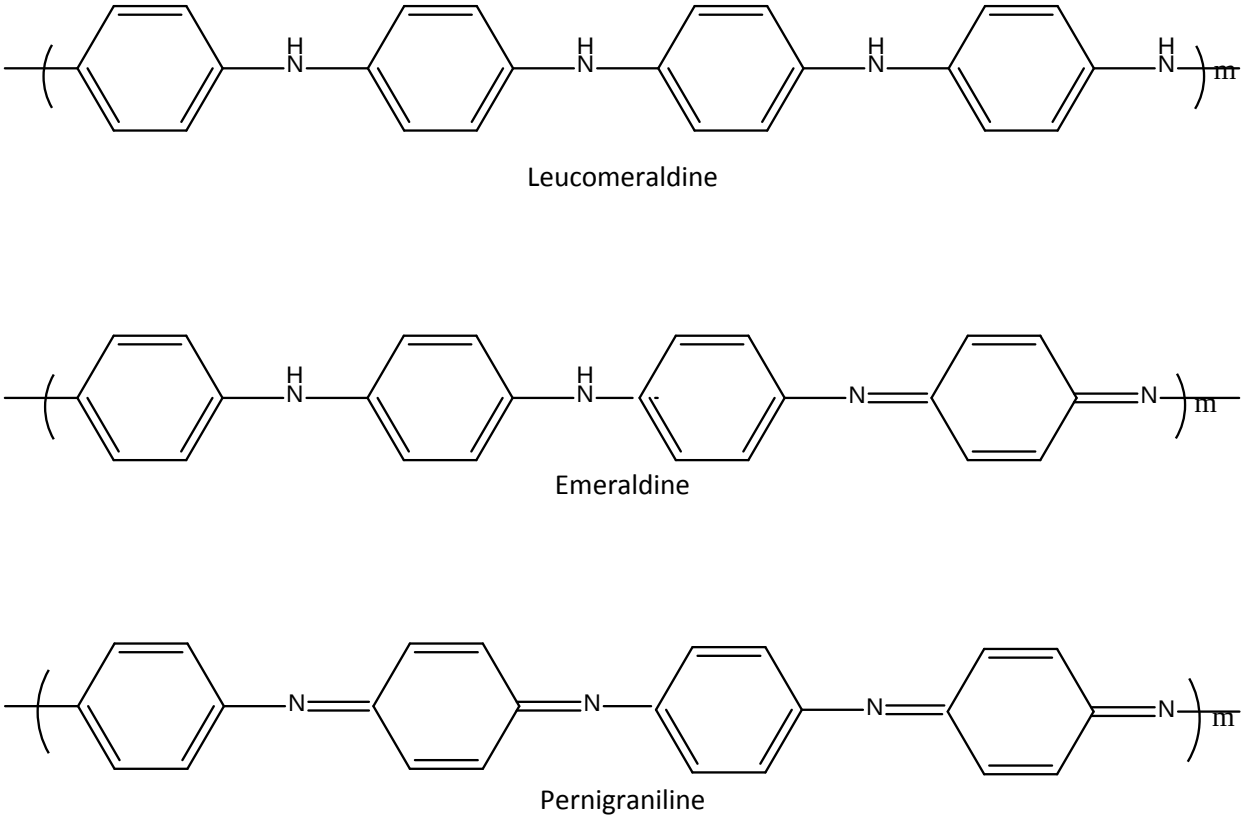

Fig. 4.2: Structure of different oxidation forms of PANI.

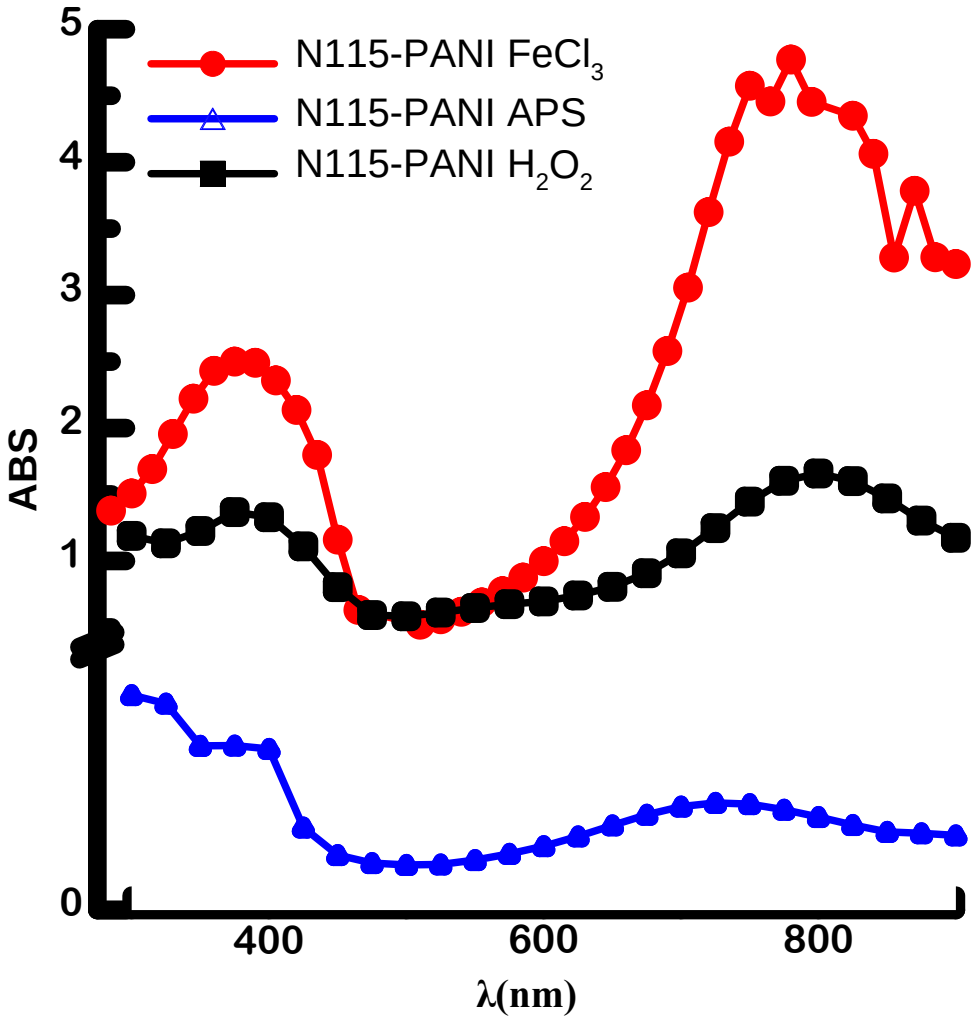

Fig. 4.3: UV-Vis spectra of N115/PANI APS, N115/PANI H_2O_2, and N115/PANI $FeCl_3$ from 300-900 nm.

4.1.3 Thermogravimetric Analysis

TGA and differential thermogravimetric (DTG) measurements were employed to investigate the thermal stability and thermal properties of N115-PANI composite membranes. Measurements were taken under two different environments; flowing air or flowing argon. A small amount of composite membranes was heated from room temperature to 1000 °C at a rate

of 10 °C min^{-1}. Fig. 4.4 (a,b,c,d) shows the TGA and DTG of N115, N115-PANI APS, N115-PANI H_2O_2, and N115-PANI $FeCl_3$ under both air and argon, respectively. Fig. 4.4 (a) shows that PANI composite membranes are generally more thermally stable than the pristine N115. The peak at *ca.* 340 °C is ascribed to the desulfonation of the hydrophilic part of the membrane which evolved as SO_2 gas. This peak is large for the composite membranes in comparison to the pristine N115 which could be due to the combustion of the organic part of the PANI composite membranes. The same observation has been reported by Jinyan et al. [64]. The peaks in the range of 425-450 °C were attributed to the combustion of the backbone of the Nafion membrane. The pristine and two composite membranes displayed two steps combustion while the N115-PANI $FeCl_3$ showed one step, as well as a small peak which could be attributed to the iron cation atoms confined in the hydrophilic channels of the membrane as ferrous chloride. It seems this peak is related to the combustion of ferrous chloride which resulted from the polymerization using ferric chloride as oxidizing agent. Moreover, Fig. 4.4 (c) shows the degradation of the PANI composite membranes and pristine N115 under a flow of argon. These thermograms are similar to the one obtained under air with the exception of *ca.* 10-15 % mass residue which is thermostable up to 1000 °C for the N115-PANI $FeCl_3$ membrane. Additionally, Fig. 4.4 (d) shows that the DTG under argon has the same range of degradation peaks at 330 °C and 490-500 °C. It is generally noticeable that the combustion peak of the backbone of the polymer in air occurred at lower temperatures compared to the same peak under argon. The thermograms of the PANI composite membranes with their degradation stages are in excellent agreement with the literature findings [63, 64, 106, 107]. From the thermograms, we can conclude that the PANI composite membranes have different degradation patterns and are more thermally stable than the pristine Nafion.

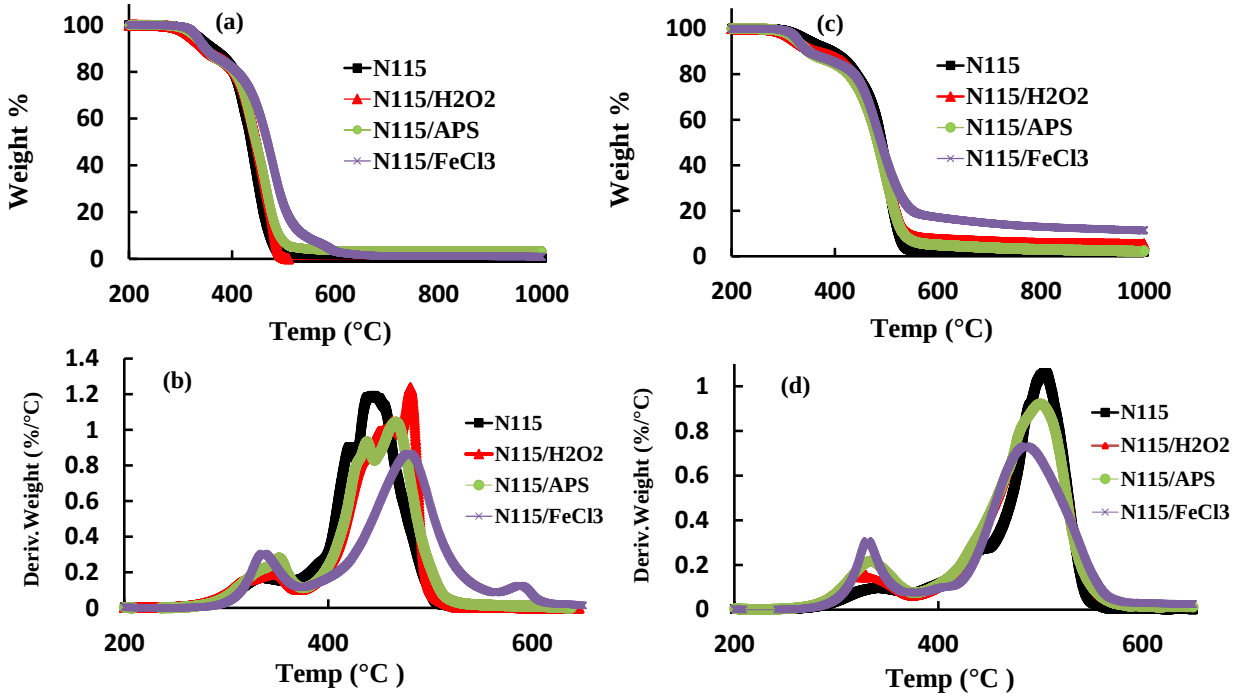

Fig. 4.4: Thermal gravimetric profile of TGA and DTG obtained for PANI composite membranes compared to N115 under flowing (a,b) air and (c,d) argon gas. All tests have been done from room temperature to 1000 ^{0}C with rate 10 ^{0}C min^{-1}.

4.1.4 Scanning Electron Microscopy

SEM micrographs were captured to characterize the properties of the formed PANI within the composite membranes. Different SEM micrographs were taken for different PANI composite membranes prepared by different oxidizing agents. Aniline was oxidized and polymerized by a cation oxidizing agent such as Fe(III), anion APS or neutral H_2O_2. The SEM images in Fig. 4.5 show significant changes in the morphology of the membranes. As can be seen in Fig. 4.5 (a), the morphology of the surface of the pristine membrane shows clear porosity with no particles on the surface, while the N115 -PANI $FeCl_3$ shows smooth surface covered

with the PANI polymer, as can be seen from Fig. 4.5 (b). Polymerization with APS is likely to occur on the surface of the Nafion membrane, as shown in Fig. 4.5 (c). It is believed that negatively charged persulfate is repelled by negative charge of the sulfonic acid groups inside the channels of the membranes pushing the polymerization to the outer surface, whereas the polymerization by hydrogen peroxide occurs inside the channels of the membrane because of the neutral charge of the oxidizing agent. This can be seen in Fig. 4.5 (d) as dispersed particles on the pores of the membrane.

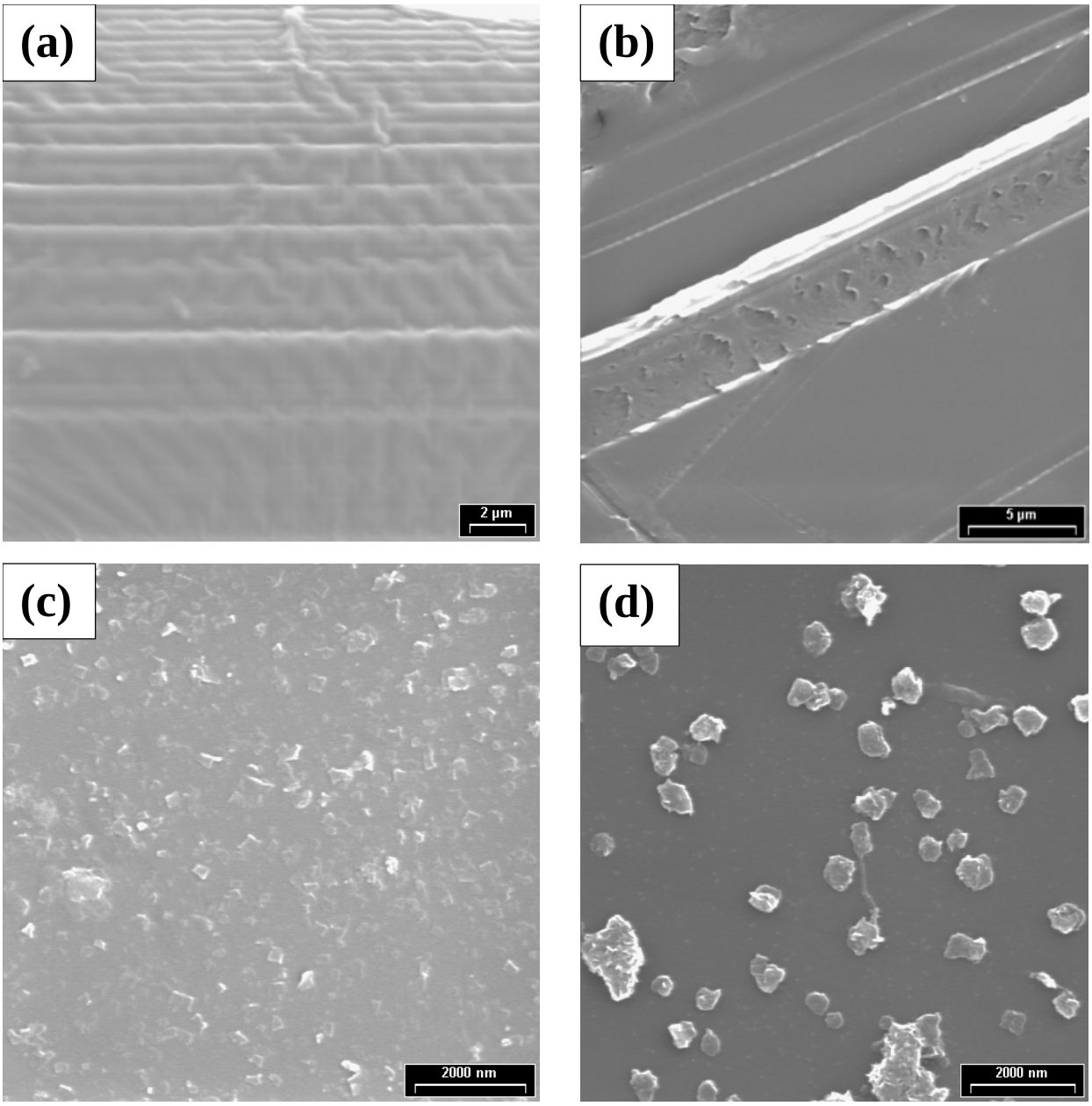

Fig. 4.5: Scanning electron micrographs of the surface of (a) the pristine N115 membrane. (b) N115 PANI $FeCl_3$. (c) N115 PANI APS. (d) N115 PANI H_2O_2.

4.2 Water Uptake Results

The water content of a membrane is an important criteria as there is a relationship between the water uptake and the conductivity of a membrane. The conductivity of a membrane increases, as the water uptake increases. The water uptake of the membranes was determined using a weight difference between a hydrated and a vacuum dried membrane according to Equation 2.1. Table 4.1 shows that the water uptake values were 31.4 and 26.8 % for pristine N117 and 115 membranes, respectively, which are in good agreement with the data from the literature [62, 63, 79]. The water uptake of N115 decreased to 13.7 and 17.1 % for N115-0.2M PANI $FeCl_3$ 24 c and N115-0.5M PANI $FeCl_3$ 24 c, respectively. Furthermore, the water uptake of the N117 membrane decreased to 20.4 and 20.1 % for N117-0.2M PANI $FeCl_3$ 24 c and N117-0.5M PANI $FeCl_3$ 24 c, respectively. This reduction in the water uptake is consistent with our finding and is most likely because the PANI occupies volume within the membrane's pores replacing the water molecules in the membrane's channels. The Ppy composite membranes showed almost similar water uptake values compared to the PANI composite membranes, which means that almost similar Ppy polymer contents formed inside the membranes.

Table 4.1: Water uptake and IEC values of some Nafion PANI composite membranes polymerized by $FeCl_3$ for 24 h compared with pristine and Ppy Nafion membranes.

membrane	% Water uptake	IEC(meq/g)
N115	26.8	0.854
N115-0.2M PANI $FeCl_3$ 24 c	13.7	0.579
N115-0.5M PANI $FeCl_3$ 24 c	17.1	0.543
N115-0.2M Ppy H_2O_2 c	14.0	0.345
N117	31.4	0.847
N117-0.2M PANI $FeCl_3$ 24 c	20.4	0.573
N117-0.5M PANI $FeCl_3$ 24 c	20.1	0.560
N117-0.2M Ppy H_2O_2 c	19.6	0.419

4.3 Ion Exchange Capacity (IEC) Results

Since IEC represents the exchangeable cationic species such as protons (H^+) which interact with the sulfonic groups, the IEC results obtained are used to determine the relative quantity of PANI in the composite membranes. From Eq. 2.2, the calculated IEC values for N115 and N117 pristine membranes are 0.854 and 0.847 meq/g, respectively which are in excellent agreement with the literature values [95]. The IEC values of the PANI modified membranes significantly decreased to *ca.* 0.5 meq/g, as can be seen from Table 4.1. This reduction which is in the range of *ca.* 32-36 % reflects the amount of PANI attached to the sulfonic groups in the membranes. As expected, when PANI chains replaced the H^+ and interacted with the sulfonic groups, the IEC value decreased as fewer protons were available for replacement. These results are supported by Tan et al. [61]. Both PANI composite membranes of N115 and N117 showed almost the same Cu and IEC reduction trend. Furthermore, changing the concentration of aniline from 0.2 M to 0.5 M had a minimal effect on the measured IEC. In

addition, comparing the values of the IEC of the PANI composite membranes with the Ppy composite membranes, we found that Ppy composite membranes had lower IEC values indicating a larger quantity of Ppy in the membrane and less exchangeable protons.

4.4 Proton Conductivity and Diffusion Results

A high proton conductivity membrane is required for electrolyzer and fuel cell applications. The proton conductivity represents the free protons that can move through the membrane. Practically, the proton conductivity was measured by EIS for each fully hydrated membrane at 25 °C. An *ex situ* diffusion cell was employed to determine the methanol and Cu permeability, which consists of two compartments A and B separated by a membrane. Compartment A contains a known concentration of methanol or Cu solution, while compartment B contains a blank solution which is regularly sampled. At the beginning, N115 has been used alone as an example to prepare different PANI composite membranes by using different oxidizing agents; 0.1 M $FeCl_3$ in 1.0 M HCl, 0.2 M aqueous solution of APS, and 30 % H_2O_2. In addition, different concentrations of aniline were used ranging from 0.1 M to 2.0 M in 1.0 M HCl.

Table 4.2 shows the conductivity, Cu permeability and selectivity of N115 PANI prepared by different oxidants for 1 h. Different concentrations of acidic solutions of aniline ranging from 0.1 to 2.0 M were used to prepare PANI composite membranes. As can be seen from Table 4.2, as the concentration of aniline increased, the measured conductivity value decreased. Furthermore, a significant reduction in the proton conductivity values was observed; i.e. *ca.* 98.7, 97.8 and 99.6 % for N115 2.0M PANI APS, N115 2.0M PANI $FeCl_3$ and N115 2.0M PANI H_2O_2, respectively. Clearly, composite membranes polymerized by 30 % H_2O_2 had the lowest values of conductivity, while composite membranes polymerized by $FeCl_3$ had the

highest values of conductivity. It is believed that using $FeCl_3$ as an oxidant for polymerization of aniline enhanced the formation of emeraldine salt which has higher conductivity than emeraldine base.

The copper permeability of these membranes was also determined using the diffusion cell. Table 4.3 shows the copper permeability of different composite membranes. It is clear that as the concentration of aniline in the composite membranes increased, the copper permeability decreased and that could be attributed to more PANI chains occupying volume within the pores and channels of the membrane, preventing the movement of the copper species. Although the capability of these membranes to prevent the copper crossover is not significantly improved compared to the pristine N115, a copper permeability reduction of *ca.* 67, 20 and 26 % was obtained for N115 2.0M PANI APS, N115 2.0M PANI $FeCl_3$ and N115 2.0M PANI H_2O_2, respectively. Since the reduction in the proton conductivity of the composite membranes was greater than the reduction in the copper permeability, the selectivity of the composite membranes seems to be lower than the pristine Nafion membrane. The copper selectivity of the pristine N115 membrane is 1.6×10^5 $S.s.cm^{-3}$ which is significantly larger than the selectivity of all other composite membranes that ranges from 6.1×10^4 to 8.1×10^2 $S.s.cm^{-3}$.

In the first modification experiment of the Nafion with PANI, a 1 h polymerization time was examined. Since this experiment did not lead to any substantial improvement in the copper selectivity, a longer polymerization times were studied. In addition to the 1 h polymerization time, 5 and 24 h were examined. Furthermore, most of the composite membranes were prepared with 0.2 M aniline as the concentrations higher than 0.2 M aniline did not support reducing the copper permeability. Table 4.3 shows the conductivity, permeability and selectivity of the PANI composite membranes prepared by using 0.2 M aniline and polymerized for either 5 or 24 h

using the three different oxidants. The conductivity of composite membranes decreased compared to the pristine membrane. However, there was a discrepancy when 5 or 24 h of polymerization was used. The Cu permeability was substantially reduced for N115 PANI APS 5 and N115 PANI APS 24 to $1.64x10^{-9}$ and $1.82x10^{-10}$ cm^2 s^{-1} compared to N115 which has a copper permeability value of $6.86x10^{-7}$ cm^2 s^{-1}. Since polymerization using APS resulted in the largest reduction in copper permeability, we decided to study this system in more detail.

Table 4.4 shows the conductivity, Cu permeability and selectivity of PANI composite Nafion membranes polymerized by APS for 24 h. N115, N117 and N212 were used to prepare different PANI composite membranes polymerized by APS for 24 h. The three composite membranes showed similar conductivity in the range 0.09- 0.1 S cm^{-1}. The copper permeability reduction was significantly improved for the N117 PANI APS 24 membrane compared to the other composite membranes. Furthermore, the selectivity of N117 0.2M PANI APS 24 is $1.2x10^8$ $S.s.cm^{-3}$ which is higher than the other pristine Nafion and composite membranes, whereas, N212 showed the lowest selectivity compared to others and was excluded from further examination.

Since both N115-0.2M PANI APS 24 and N117-0.2M PANI APS 24 showed very high resistivity when they were examined in the full cell Cu-Cl electrolyzer, lower concentrations of aniline were used to prepare the PANI composite membranes. Thus different concentrations of aniline ranging from 0.01 to 0.2 M were independently utilized to prepare the composite membranes. Table 4.5 shows the conductivity, Cu permeability and selectivity of N115 PANI and N117 PANI polymerized by APS for 24 h and coated with 5 % Nafion solution. N115 and N117 PANI composite membranes, that have been prepared using aniline concentrations, ranging from 0.01-0.075 M, showed almost similar conductivity to their pristine membranes,

whereas higher concentrations showed a reduction in conductivity. For example, the conductivity was reduced from 0.0997 to 0.0839 and 0.0659 S cm^{-1} for N115-0.1M PANI APS 24 c and N115-0.2M PANI APS 24 c, respectively. Furthermore, a similar trend was obtained for N117 composite membranes, as can be seen in Table 4.5. The best value of copper permeability reduction was observed as 4.86×10^{-11} and 3.40×10^{-10} cm^2 s^{-1} for N115-0.1M PANI APS 24 c and N115-0.1M PANI APS 24 c, respectively. A membrane with high proton conductivity and low copper permeability would have high selectivity value and is the preferred membrane to be tested in the Cu-Cl electrolyzer. The lower copper permeability of both N115-0.1M PANI APS 24 c and N117-0.1M PANI APS 24 c resulted in higher selectivity, making them good candidates to be tested in the full Cu-Cl electrolyzer.

Fig. 4.6 (a,b) shows the change in Cu permeability and proton conductivity with the concentration of aniline polymerized for 1h by different oxidants. Fig. 4.6 (a) shows that 1h polymerization is not sufficient to reduce the Cu permeability using these concentrations of aniline regardless of the oxidant used. However, proton conductivity was significantly reduced over all conditions tested, particularly when the concentration of aniline exceeds 0.5 M.

Table 4.2: The conductivity, Cu permeability and selectivity of N115 PANI polymerized by different oxidants for 1 h.

Membrane	Conductivity S/cm	Permeability cm^2/s	Selectivity $S.s/cm^3$
N115	1.09E-01	6.86E-07	1.58E+05
N115 0.1M PANI APS	1.73E-02	6.64E-07	2.60E+04
N115 0.2M PANI APS	1.43E-02	7.39E-07	1.94E+04
N115 0.5M PANI APS	1.31E-02	7.31E-07	1.79E+04
N115 1.0M PANI APS	1.07E-02	8.25E-07	1.30E+04
N115 2.0M PANI APS	1.38E-03	2.24E-07	6.14E+03
N115 0.1M PANI $FeCl_3$	3.65E-02	7.31E-07	5.00E+04
N115 0.2M PANI $FeCl_3$	3.20E-02	6.95E-07	4.60E+04
N115 0.5M PANI $FeCl_3$	2.63E-02	7.15E-07	3.68E+04
N115 1.0M PANI $FeCl_3$	2.53E-02	7.26E-07	3.49E+04
N115 2.0M PANI $FeCl_3$	2.39E-03	5.52E-07	4.32E+03
N115 0.1M PANI H_2O_2	1.71E-02	6.73E-07	2.54E+04
N115 0.2M PANI H_2O_2	1.61E-02	5.86E-07	2.75E+04
N115 0.5M PANI H_2O_2	2.09E-03	6.08E-07	3.44E+03
N115 1.0M PANI H_2O_2	1.62E-03	6.15E-07	2.64E+03
N115 2.0M PANI H_2O_2	4.11E-04	5.05E-07	8.13E+02

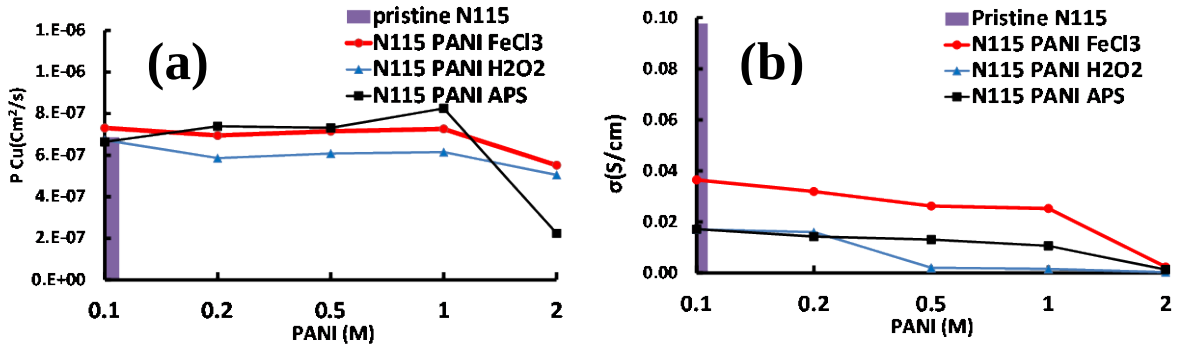

Fig. 4.6: The relationship between (a) the copper permeability (b) the proton conductivity, versus the concentration of PANI by using different oxidizing agents for 1 h polymerization for N115 membrane.

Table 4.3: The conductivity, Cu permeability and selectivity of N115 PANI polymerized by different oxidants for 5 and 24 h.

Membrane	Conductivity S/cm	Permeability cm^2/s	Selectivity $S.s/cm^3$
N115	1.09E-01	6.86E-07	1.58E+05
N115 0.2M PANI APS 5	4.17E-02	1.64E-09	2.54E+07
N115 0.2M PANI APS 24	5.74E-02	1.82E-10	3.15E+08
N115 0.2M PANI $FeCl_3$ 5	4.54E-02	6.44E-07	7.06E+04
N115 0.2M PANI $FeCl_3$ 24	3.22E-02	4.46E-07	7.21E+04
N115 0.2M PANI H_2O_2 5	3.93E-02	7.73E-07	5.08E+04
N115 0.2M PANI H_2O_2 24	7.54E-02	6.96E-07	1.08E+05

Table 4.4: The conductivity, Cu permeability and selectivity of PANI composite Nafion membranes polymerized by APS for 24 h.

Membrane	Conductivity S/cm	Permeability cm^2/s	Selectivity $S.s/cm^3$
N115	1.04E-01	6.86E-07	1.52E+05
N115 0.2M PANI APS 24	9.82E-02	6.92E-07	1.42E+05
N117 0.2M PANI APS 24	8.53E-02	7.00E-10	1.22E+08
N212 0.2M PANI APS 24	9.97E-02	4.96E-06	2.01E+04

Table 4.5: The conductivity, Cu permeability and selectivity of N115 PANI and N117 PANI polymerized by APS for 24 h and coated with 5 % Nafion solution.

Membrane	Conductivity S/cm	Permeability cm^2/s	Selectivity $S.s/cm^3$
N115	9.97E-02	6.86E-07	1.45E+05
N115 0.01M PANI APS 24 c	1.06E-01	7.10E-07	1.49E+05
N115 0.03M PANI APS 24 c	1.05E-01	6.04E-07	1.73E+05
N115 0.05M PANI APS 24 c	1.04E-01	7.50E-07	1.39E+05
N115 0.075M PANI APS 24 c	1.11E-01	5.99E-07	1.86E+05
N115 0.1M PANI APS 24 c	8.39E-02	4.86E-11	1.73E+09
N115 0.2M PANI APS 24 c	6.59E-02	6.92E-07	9.53E+04
N117	1.14E-01	1.05E-06	1.09E+05
N117 0.01M PANI APS 24 c	1.07E-01	7.76E-07	1.38E+05
N117 0.03M PANI APS 24 c	1.25E-01	7.15E-07	1.75E+05
N117 0.05M PANI APS 24 c	1.12E-01	6.90E-07	1.63E+05
N117 0.075M PANI APS 24 c	1.07E-01	6.88E-07	1.55E+05
N117 0.1M PANI APS 24 c	6.95E-02	3.40E-10	2.04E+08
N117 0.2M PANI APS 24 c	7.08E-02	1.53E-09	4.63E+07

Fig. 4.7 (a) shows the relationship between the proton conductivity and the concentration of PANI. It is clear from the graph that the proton conductivity of both N115 and N117 PANI composite membranes was substantially lower when 0.1 and 0.2 M aniline concentrations were used. Composite membranes prepared using aniline concentrations of less than 0.075 M displayed conductivities that were similar values to the pristine Nafion. This could imply that there was insufficient PANI in the membrane to have a significant interaction with the sulfonic groups, leading to minimal disruption of proton conductivity. However, when the aniline concentration is higher, the PANI inside the membrane has a far greater interaction with the sulfonic acid groups, leading to a substantial drop in proton conductivity. Fig. 4.7 (b) shows that a similar trend has been observed for the copper permeability, although a discrepancy was found

for N115-0.2M PANI APS 24 c which showed a shift to a higher permeability for copper species.

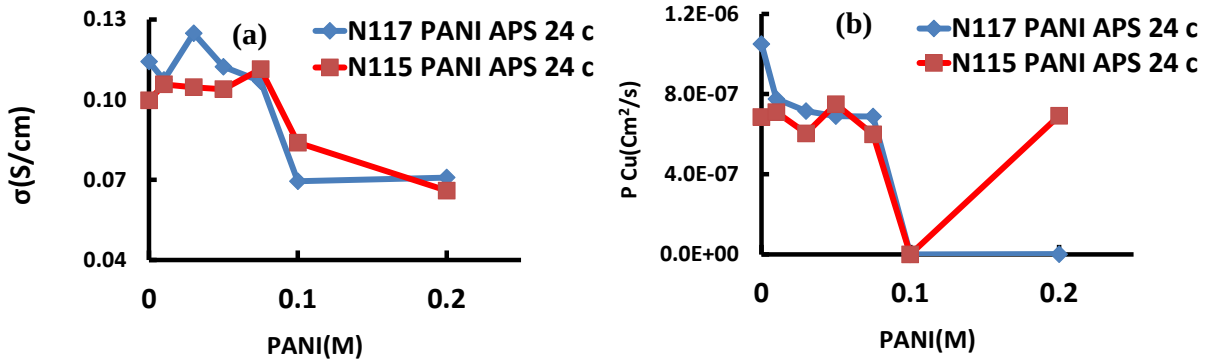

Fig. 4.7: The relationship between (a) the proton conductivity and the concentration of PANI and (b) the copper permeability and the concentration of PANI for both N115 and N117 composite membranes.

A membrane that can maintain its conductivity and show a noticeable reduction in copper permeability is required. Almost all the PANI composite membranes that were prepared failed to meet the selectivity criteria and/or poorly performed in the Cu-Cl electrolyzer due to high resistivity. From previous experiments, PANI composite membranes that used aniline 0.2-0.5 M showed suitable properties. In addition, using $FeCl_3$ as the oxidant was more successful in maintaining of sufficient proton conductivity. Table 4.6 shows the conductivity, Cu permeability and selectivity of N115 PANI and N117 PANI polymerized by $FeCl_3$ for 24 h and coated with 5 % Nafion solution. N115-0.2M PANI $FeCl_3$ 24 h c and N115-0.5M PANI $FeCl_3$ 24 h c showed almost the same conductivity *ca.* 0.024 S cm^{-1}, whereas N115-0.5M PANI $FeCl_3$ 24 h c showed lower permeability than N115-0.2M PANI $FeCl_3$ 24 h c. Therefore, the measured selectivity was 5.60×10^4 and 6.29×10^4 S.s.cm^{-3} for N115-0.2M PANI $FeCl_3$ 24 h c and N115-0.5M PANI

$FeCl_3$ 24 h c, respectively. In comparison, the N115/Ppy H_2O_2 c composite membrane showed lower conductivity; 0.009 S cm^{-1} and lower copper permeability; 9.13×10^{-8} cm^2 s^{-1} and its selectivity was 1.01×10^5 S.s.cm^{-3} which is greater than both the PANI composite membranes and almost similar to N115 pristine membranes. Additionally, N117-0.5M PANI $FeCl_3$ 24 h c showed lower conductivity than N117 0.2M PANI $FeCl_3$ 24 h c as expected as a larger amount of PANI chains replaced protons that are important for conductivity. In comparison, their conductivity was a little higher than the N115 PANI composite membranes but their copper permeability was lower than the N115 PANI composite membranes. Therefore, the selectivity of both N115 and N117 PANI composite membranes resulted in almost similar values. Compared to N117 PANI composite membranes, N117/Ppy H_2O_2 c showed almost 50 % reduction in both proton conductivity and copper permeability, therefore its selectivity was similar to others.

Table 4.6: The conductivity, Cu permeability and selectivity of N115 PANI and N117 PANI polymerized by $FeCl_3$ for 24 h and coated with 5 % Nafion solution. In addition, the pristine N115, N117 and their Ppy composite membranes were added for comparison.

Membrane	Conductivity S/cm	Permeability cm^2/s	Selectivity $S.s/cm^3$
N115	9.78E-02	6.86E-07	1.43E+05
N115 0.2M PANI $FeCl_3$ 24 c	2.35E-02	4.20E-07	5.60E+04
N115 0.5M PANI $FeCl_3$ 24 c	2.37E-02	3.76E-07	6.29E+04
N115 0.2M Ppy H_2O_2 c	9.19E-03	9.13E-08	1.01E+05
N117	1.19E-01	1.05E-06	1.13E+05
N117 0.2M PANI $FeCl_3$ 24 c	3.53E-02	4.94E-07	7.14E+04
N117 0.5M PANI $FeCl_3$ 24 c	2.77E-02	4.78E-07	5.80E+04
N117 0.2M Ppy H_2O_2 c	1.52E-02	1.96E-07	7.77E+04

4.5 Full Cell Electrochemical Characterization Results

4.5.1 Cu-Cl Electrolysis

One of the membranes that showed high selectivity due to a superior high copper reduction was N117-0.2M PANI APS 24 h. After measuring the conductivity and copper permeability, the next step was to evaluate the performance of the membrane in the CuCl/HCl electrolysis cell. As mentioned in the methodology, this membrane was hot pressed with the cathode membrane. After preparing the MEA and assembling the cell, the sample was first analyzed in the electrochemical diagnostic mode, as detailed in Table 2.1. Fig. 4.8 shows the CV obtained for N117-0.2M PANI APS 24 h d1 membrane. The CV showed high resistivity which is resulted from the only variable in this cell; the membrane. Furthermore, Fig. 4.9 shows the polarization curve for the electrolysis of the CuCl/HCl solution for N117-0.2M PANI APS 24 h d1 which supports the CV data. The N117-0.2M PANI APS 24 h membrane polarization curve showed a very low current density response which was about 0.00014 A cm^{-2} at 0.7 V. This high resistivity can be attributed to the PANI chains that replaced the protons attached to the sulfonate groups.

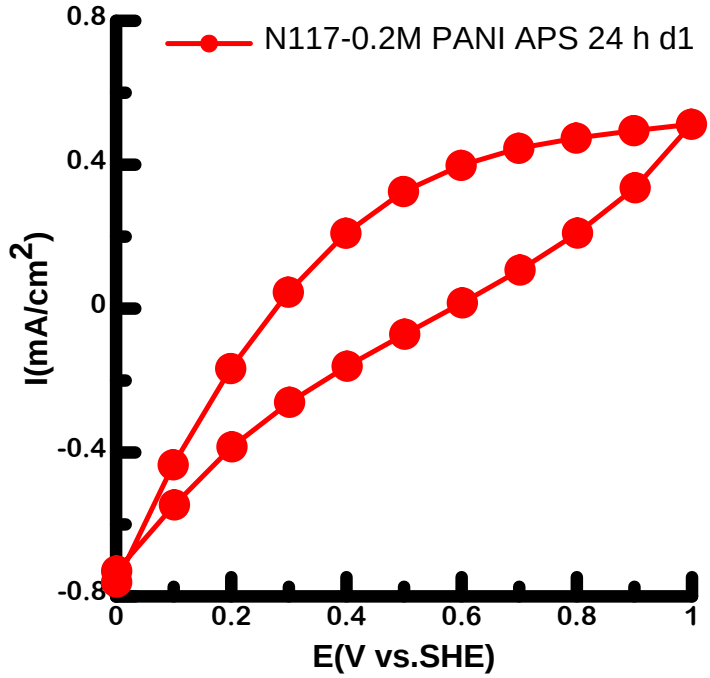

Fig. 4.8: Diagnostic mode full cell CV for N117-0.2M PANI APS 24 h d1 membrane. Measurements were taken at a sweep rate of 50 mV s^{-1} at 25.0 °C with 2.0 M HCl flowing in the left side of the cell at 60 mL min^{-1} and H_2 flowing in the right side at 25 mL min^{-1}.

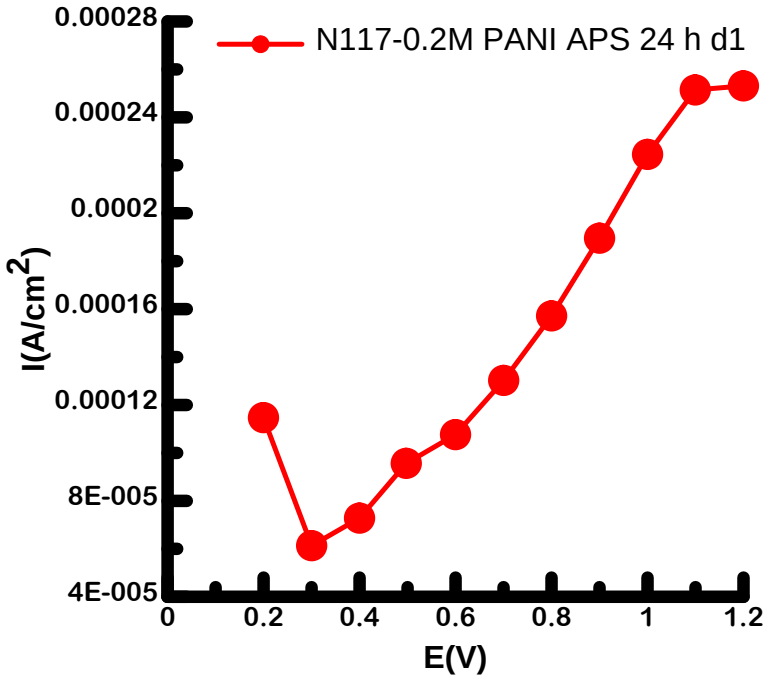

Fig. 4.9: Full cell polarization curve for the electrolysis of CuCl/HCl solution for N117-0.2M PANI APS 24 h d1. A measurement was performed at 25.0 ^{0}C with 0.2 M CuCl in 2.0

M HCl flowing at the anode, and deionized water flowing at the cathode with a rate of 60 mL min^{-1}, under nitrogen atmosphere.

As N117-0.2M PANI APS 24 h showed very high resistivity, a small change on the modification of the membranes has been taken. The membranes were coated with 5 % Nafion solution (abbreviated c) to preserve the surface of the membranes and support the conductivity of the membranes. In another experiment, N115-0.2M PANI APS 24 h c was prepared and tested in the full cell with the same setup and it showed similar high resistivity during the CV and the linear stair step measurements. Other membranes were prepared and those which had lower resistivity were chosen to be tested by the Cu-Cl electrolysis cell. According to the preliminary data, these membranes had high selectivity. Fig. 4.10 (c) shows full cell polarization curves for the electrolysis of the CuCl/HCl solution for the N115/Ppy c membrane for 3 working days (abbreviated d). The polarization curves showed an onset potential around 0.4 V during the three days of Cu-Cl electrolysis. During the first two days the curves looked very similar. However, on the third day the polarization curve showed improved performance. In contrast, the pristine N115 membrane had onset potential of *ca.* 0.4 V on the first day which increased over the second and third days to around 0.6 V, as shown in Fig. 4.10 (a). This instability and onset potential shift can be ascribed to the copper crossover from the anode to the cathode side, which deteriorated the MEA and the cell performance. In addition, two other membranes were tested, N117/Ppy c and N117-0.2M PANI $FeCl_3$ 24 h c. Fig. 4.11 (a) illustrates full cell polarization curves for the electrolysis of the CuCl/HCl solution for the N117/Ppy c membrane for three days. The polarization curves showed onset potential around 0.4 V and fair stability for the three working days. N117-0.2M PANI $FeCl_3$ 24 h c displayed onset potential at 0.4 V for almost the three days but the performance on the first day was better than the other two days, as shown in Fig. 4.11 (c).

Fig. 4.10 (b,d) and Fig. 4.11 (b,d) show the polarization curves with the IR-corrected cell potential. These IR-corrected cell potential curves showed that the performance was improved when the effect of the membrane resistivity was eliminated, particularly for the composite membranes.

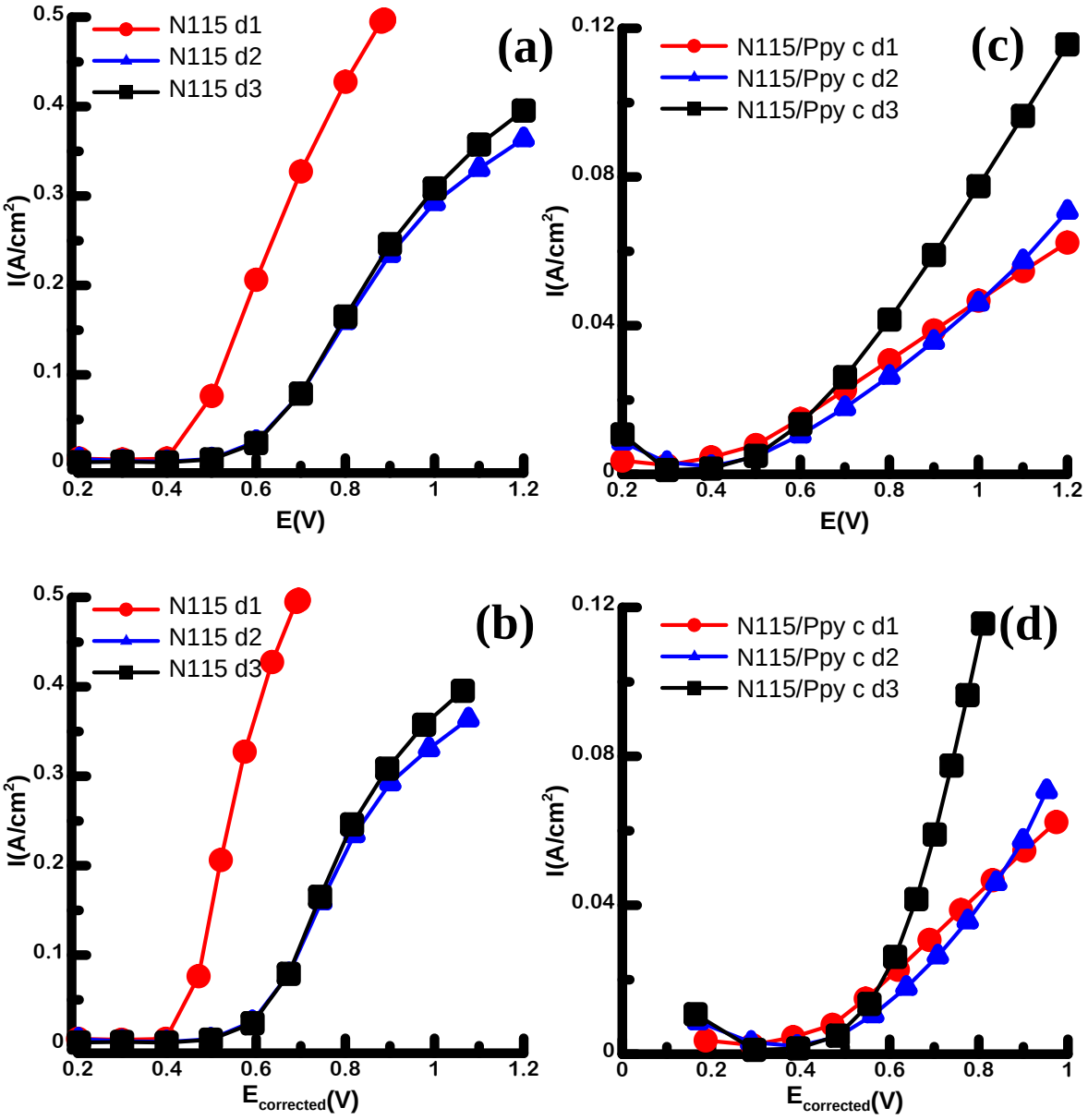

Fig. 4.10: Full cell polarization curves for the electrolysis of CuCl/HCl solution for membranes (a) N115 (b) N115 IR-corrected (c) N115/Ppy c (d) N115/Ppy c IR-corrected, after certain working days (abbreviated d). Measurements were performed at 25.0 ^{0}C with 0.2 M CuCl in 2.0 M HCl flowing at the anode, and deionized water flowing at the cathode, with a rate of 60 mL min^{-1}, under nitrogen atmosphere.

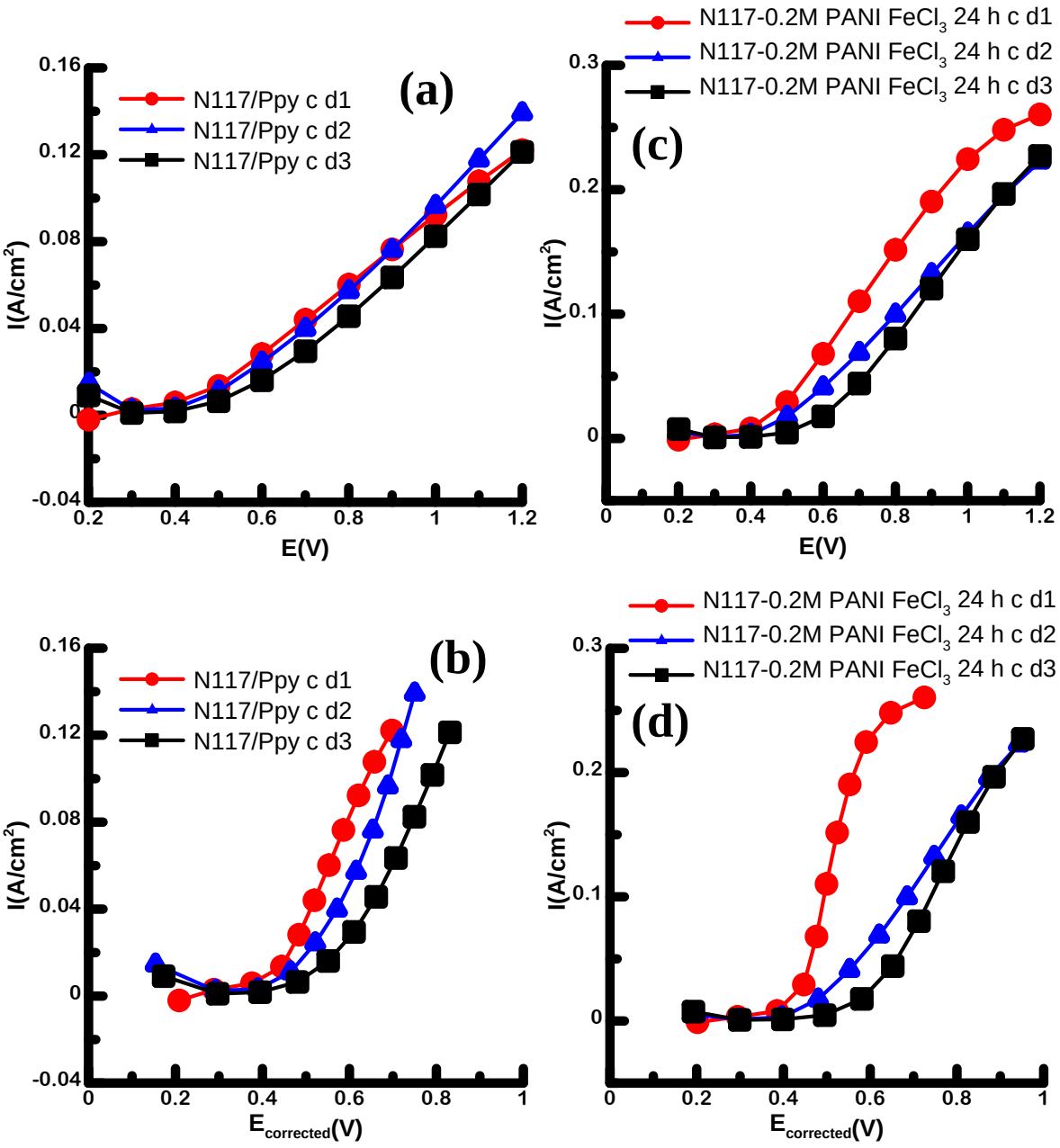

Fig. 4.11: Full cell polarization curves for the electrolysis of CuCl/HCl solution for membranes (a) N117/Ppy c (b) N117/Ppy c IR-corrected (c) N117-0.2M PANI $FeCl_3$ 24 h c (d) N117-0.2M PANI $FeCl_3$ 24 h c IR-corrected, after certain working days (abbreviated d). Measurements were performed at 25.0 ^{0}C with 0.2 M CuCl in 2.0 M HCl flowing at the anode, and deionized water flowing at the cathode, with a rate of 60 mL min^{-1}, under nitrogen atmosphere.

Another experiment to evaluate the performance of the membranes in the Cu-Cl electrolyzer was the potentiostatic hold. This test was performed at a constant potential of 0.7 V for 1 h. During the test the current was measured as a function of time. Four membranes were examined by this potentiostatic test: N115/Ppy c, N115, N117/Ppy c and N117-0.2M PANI $FeCl_3$ 24 h c. Fig. 4.12 (a) illustrates full cell potentiostatic curves at 0.7 V for the electrolysis of CuCl/HCl solution of the N115/Ppy c membrane for 3 working days. The current density was around 0.029, 0.027 and 0.025 A cm^{-2} for day 1, 2, and 3, respectively. These current densities were reached and stabilized after 500 s. For comparison, the N115 membrane was tested as shown in Fig. 4.12 (b). The current density was started at 0.3 and 0.4 A cm^{-2} for the first and second day, respectively, then it increased to *ca.* 0.55 A cm^{-2} during the first 2000 s. This significant increase in the current density was attributed to copper permeating through the membrane and plating at the cathode [87]. However, on the third day the current density stabilized at *ca.* 0.55 A cm^{-2} which can likely be explained by saturation of the copper species on both sides of the membrane. Fig. 4.12 (c) shows the potentiostatic curves of N117/Ppy c for three days. The current density stabilized at 0.05, 0.035, and 0.025 A cm^{-2} for day 1, 2, and 3, respectively. In addition, on each day it required *ca.* 500 s to reach the stabilized values. Fig. 4.12 (d) illustrates the potentiostatic curves of N117-0.2M PANI $FeCl_3$ 24 h c for three days. The current density started at 0.055, 0.04, and 0.03 A cm^{-2} for day 1, 2, and 3, respectively. At *ca.* 500 s the values stabilized at 0.06, 0.055, and 0.045 A cm^{-2} for day 1, 2, and 3, respectively. It can be concluded that all the membranes tested by the potentiostatic measurements showed good stability compared to N115 that showed copper crossover by continuously increasing the current density.

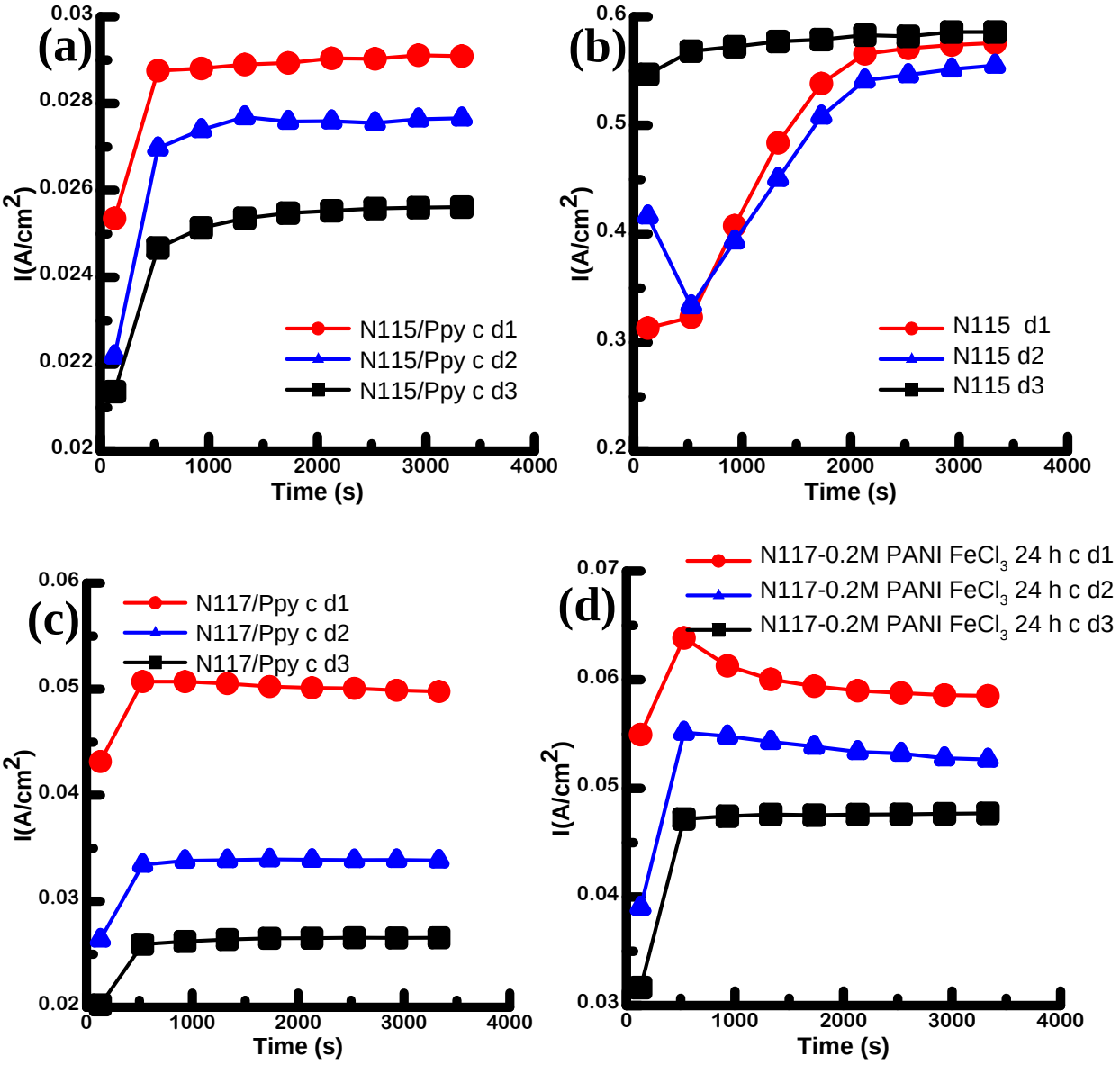

Fig. 4.12: Full cell polarization curves for the electrolysis of CuCl/HCl solution for membranes (a) N117/Ppy c (b) N117/Ppy c IR-corrected (c) N117-0.2M PANI $FeCl_3$ 24 h c (d) N117-0.2M PANI $FeCl_3$ 24 h c IR-corrected, after certain working days (abbreviated d). Measurements were performed at 25.0 ^{0}C with 0.2 M CuCl in 2.0 M HCl flowing at the anode, and deionized water flowing at the cathode, with a rate of 60 mL min^{-1}, under nitrogen atmosphere.

Fig. 4.13 illustrates full cell CV measurements in the diagnostic mode for the pure Nafion N115 membrane and other composite membranes after 3 working days. This test was used to

detect any copper species deposited from the copper crossover and conducted at the beginning of each day before starting other tests. Therefore, all membranes, on the first day of the CV measurement, as expected did not show any traces of copper deposition. For the 3 days, the CV measurement of the N115/Ppy c membranes did not display any oxidation or reduction peaks at *ca.* 0.4-0.5 V, as can be seen in Fig. 4.13 (a), which could be a positive sign of absence of any copper crossover. Fig. 4.13 (b) illustrates the CV measurements of the N115 pristine membrane. It clearly shows the oxidation and reduction peaks on the second and third testing days, whereas these peaks were absent on the first day, as mentioned before. It is believed that the developed peaks are attributed to the copper accumulation at the membrane-electrode interface. Furthermore, CV measurements were obtained for N117/Ppy c and N1170.2M PANI $FeCl_3$ 24 h c as can be seen from Fig. 4.13 (c) and (d), respectively. The CV measurements of the N117/Ppy c membrane did not show any oxidation or reduction peaks for the first and second day. An oxidation peak appeared at *ca.* 0.3 V without any clear reduction peak. Most probably, this peak is not related to the copper crossover as it does not match the *ca.* 0.4-0.5 value. The CV measurements of the N117-0.2M PANI $FeCl_3$ 24 h c membrane showed small oxidation reduction peaks as illustrated in Fig. 4.13 (d). These small peaks prove that there was some copper deposition. Compared to N115, It is clear that N115/Ppy c performance is the best amongst all the tested membranes.

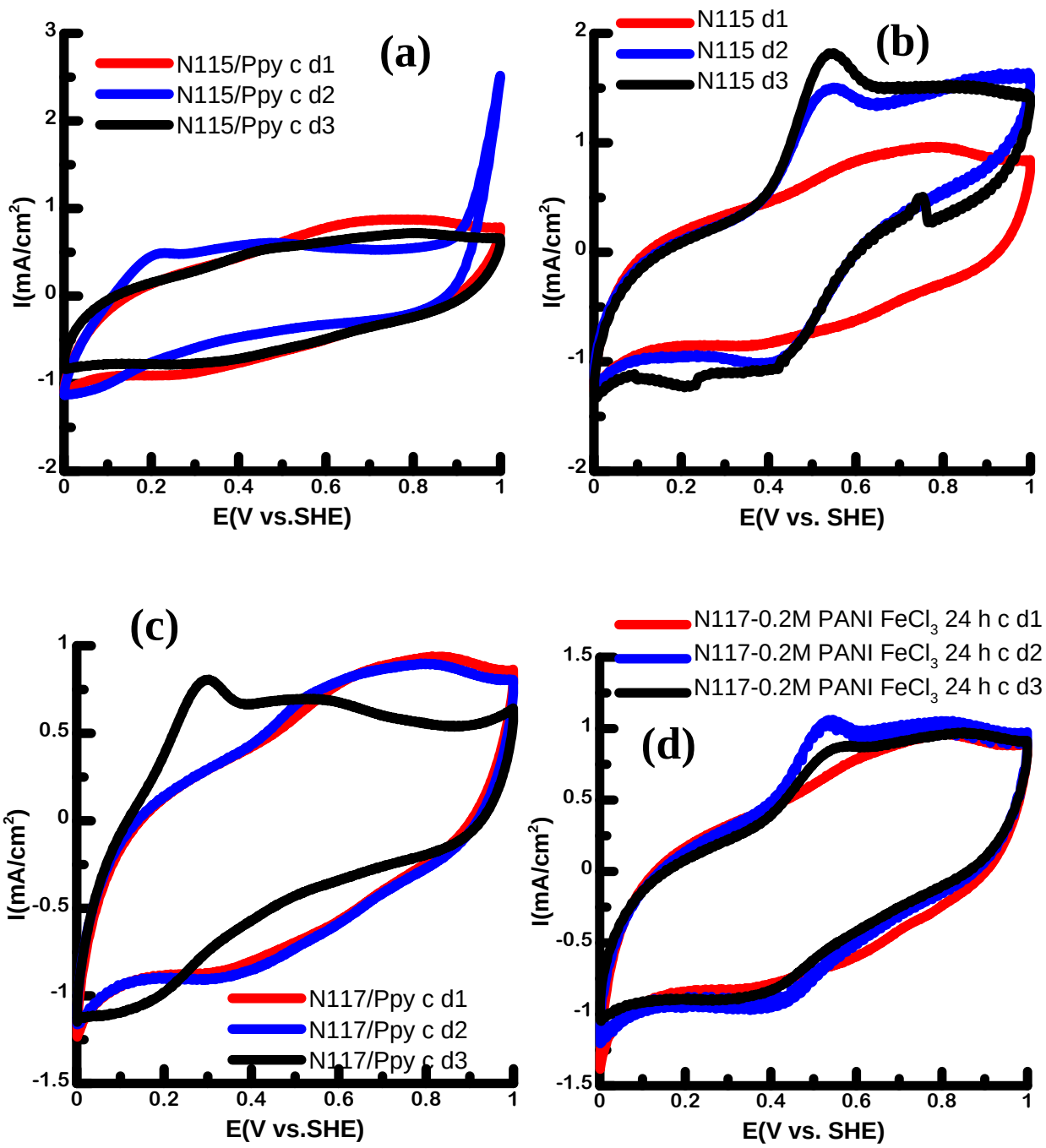

Fig. 4.13: Diagnostic mode full cell CV for pure Nafion N115 membrane and other composite membranes after certain working days (abbreviated d). (a) N115/Ppy c (b) N115 (c) N117/Ppy c (d) N117-0.2M PANI $FeCl_3$ 24 h c. Measurements were taken at a sweep rate of 50 mV s^{-1} at 25.0 °C with 2.0 M HCl flowing in the left side of the cell at 60 mL min^{-1} and H_2 flowing in the right side at 25 mL min^{-1}.

4.6 Hydrogen Collection

Hydrogen collection is another way of testing cell performance. It can be performed through passing a fixed current for a specific time and measure the voltage while collecting the hydrogen produced in the cathode side. Fig. 4.14 shows the galvanostatic curves of the full cell test for the pure Nafion membranes and their composites at a constant current of 0.5 A during the H_2 production measurements. From Fig. 4.14 (a), it can be seen that N115 needs around 0.6 V to generate this constant current during almost all the three testing days, while for the Nafion 115/Ppy c the potential starts at 1.4 V on the first day, then decreases to 1.2 and 1.1 V for the second and third days, respectively, as can be seen in Fig. 4.14 (b). The galvanostatic curves for N117-0.2M PANI $FeCl_3$ 24 h c showed that to generate 0.5 A current, a voltage of *ca.* 0.8 V has to be applied as illustrated in Fig. 4.14 (c). Although the performance of the composite membranes seems significantly poor due to high resistivity, looking carefully on these galvanostaic curves, we can notice that both N115/Ppy c and N117-0.2M PANI $FeCl_3$ 24 h c had smooth curves during the three testing days. However, the galvanostatic curves of the pristine N115 showed a noisy trend that can be noticed from the thickness of the curves especially on testing days 2 and 3. This might be explained by the penetration of copper to the cathode side causing deterioration of the cell performance. To verify this assumption, a Faradic current efficiency test is conducted using hydrogen collection for each membrane.

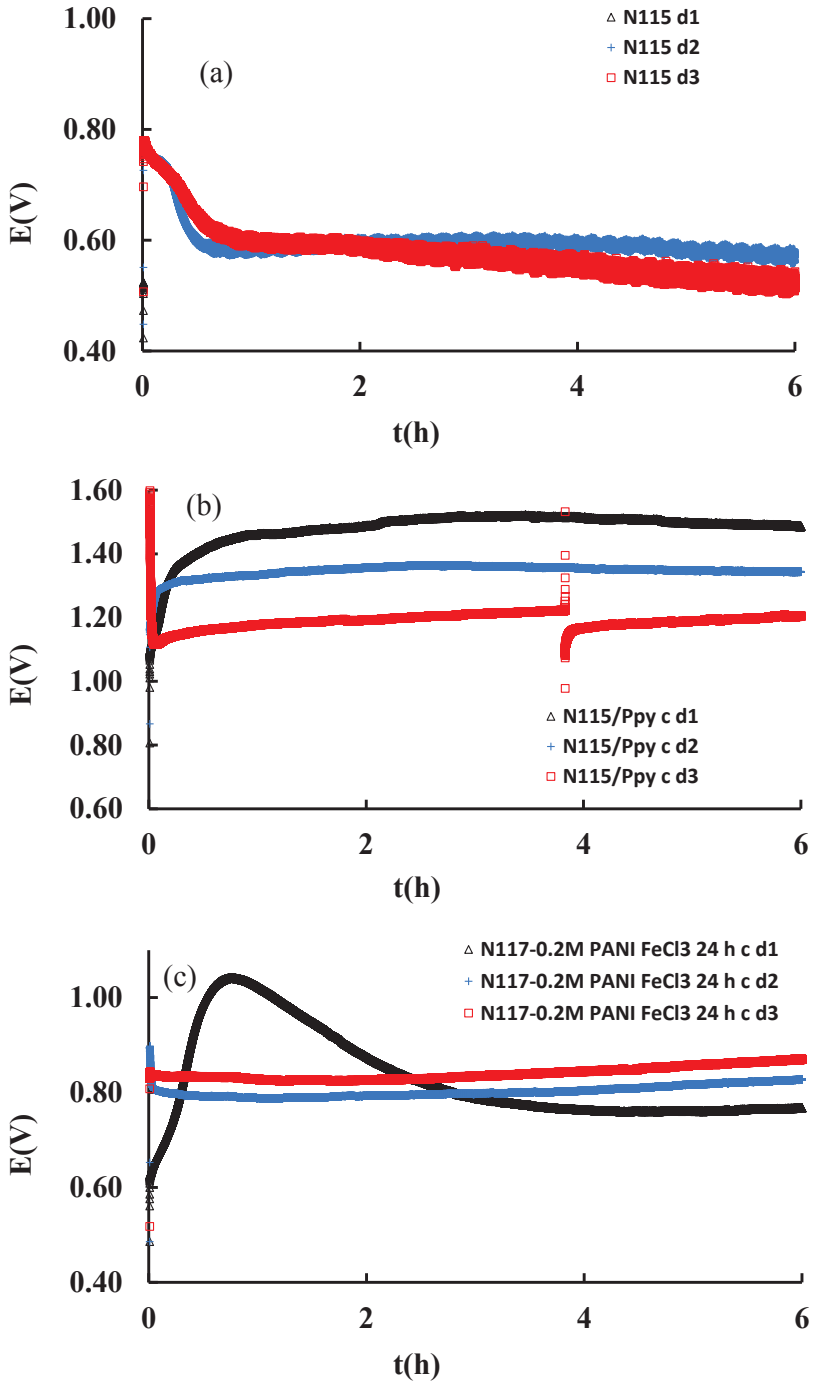

Fig. 4.14: Full cell galvanostatic curves at 0.5 A for the electrolysis of CuCl/HCl soln. for 6 h after certain working days (abbreviated d) (a) N115 (b) N115/Ppy c (c) N117-0.2M PANI $FeCl_3$ 24 h c. Measurements were made at 25.0 °C with 0.2 M CuCl in 2.0 M HCl flowing at the anode and deionized water flowing at the cathode, with a rate of 60 mL min^{-1}, under nitrogen atmosphere.

The current efficiency of the Cu-Cl electrolysis for different MEAs can be calculated from a ratio of the amount of hydrogen produced experimentally to the theoretical amount calculated from Faraday's law, as can be seen in Eq. 4.1

$$\eta c = \frac{H_2}{H_2}\frac{(\exp)}{(theor)} X100 \qquad Eq.4.1$$

Data obtained from Lvov et al. [12] indicated that the Faradic efficiency for pristine Nafion in the Cu-Cl electrolysis was 98 % based on a 5 h electrolysis. Furthermore, they suggested that a lengthy electrolysis experiment should be examined to discover any copper permeation. In our study, we initially performed conventional water electrolysis and collected the produced H_2 to evaluate our apparatus and methodology. From replicate experiments we determined a 99.2 % current efficiency towards water electrolysis, which validates the experimental design. We later tested the MEAs in the Cu-Cl/HCl electrolysis cell for 6 h each day for three days and collected the H_2 to calculate the current efficiency. Each MEA should produce the same amount of H_2 if the Faradic current efficiency is the same. Table 4.7 shows that when N115 was used in the Cu-Cl electrolysis, and current efficiency was calculated from H_2 collection, only *ca.* 79 % and 18 % were collected for day 1 and 3, respectively. In contrast, N115/Ppy c shows superior and constant H_2 production with current efficiency around 100 % for day 1 and 3. In another experiment, N117-0.2M PANI $FeCl_3$ 24 c showed Faradic current efficiency of 97 % and 90 % for day 1 and 3, respectively. All Faradic current efficiency data are also illustrated in Fig. 4.15. These results support the idea that the applied current in the N115 membrane not only produces hydrogen but also drives other side reactions, most probably Cu deposition. Furthermore, both N115/Ppy c and N117-0.2M PANI $FeCl_3$ 24 h c used most of the

applied current to generate H_2 gas, which proves the high performance of these membranes to be used in the Cu-Cl cycle.

Table 4.7: The percentage of hydrogen efficiency of pure Nafion membrane N115, Ppy and PANI composite membrane during 6 h of fixed current of 0.5A at 25.0 ^{0}C for certain working days. Anolyte is 0.2 M CuCl in 2.0 M HCl and catholyte is water. Both flow at rate 60 mL min^{-1}.

H_2 production effeciency %			
	N115	N115/Ppy c	N117 PANI $FeCl_3$ 24 h c
d1	79.3	99.0	97.1
d3	18.3	99.8	90.0

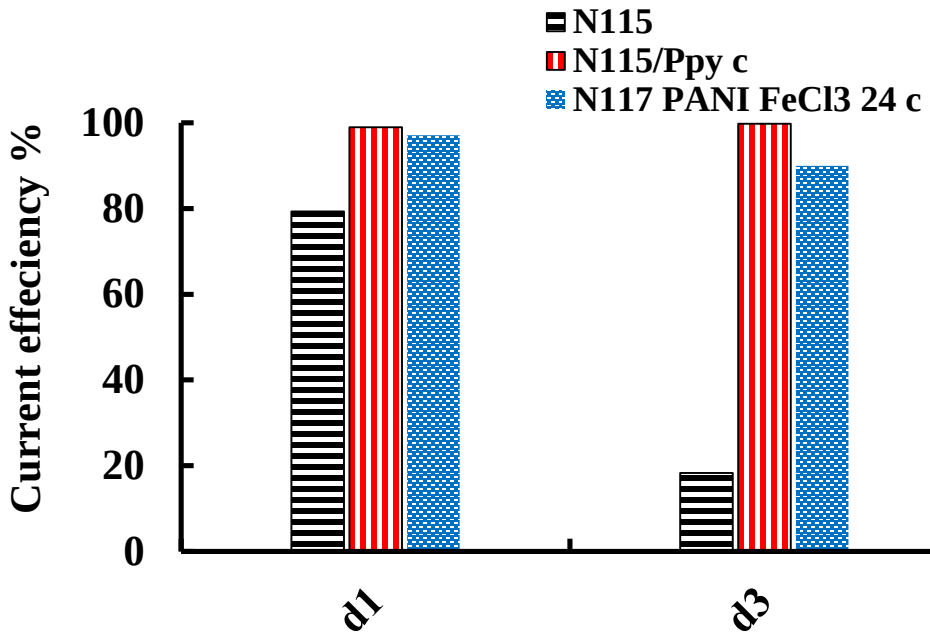

Fig. 4.15: The percentage of hydrogen efficiency of pure Nafion membrane N115, and its Ppy, and PANI composite membranes during 6 h of fixed current at 0.5 A and 25.0 ^{0}C for certain working days. Anolyte is 0.2 M CuCl in 2.0 M HCl and catholyte is water. Both flow at rate 60 mL min^{-1}.

From the data in Table 4.7, we can estimate the H_2 production rate for N115 and N115/Ppy c. On day 1, the rate of hydrogen production was 3.0 and 3.8 cm^3 min^{-1} for N115 and N115/Ppy c, respectively, as illustrated in Table 4.8. By day 3, the hydrogen production rate for the pristine membrane dropped to 0.7 cm^3 min^{-1} while N117/Ppy c showed stability at the same value of 3.8 cm^3 min^{-1}. Such measurements and calculations support the idea of the superiority of the Ppy and PANI composite membranes compared to the pristine Nafion membranes.

Table 4.8: The rate of hydrogen production of pure Nafion membrane N115 and its Ppy composite membrane during 6 h of fixed current of 0.5 A at 25.0 ^{0}C for certain working days. Anolyte is 0.2 M CuCl in 2.0 M HCl and catholyte is water. Both flow at rate 60 mL min^{-1}.

H_2 Production rate cm^3/min		
	N115	N115/Ppy c
d1	3.0	3.8
d3	0.7	3.8

4.7 Summary

In this chapter, the Nafion membranes were modified by *in situ* polymerization of aniline. The modified membranes were identified and characterized by FT-IR, UV-Vis spectroscopy, TGA, and SEM. The proton conductivity was determined by EIS and the Cu permeability was determined by an *ex situ* diffusion cell. In addition, selectivity was calculated for each PANI modified membrane. Different parameters were studied to optimize the proton conductivity and Cu permeability, such as the concentration of the monomer, different polymerizing agents, and the time of polymerization. Our experiments showed that a high selectivity membrane can be obtained by using an acidic solution of 0.2 M aniline as a monomer, an acidic solution of $FeCl_3$

as an oxidizing agent and a polymerization time of 24 hours. N117-0.2M PANI $FeCl_3$ 24 h membrane showed a reduction in the Cu permeability rate with good conductivity.

Potential candidates modified membranes that can mitigate the Cu permeation were tested in the CuCl/HCl electrolyzer. MEAs of N115/Ppy, N117/Ppy, and N117-0.2M PANI $FeCl_3$ 24 h membranes were prepared and assembled in the cell in separate experiments, then tested using CuCl/ HCl electrolysis and the electrochemical diagnostic mode. In the diagnostic mode, the CVs clearly showed a peak for the copper deposition in the MEA of the pristine membrane, while it is unclear or absent in the composite membranes after certain working days. Visually inspecting the MEAs confirmed that the composite membranes blocked the copper species from permeating through the membranes, while the pristine Nafion membrane showed a solid Cu deposition. The presence of Cu in the catholyte has a longer influence on the membrane and the electrolysis cell. Deposition of Cu on the cathode can physically damage the membranes and in turn can deteriorate electrolysis cell efficiency. Moreover, reducing the Cu transport rate through a membrane can enhance the performance of the electrolysis cell by keeping the cathode catalyst layer clean from any Cu deposition.

The Galvanostatic hold data showed that a higher potential is required to draw a fixed current of 0.5 A compared to a pristine Nafion membrane. This measurement was misleading and could be due to high resistivity of the composite membranes. However, to clear the misleading result from the voltage current curves, a Faradic current efficiency test through H_2 collection measurements was conducted for each membrane. Each MEA should theoretically produce the same amount of H_2 if they have similar Faradic efficiency. The % of H_2 collection efficiency of N115 was 79.3 % during the first electrolysis day but drastically dropped to 18.3 % during the third hydrogen collection day. Both N115/Ppy c and N117 PANI $FeCl_3$ 24 h C

showed excellent high Faradic efficiency of 99.0 and 97.1 %, respectively during the first day of CuCl/HCl electrolysis, and both of them maintained high Faradic current efficiency during the third H_2 collection day. It seems that the current in the composite membranes was totally devoted towards producing H_2, while in the pristine membrane the current was diverted from H_2 production towards Cu deposition.

Although composite membranes showed high resistivity compared to the pristine Nafions which resulted in low voltage efficiency, they showed outstanding Faradic current efficiency. This high Faradic current efficiency indicated that, except for production of H_2 gas, no other parasitic reaction occurred.

Chapter 5

Electrochemical Monitoring of Copper in the Catholyte Solution

The previous chapter has shown us that there is a clear correlation between the rate of Cu permeation and the long term hydrogen production efficiency of the membrane electrolyte assemblies (MEAs). With all this evidence of Cu accumulation (diagnostic cyclic voltammetry (CV), and visual Cu deposition) we would like to have a simple, efficient method to monitor the Cu in the catholyte solution. Differential pulse anodic stripping voltammetry (DPASV) is an electrochemical method that has the capability to monitor the Cu crossover in the actual cell effluent. In this chapter, we want to compare Nafion, which is considered a cation exchange membrane, with an anionic exchange membrane such as polysulfone based tetramethylammonium cation in chloride form (TMA) and, for curiosity, examine it in the full Cu-Cl/HCl electrolysis cell. TMA which is a linear polysulfone with benzyl quaternary, was procured from researchers in the membrane field at Illinois Institute of Technology. It is an anionic exchange membrane with 50 μm thickness.

5.1 TMA Full Cell Analysis

The full tests were performed on hot pressed membranes with the cathode electrode at T (135-140 ^{0}C) for 70 s under a load of 300 kg cm^{-2}. Daily, fresh solutions of HCl 2.0 M and 0.2 M CuCl in 2.0 M HCl were used. A solution of HCl 2.0 M was used as a catholyte instead of deionized water to keep the membrane balanced in the chloride form, and a CuCl solution was utilized as an anolyte at 25 °C. N115 and N117 and their composite Ppy membranes were examined under the same conditions for comparison.

Fig. 5.1 shows full cell polarization curves for the electrolysis of the CuCl/HCl solution for membranes N115, N115/Ppy, N117, N117/Ppy and TMA. Fig. 5.1 (a,b) shows that pristine membranes and Ppy composite membranes have similar onset potential with a lower limiting

current of the composite membranes. Fig. 5.1 (c) demonstrates that TMA had higher onset potential and limiting current lower than either pristine or composite membranes. These results can be attributed to the more activation resistive TMA due to the anionic nature of this membrane.

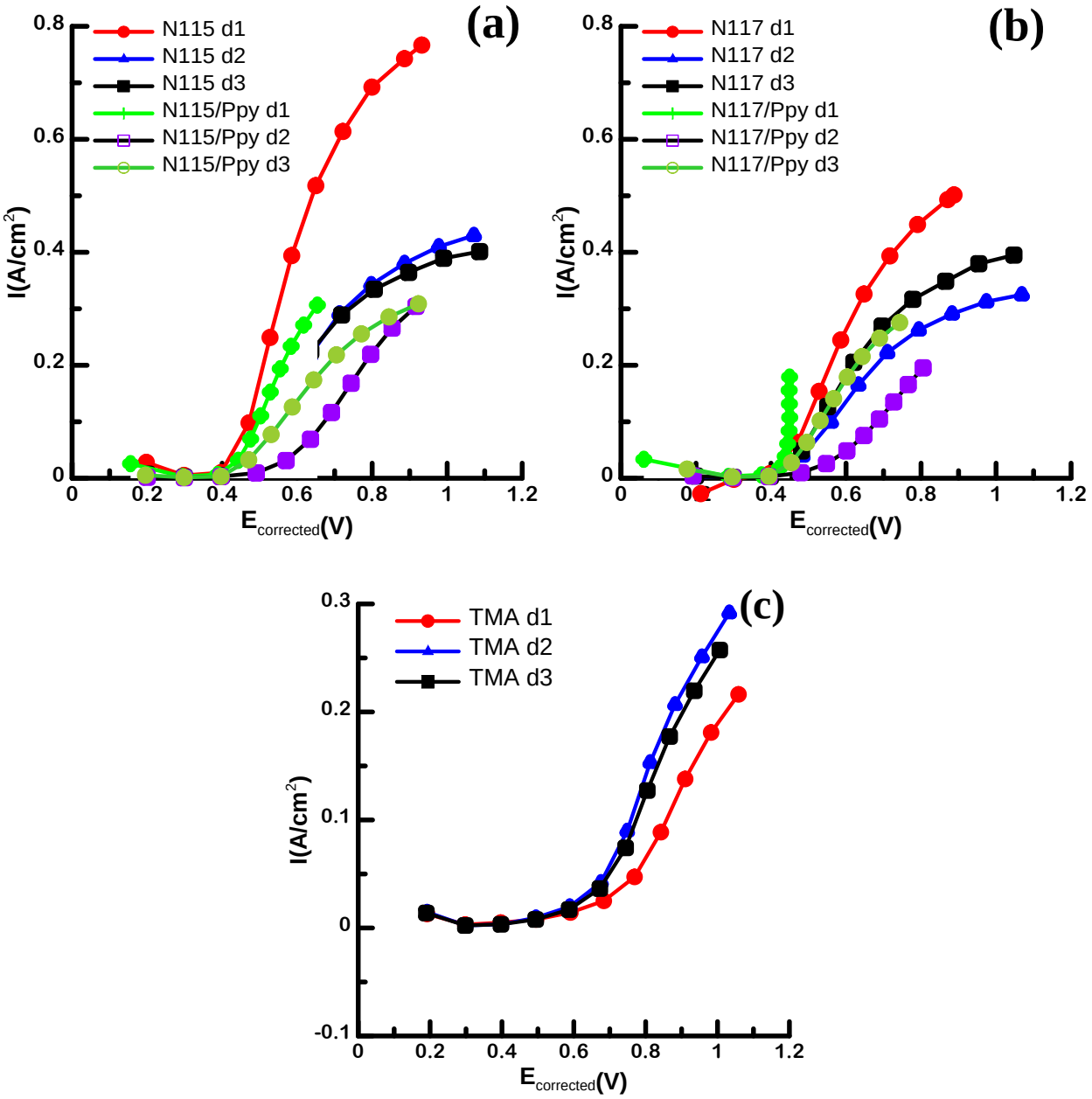

Fig. 5.1: Full cell polarization curves for the electrolysis of CuCl/HCl solution for membranes (a) N115 and N115/Ppy (b) N117 and N117/Ppy (c) TMA, after certain working days (abbreviated d). Measurements were performed at 25 ^{0}C with 0.2 M CuCl in 2.0 M HCl flowing at the anode, and HCl 2.0 M flowing at the cathode, with a rate of 60 mL min^{-1}, under nitrogen atmosphere.

Fig. 5.2 shows full cell potentiostatic curves at 0.7 V for the electrolysis of the CuCl/HCl solution of N115, N115/Ppy, N117, N117/Ppy and TMA membranes. The N115/Ppy membrane

showed stability in the current generated at a fixed voltage, while N115 showed a significant change in the current with time, as can be seen in Fig. 5.2 (a,b). Similarly, N117 showed stability during the first two days then the current sharply increased on the third day, as shown in Fig. 5.2 (c). To the contrary, N117/Ppy showed stability of the current with time during the three working days, as illustrated in Fig. 5.2 (d). Nafion Ppy composite membranes showed lower generated current compared to the pristine membranes as the Ppy polymer exchanged a noticeable number of protons which were responsible for transferring the charge through the membrane. TMA showed that 0.7 V can generate a current density of 0.05 A/cm^2 or less, while the same voltage can generate 0.1 A/cm^2 or more for N115 and N117, as shown in Fig. 5.2 (e).

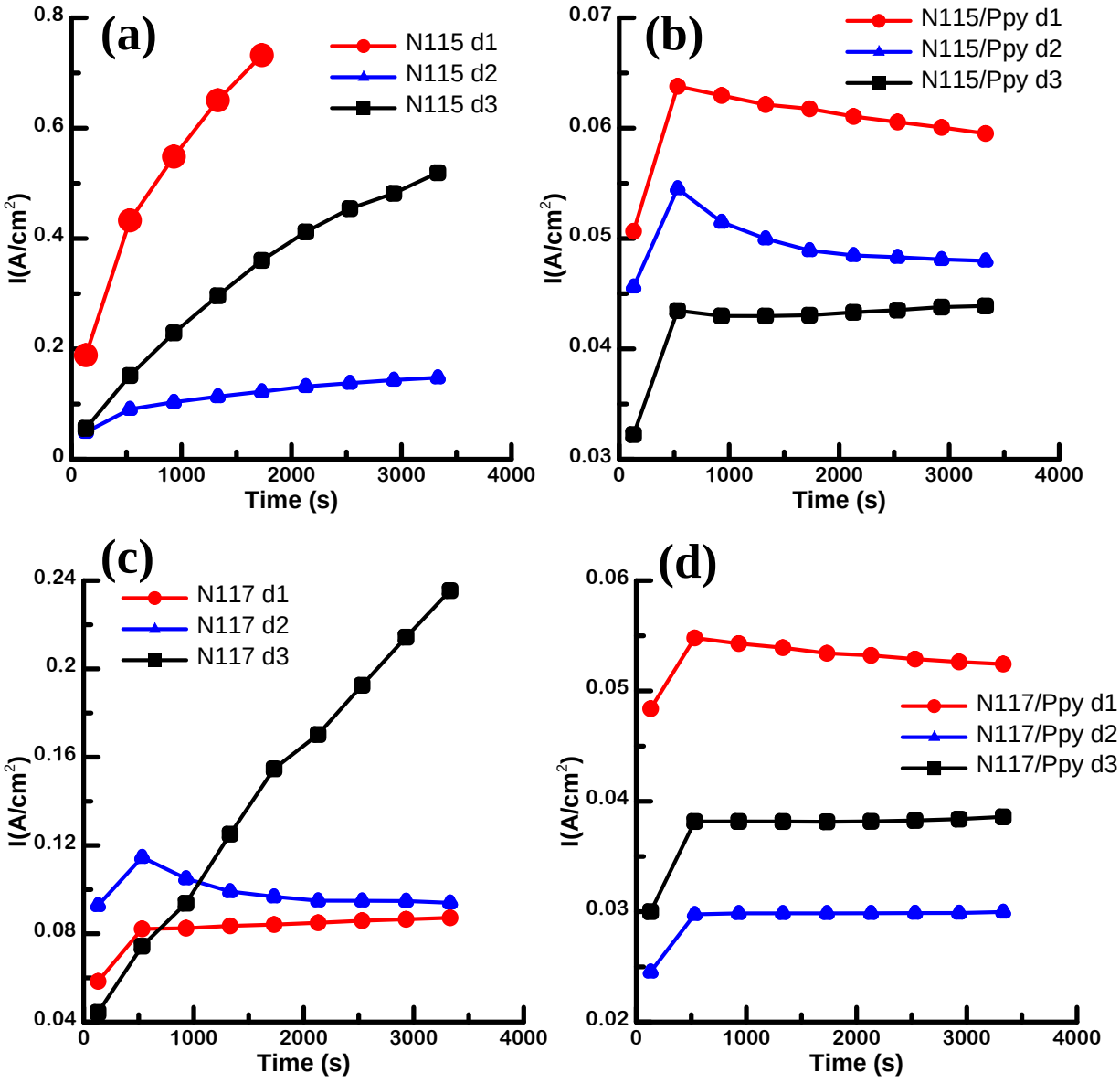
(a)
N115 d1
N115 d2
N115 d3
I(A/cm^2)
Time (s)
(b)
N115/Ppy d1
N115/Ppy d2
N115/Ppy d3
I(A/cm^2)
Time (s)
(c)
N117 d1
N117 d2
N117 d3
I(A/cm^2)
Time (s)
(d)
N117/Ppy d1
N117/Ppy d2
N117/Ppy d3
I(A/cm^2)
Time (s)

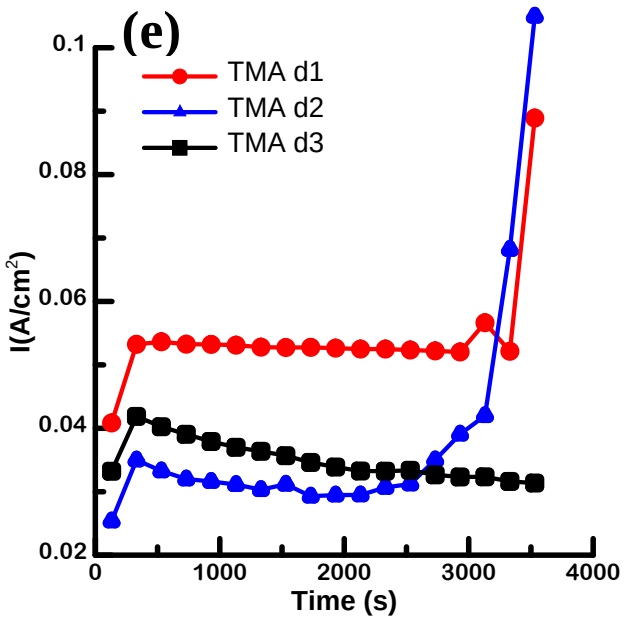

Fig. 5.2: Full cell potentiostatic curves at 0.7 V for the electrolysis of CuCl/HCl soln. of (a) N115 (b) N115/Ppy (c) N117 (d) N117/Ppy (e) TMA membranes, after certain working days (abbreviated d). Measurement were made at 25 °C with 0.2 M CuCl in 2.0 M HCl flowing at the anode, and HCl 2.0 M flowing at the cathode, with a rate of 60 mL min^{-1}, under nitrogen atmosphere.

Fig. 5.3 shows full cell galvanostatic curves at 0.5 A for the electrolysis of the CuCl/HCl solution for 6 h after three working days. The cell voltage was decreased with time for both pristine Nafion membranes, while it was stable for the composites, as shown in Fig. 5.3 (a-d). At the beginning, TMA required more than 0.8 V to generate a fixed current of 0.5 A; later, during the test this voltage dropped to about 0.4 V which did not occur for other composite membranes. This severe reduction in the cell voltage indicates the Cu crossover, as shown in the previous chapter.

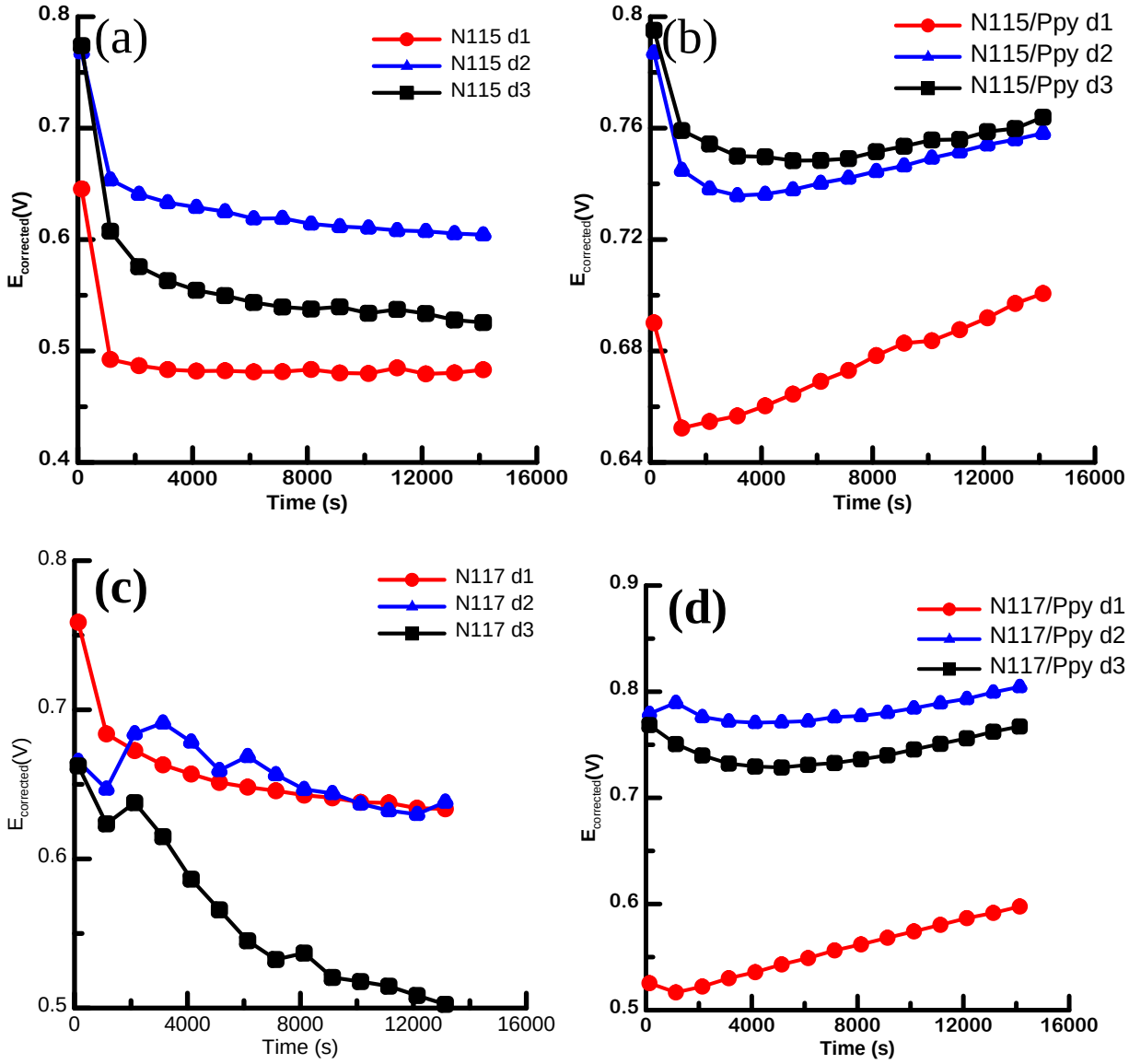
(a)
N115 d1
N115 d2
N115 d3
E corrected (V)
Time (s)
(b)
N115/Ppy d1
N115/Ppy d2
N115/Ppy d3
E corrected (V)
Time (s)
(c)
N117 d1
N117 d2
N117 d3
E corrected (V)
Time (s)
(d)
N117/Ppy d1
N117/Ppy d2
N117/Ppy d3
E corrected (V)
Time (s)

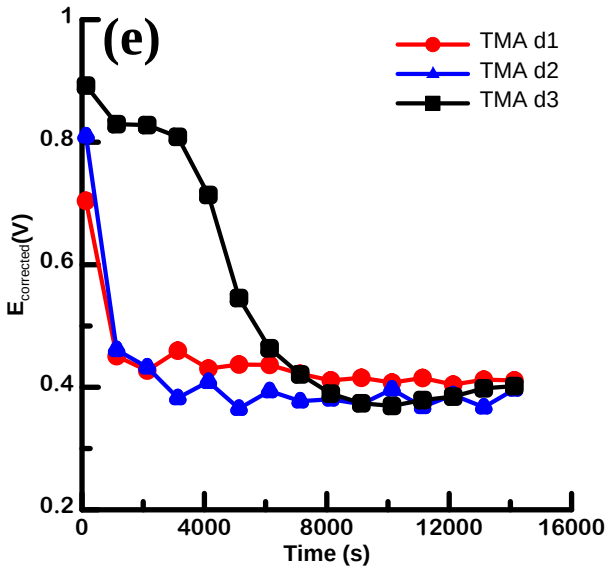

Fig. 5.3: Full cell galvanostatic curves at 0.5 A for the electrolysis of CuCl/HCl soln. for 6 h after certain working days (abbreviated d). (a) N115 (b) N115/Ppy (c) N117 (d) N117/Ppy (e) TMA. Measurements were made at 25 °C with 0.2 M CuCl in 2.0 M HCl flowing at the anode and HCl 2.0 M flowing at the cathode, with a rate of 60 mL min^{-1}, under nitrogen atmosphere.

Fig. 5.4 shows the full cell CV measurements in diagnostic mode for pure Nafion N117 membranes, its Ppy composite membranes and TMA for three working days. The CVs show that the pure Nafion 115 membrane had oxidation and reduction peaks at around 0.4 V on the 2nd and 3rd day, likely due to copper deposition in the membrane electrolyte assembly (MEA). These peaks are absent for MEAs made with the Ppy composite membranes. The same result was observed for N117 and its Ppy composite membrane, as can be seen in Fig. 5.4 (c,d). The CVs obtained with TMA showed high resistivity making it impossible to see any trace of redox peaks, as shown in Fig. 5.4 (e). The deposition of copper on the pure membranes was also confirmed by photographs showing this deposition in Fig. 5.6. In contrast, the photographs of the composite membranes reveal the absence of any deposition, as shown in Fig. 5.6 (c,e). The MEA photo of

the TMA showed some Cu deposition on the membrane but it was less intense than pristine membranes.

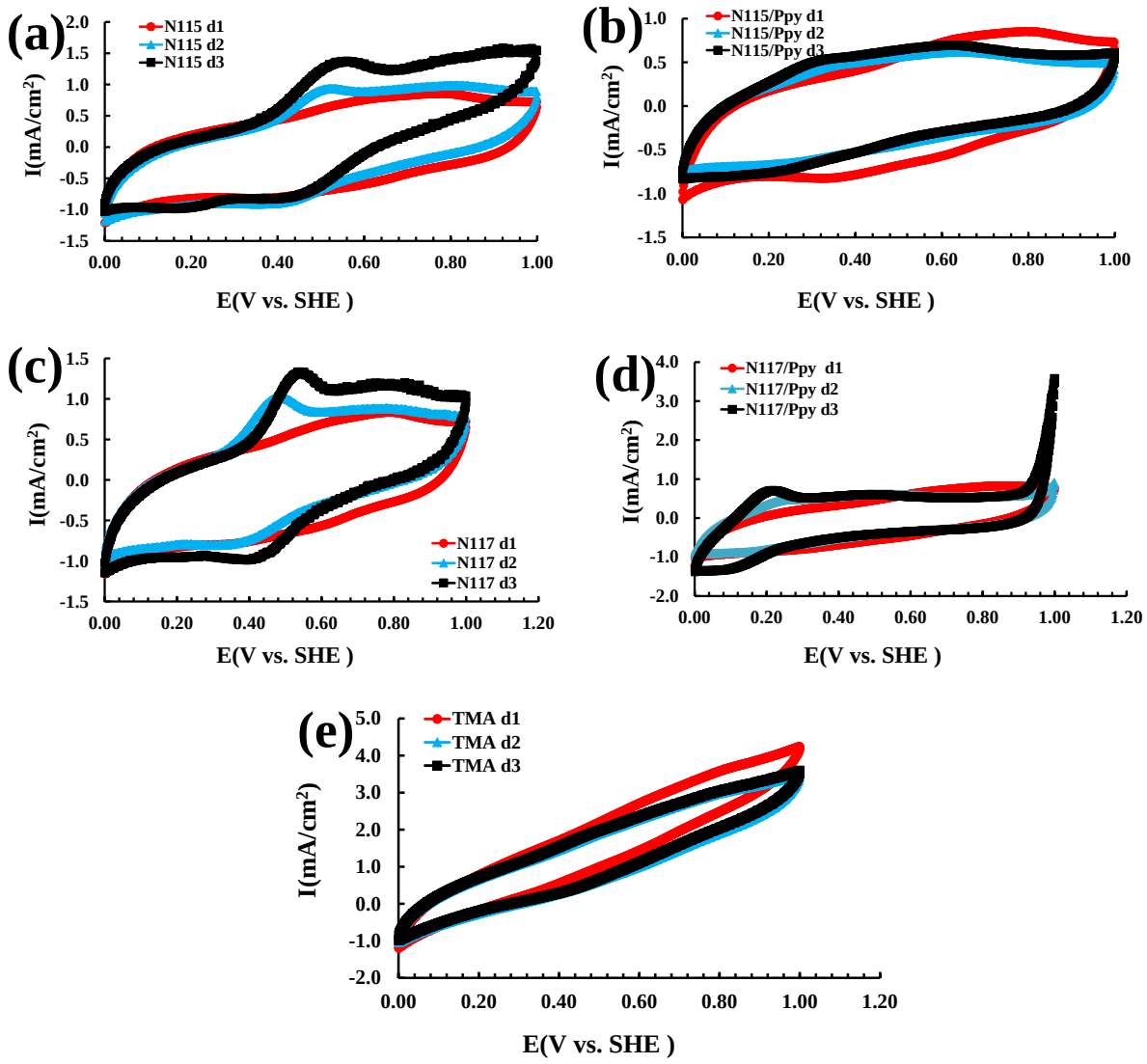

Fig. 5.4: Diagnostic mode full cell CV for pure Nafion membranes and other composite membranes (abbreviated d). (a) N115 (b) N115/Ppy (c) N117 (d) N117/Ppy (e) TMA, after certain working days Measurements were taken at a sweep rate of 50 mV s^{-1} at 25 °C with 2.0 M HCl flowing in the left side of the cell at 60 mL min^{-1} and H_2 flowing in the right side at 25 mL min^{-1}.

Fig. 5.5 displays the impedance plots of pure Nafion membrane N115, N115/Ppy and TMA. As can be seen from the embedded plot in Fig. 5.5 (a), the semi-circle in the Nyquist plot

and Warburg impedance for N115 on d3 was high compared to the first two days which could be due to Cu deposition. Although Fig. 5.5 (b) shows high membrane impedance at d1 for N115-Ppy, it shows more stability and less impedance during the 2nd and 3rd days of testing due to mass transfer control. TMA had a considerable impedance compared to N115 and N115/Ppy due to charge transfer as shown in Fig. 5.5 (c), which could be explained by the anion exchange property of TMA that inhibits the proton exchange.

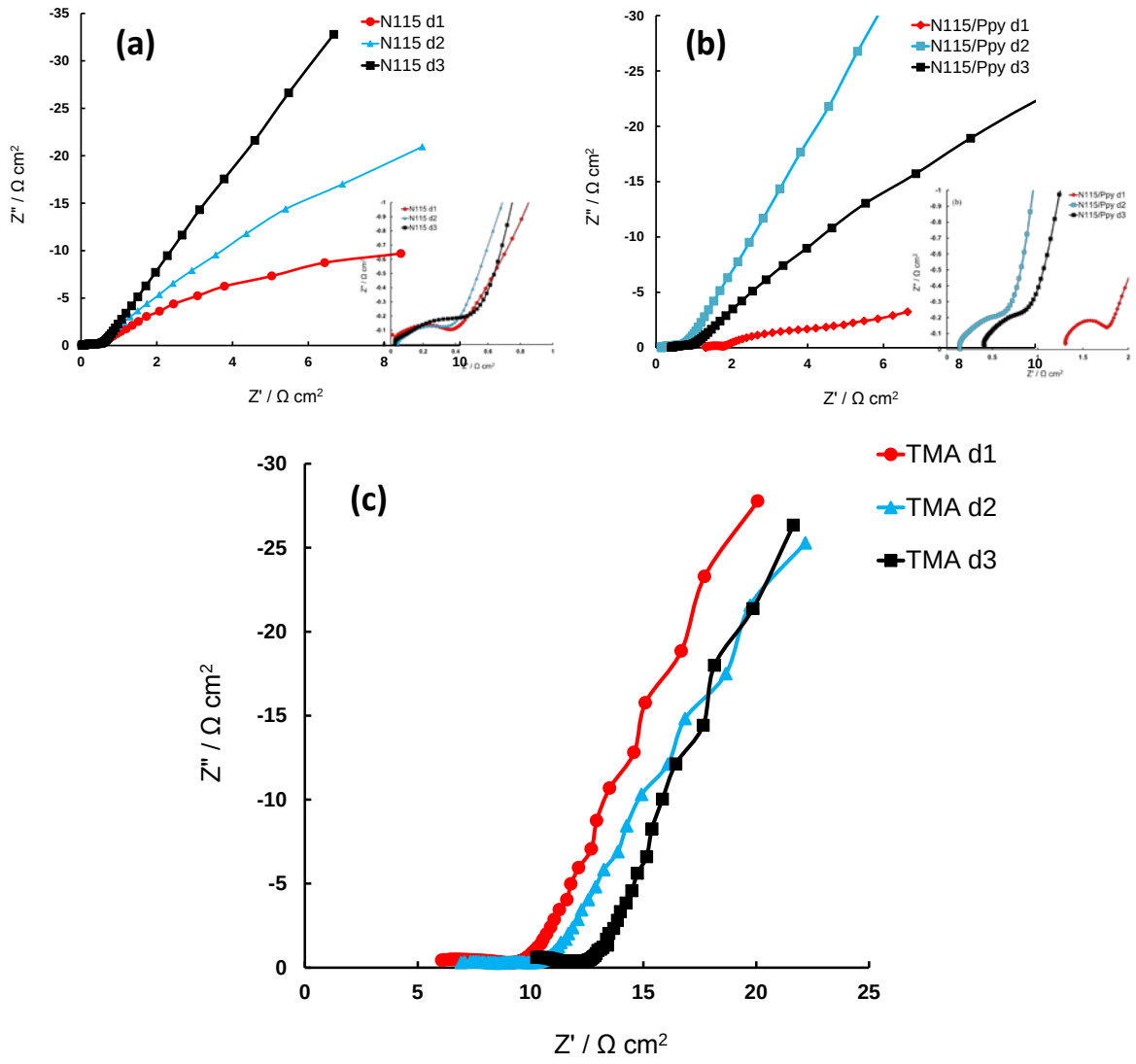

Fig. 5.5: Impedance plots of (a) N115 (b) N115/Ppy (c) TMA membranes after certain working days (abbreviated d). Measurements were made at 25 °C with 0.2 M CuCl in 2.0 M HCl flowing at the anode and HCl 2.0 M flowing at the cathode, with a rate of 60 mL min^{-1}, under nitrogen atmosphere.

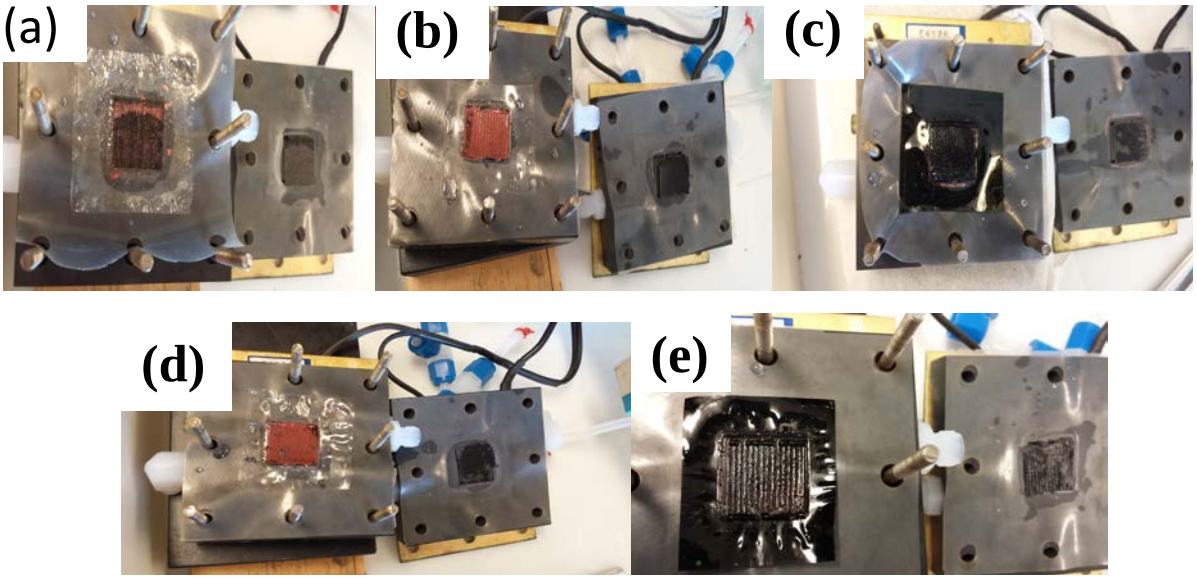

Fig. 5.6: Pictures of the Cu deposition of Cu-Cl electrolysis. (a) TMA (b) N115 (c) N115/Ppy (d) N117 (e) N117/Ppy membrane after three working days.

5.2 Analysis of the Catholyte by Differential Pulse Anodic Stripping Voltammetry (DPASV)

To further evaluate these membranes, the catholyte solution was analyzed after each working day. Samples from the fresh catholyte solution were taken each day, before and after the Cu-Cl electrolysis. DPASV was used to quantify any copper permeated through the membranes to the catholyte solution. A three-electrode cell set up was utilized using UMEs and Pine Instruments Wave Driver potentiostat under N_2 and at ambient temperatures. A 25 μm Pt working disc electrode, a silver/silver chloride (Ag/AgCl) reference electrode, and a Pt wire as a counter electrode were employed. Different concentrations of Cu standards were prepared in a 2.0 M HCl acid solution and measured by DPASV. A calibration graph of peak areas *vs*. the Cu concentrations was constructed, as can be seen in the inset of Fig. 5.7. The DPASV method was implemented as it showed excellent linearity and stability. Furthermore, it is fast, simple and cost

effective. Fig. 5.7 shows the DPASV response for 1, 2, 5, and 10 ppm Cu solution. In addition, the results from DPASV showed outstanding agreement with AAS analysis results.

Table 5.1 shows the catholyte analysis after each working day in the full cell Cu-Cl electrolyzer, for N115, N117, N115/Ppy, N117/Ppy and TMA. The unmodified Nafion membranes showed that the amount of Cu in the catholyte after each working day in the full cell is between 3-6 ppm, while in Ppy composite membranes it is in the range of 0.9-2.5 ppm. Furthermore, TMA showed a large amount of Cu in the catholyte compared to both Nafion and Ppy composite membranes. The amount of Cu in the catholyte for TMA was 33, 42, and 39 ppm for d1, d2 and d3, respectively. In the HCl solution, The Cu species, such as neutral $CuCl_2$ (aq) and negatively charged $CuCl_3^{2-}$, $CuCl_3^{-}$, $CuCl_4^{2-}$, could easily permeate through an anion exchange membrane as TMA. In contrast, only neutral Cu species such as $CuCl_2$ (aq) can permeate to the cathode side of the Nafions.

We can see from Fig. 5.8. that the catholyte of TMA had a significant amount of Cu permeated through the membrane, as an anion exchange membrane easily permeates the most prevalent negatively charged Cu species of Cu(I) and Cu(II) such as $CuCl_3^{2-}$, $CuCl_3^{-}$, $CuCl_4^{2-}$ [108]. Nafion as a cation exchange membrane showed a lower rate of Cu permeation compared to TMA. Fig. 5.9 shows,as expected, that the composite membranes, N115/Ppy and N117/Ppy, showed minimal concentration of Cu in the catholyte compared to the pristine membranes, which supports the data from previous chapters such as *ex situ* diffusion cell, electrochemical measurements and Faradic current efficiency.

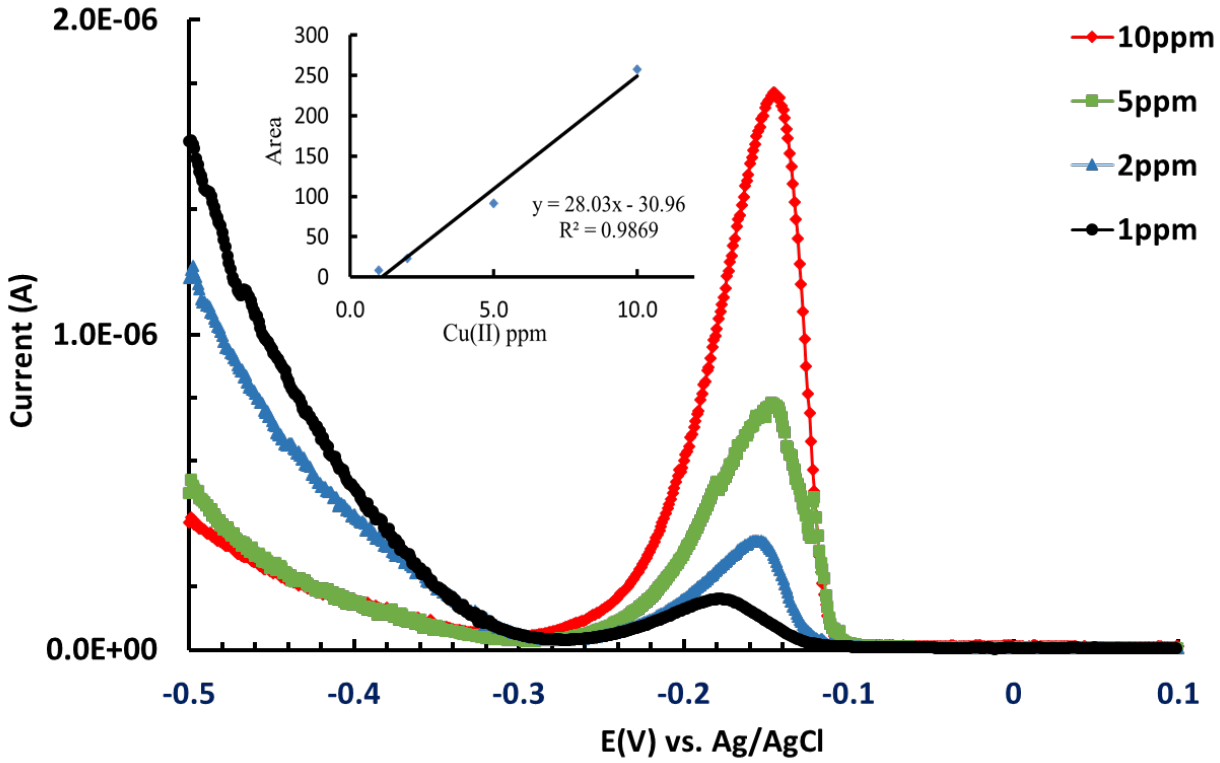

Fig. 5.7: DPASV responses of 1, 2, 5, and 10 ppm Cu^{2+}. Analysis was performed by a three-electrode cell set up using UMEs and Pine Instruments Wave Driver potentiostat under N_2 and at ambient temperatures using 25 µm Pt disc working electrode, a silver/silver chloride (Ag/AgCl) reference electrode, and a Pt wire as a counter electrode. The inset shows the corresponding calibration curve.

Table 5.1: Catholyte analysis after each working day in full cell Cu-Cl electrolyzer, for N115, N117, N115/Ppy, N117/Ppy and TMA. Analysis was performed by DPASV technique and three-electrode cell set up using UMEs and Pine Instruments Wave Driver potentiostat under N_2 and at ambient temperature using 25 µm Pt working disc electrode, a silver/silver chloride (Ag/AgCl) reference electrode, and a Pt wire as a counter electrode.

Membrane	Catholyte Cu(ppm)
N117 d1	3.4
N117 d2	6.3
N117 d3	4.8
N117/Ppy d1	1.4
N117/Ppy d2	0.9
N117/Ppy d3	1.3
N115 d1	3.6
N115 d2	3.0
N115 d3	3.0
N115/Ppy d1	2.5
N115/Ppy d2	1.5
N115/Ppy d3	1.8
TMA d1	33.4
TMA d2	41.6
TMA d3	39.3

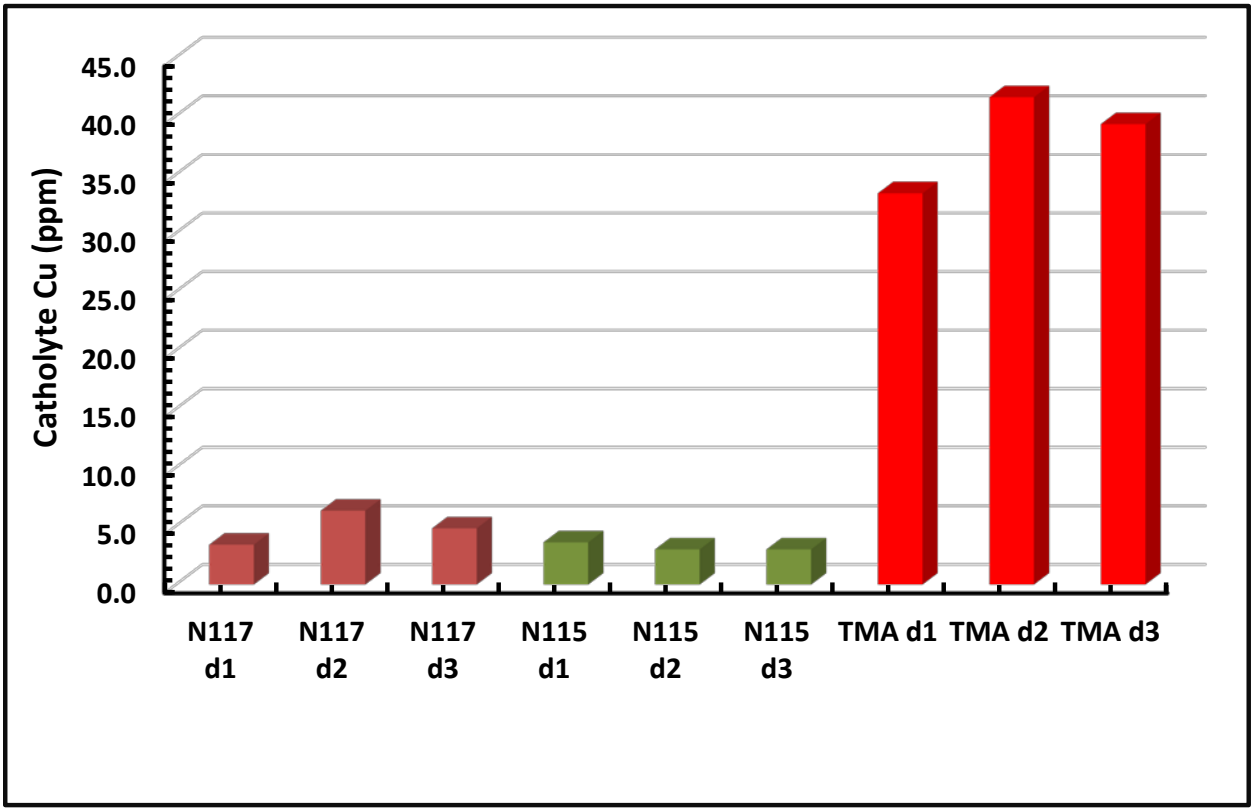

Fig. 5.8: Catholyte analysis after each working day in full cell Cu-Cl electrolyzer, for N115, N117, and TMA. Analysis was performed by DPASV technique and three-electrode cell set up using UMEs and Pine Instruments Wave Driver potentiostat under N_2 and at ambient temperature using 25 µm Pt working disc electrode, a silver/silver chloride (Ag/AgCl) reference electrode, and a Pt wire as a counter electrode.

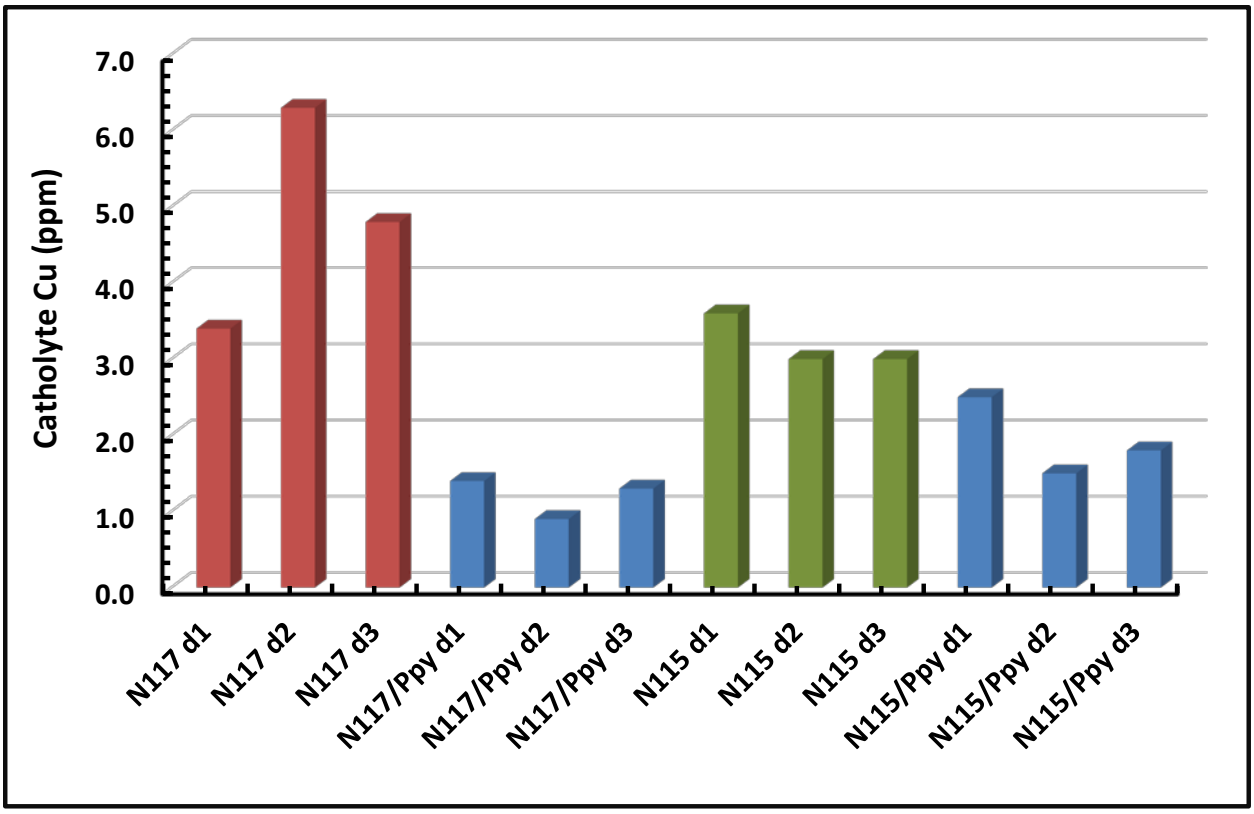

Fig. 5.9: Catholyte analysis after each working day in full cell Cu-Cl electrolyzer, for N115, N117, N115/Ppy, and N117/Ppy . Analysis was performed by DPASV technique and three-electrode cell set up using UMEs and Pine Instruments Wave Driver potentiostat under N_2 and at ambient temperature using 25 µm Pt working disc electrode, a silver/silver chloride (Ag/AgCl) reference electrode, and a Pt wire as a counter electrode.

5.3 Analysis of the Anolyte by Ultramicroelectrode Cyclic Voltammetry (UME CV)

Understanding the process of oxidation of the CuCl at the anode, and monitoring the varied copper oxidation state in the full cell system during operation, makes it crucial to have a suitable method to determine the speciation of Cu. An electrochemical method would be totally advantageous due to its real-time monitoring capability and the proximity to electrochemical equipment during electrolysis testing. UME CV is a facile electrochemical three electrode-system technique that shows some very consistently promising results to estimate the wt. % of Cu(I) and Cu(II) in the anolyte. As a matter of fact we started with 100 % of Cu(I) as CuCl, and

with electrolysis at specific current of 0.5 A, Cu(I) oxidized to Cu(II). According to Faradic law, theoretically 28 % of Cu(I) should be oxidized to Cu(II) during the 6 h of electrolysis. Fig. 5.10 (a,b,c) shows the CV analysis of mixed standard solutions of CuCl and $CuCl_2$ by using a Pt disc microelectrode and that when only Cu(I) is available, an anodic current will only be available for the oxidation. Furthermore, when Cu(II) is available, the CV shows only a cathodic current for the reduction. Fig. 5.11 (a,b) shows the calibration curves of the anodic and cathodic currents as a function of normalized wt. % CuCl and $CuCl_2$, respectively. Both curves display a linear relationship between the peak current and concentration of copper species. However, the value of slope for the oxidation of Cu(I) to Cu(II) (peak anodic current) is larger than that for the reverse reaction (peak cathodic current). The reason for this is likely due to the reduction of Cu(II) to Cu(0). Although different constants for the oxidation of Cu(I) and the reduction of Cu(II) were obtained, this method can still be used to monitor the relative concentration of the CuCl in the anolyte. Moreover, the anolyte of the N115 membrane showed that the amount of Cu(I) oxidized to Cu(II), by the end of day 1 and day 3 tested at a fixed current of 0.5 A for 6h, was only *ca*. 25 % and 8 % , respectively as can be seen in Fig. 5.10 (a). N115/Ppy membrane was able to constantly oxidize *ca*. 28 % of Cu(I) to Cu(II) after each day, which is the maximum amount that can be oxidized according to Faradic law, as detailed in Fig. 5.10 (b). Similarly, N117/PANI $FeCl_3$ was able to oxidize *ca*. 25 and 28 % of Cu(I) to Cu(II) after day 1 and day 3, respectively as shown in Fig. 5.10 (c). It can be concluded that the performance of the pristine membrane is deteriorated by day 3, whereas N115/Ppy and N117/PANI $FeCl_3$ membranes showed superiority and stability in performance during the three days of Cu-Cl electrolysis as can be seen in Fig. 5.12.

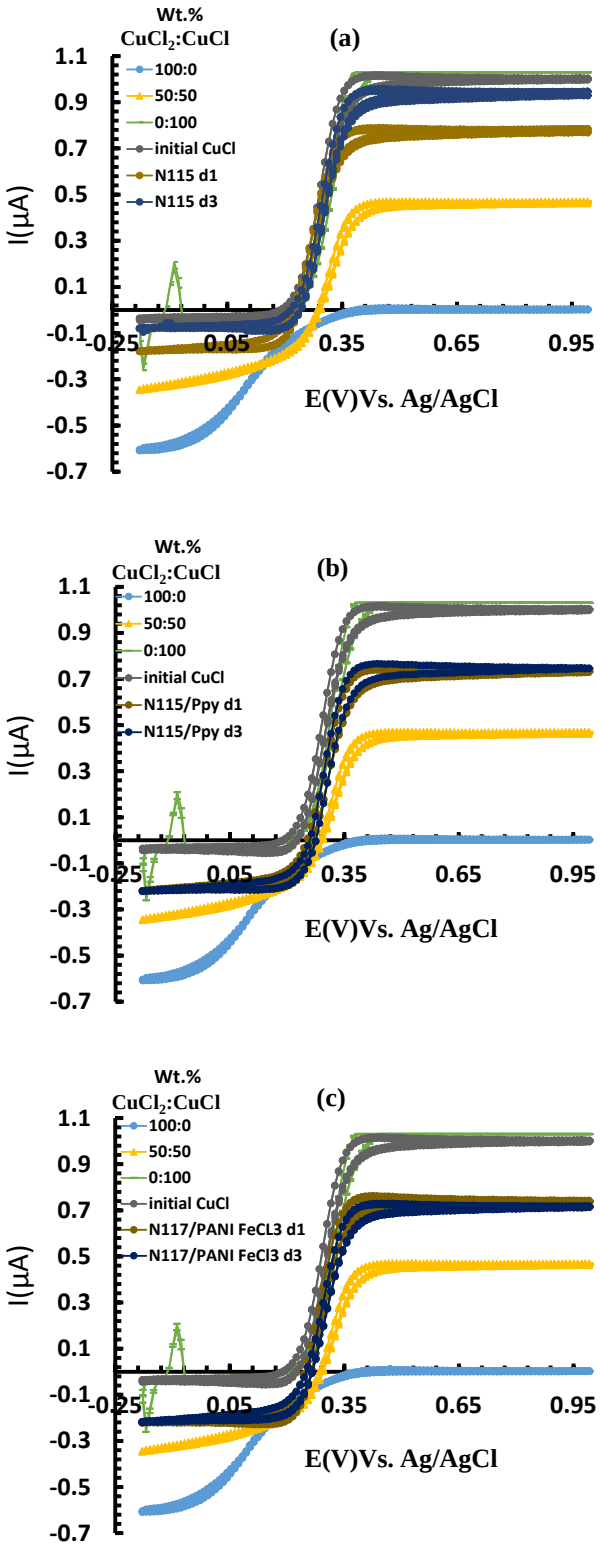

Fig. 5.10: Ultramicroelectrode CVs for mixtures of specific weight percentage of $CuCl_2$, CuCl and the anolyte after certain working days at fixed current of 0.5 A for 6 h (a) Pure Nafion membrane N115 (b) N115/Ppy membrane (c) N117/PANI $FeCl_3$.

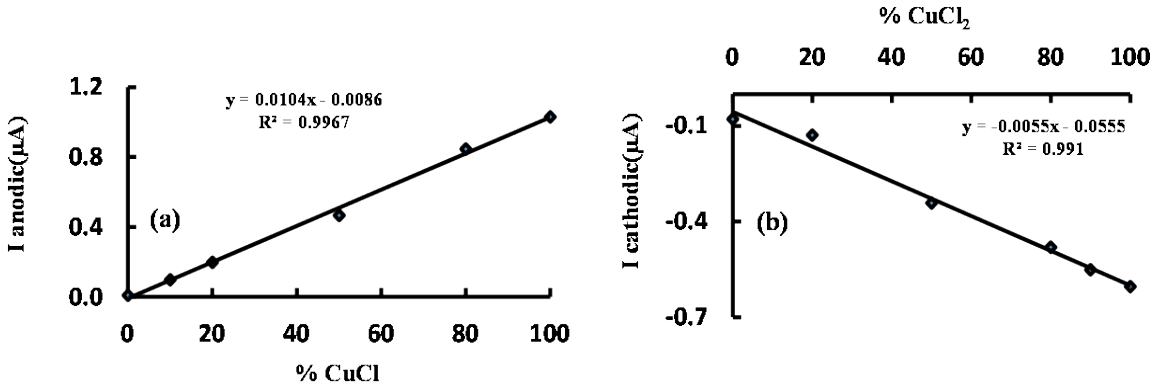

Fig. 5.11: Calibration curves of mixtures of specific wt. % of $CuCl_2$ and CuCl based on anodic and cathodic current, respectively.

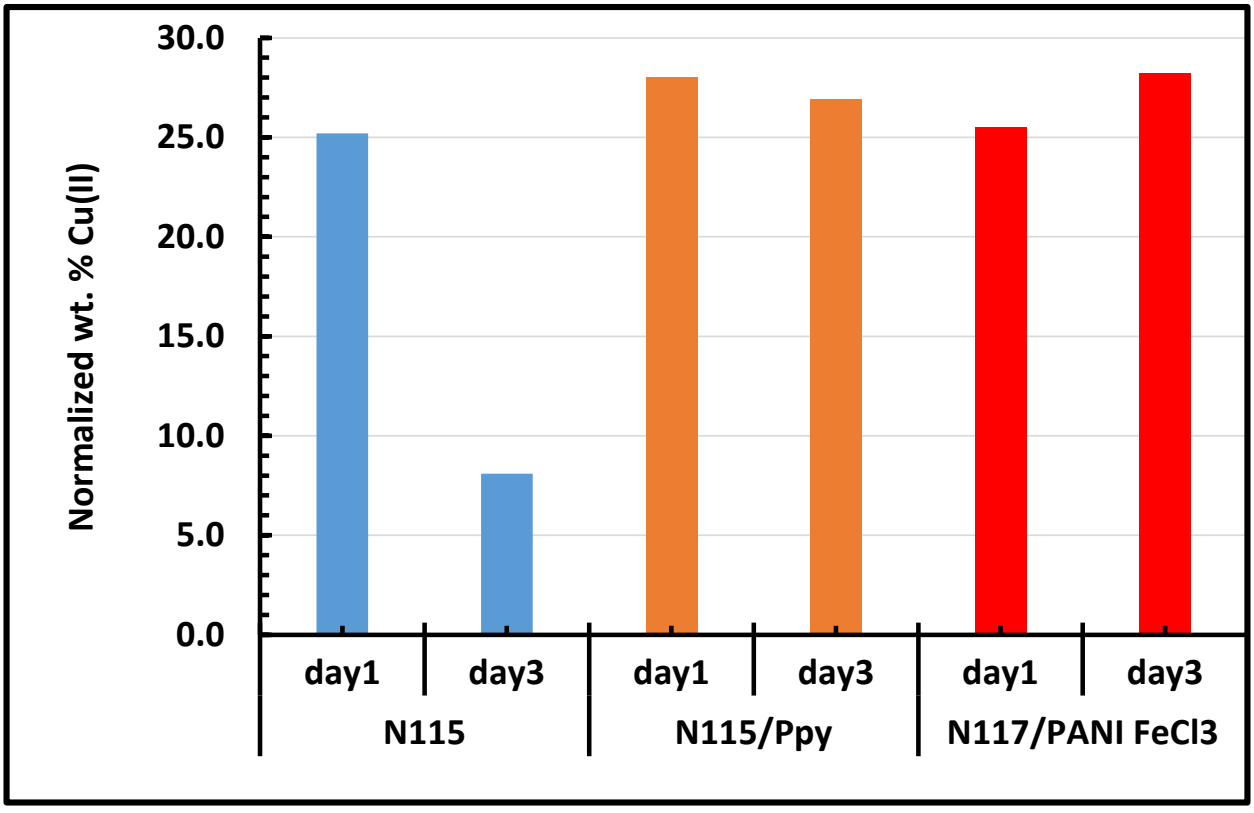

Fig. 5.12: Normalized wt. % of Cu(II) found in the anolyte after electrolysis for certain working days at fixed current of 0.5 A for 6 h for pristine Nafion membrane N115, N115/Ppy membrane and N117/PANI $FeCl_3$.

5.4 Summary

In this chapter, we investigated a way to monitor the Cu crossover in the catholyte. An electrochemical experiment was used because it is simple, fast and available in most electrochemical laboratories. The actual cell effluent was monitored using DPASV. In this method, a calibration curve was constructed for different concentration of Cu in ppm range and a small amount of the catholyte sample was measured using a Pt ultramicroelectrode and Ag/AgCl as a reference electrode. TMA was used as an anion exchange membrane. Its electrochemical behavior and efficiency were examined and compared to the pristine and composite Nafion membranes. By measuring the Cu in the catholyte, TMA showed high Cu permeability as copper complexes consisting mainly of negatively charged species. In addition, TMA showed high resistivity as it resists the movement of the positively charged species (H^+). To the contrary, composite membranes showed a significant reduction in Cu permeability in the catholyte which supports the findings using *ex situ* diffusion cells in the previous chapters.

DPASV is a simple method that can be conducted on a small volume of catholyte using a three electrode system in a small cell. This configuration could also be readily introduced into the catholyte tank itself, enabling continuous monitoring of Cu permeation. This would be highly beneficial since small concentrations of Cu has a significant influence on the current efficiency of the cell.

UME CV can be used to determine the amount of Cu(I) and Cu(II) species in the anolyte. We expect that for a high efficient electrolysis membrane that 28 % of Cu(I) should be oxidized to Cu(II) by 6 h of applying a fixed current of 0.5 A according to Faraday's law. The pristine Nafion membrane showed deteriorated performance by day three of the CuCl electrolysis at

fixed current, whereas the composites membranes showed high consistency and performance during the three working days.

In general, anion exchange membranes are not suitable to be used in the CuCl/HCl electrolyzer, because negatively charged species such as $CuCl_3^{2-}$, $CuCl^{3-}$, and $CuCl_4^{2-}$ are in high concentration and permeate the membrane. In addition, they have very low ionic conductivity as the positively charged functional groups on them prevent the protons to permeate through the membrane.

Chapter 6

Conclusions and Future Directions

The CuCl thermochemical cycle is a promising cycle to produce H_2 gas on a large scale. A hybrid cycle contains one electrochemical step. In this step, an electrolyzer is used which consists of an anode and a cathode separated by a membrane. Cu(I) is oxidized to Cu(II) at the anode and H_2 is produced at the cathode. CuCl electrolysis requires electrical energy to split water to produce H_2 gas. The hydrogen production by CuCl/HCl electrolyzer requires much less electrical energy than a regular water electrolysis. The onset potential for water electrolysis is *ca*. 1.75-2.0 V, whereas in the CuCl electrolyzer it is *ca*. 0.4 V. This electrical energy saving is one of the advantages of the CuCl thermochemical cycle. On the other side, Cu crossover is one of the drawback of CuCl cycle. Cu can permeate through the membrane of the electrochemical cell to the cathode side, reduced to metallic Cu and deposited on the catalyst layer of the cathode. As a result, the efficiency of the cell is reduced.

In this thesis, we modified Nafion membranes by two organic conducting polymers: polypyrrole (Ppy) and polyaniline (PANI). They were characterized by different techniques and their physical properties were studied. In addition, the electrochemical behaviors of the new membranes were investigated by a full cell Cu-Cl electrolyzer.

First, we modified the Nafion membranes, NRE212, N115 and N117, by *in situ* chemical polymerization with a pyrrole compound using a hydrogen peroxide solution as an oxidant. Methanol and copper permeability were measured by an *ex situ* diffusion cell. The composite membranes showed a noticeable reduction in the methanol and copper permeability. For example, the composite membranes demonstrated significant reduction in methanol and copper permeability over their unmodified counterpart *ca.* (50-63 %) and (56-69 %) reduction, respectively. Furthermore, there was a linear relationship between methanol and copper permeability. Therefore, if we know the methanol permeability of a membrane, we can predict

its copper permeability. It is worth noting that N115/Ppy had the lowest Cu permeability amongst the modified and unmodified membranes. Selectivity (α) is defined as the ratio of fluxes of protons (proton conductivity-desired) to the fluxes of methanol (methanol permeability-undesired) or copper (Cu permeability-undesired). N117/Ppy displayed the highest methanol and Cu selectivity values compared to the other composite membranes. The copper selectivity ranged from highest to lowest as N117/Ppy, N115/Ppy then NRE212/Ppy. Accordingly, we chose to test both N115/Ppy and N117/Ppy by a full cell Cu-Cl electrolyzer.

The data from the full cell Cu-Cl electrolyzer showed that both N115/Ppy and N117/Ppy demonstrated high efficency in reducing the rate of Cu permeation compared to the pristine Nafion membranes. This was confirmed by the absence of the redox peaks corresponding to Cu in CVs and visually by inspecting the MEAs which showed no Cu deposition present on the composite membranes.

Anion exchange membranes have low efficiency in blocking the Cu species compared to cation exchange membranes. In our study, we found that an anion exchange membrane, such as polysulfone based tetramethylammonium cation (TMA), allows Cu species to permeate more rapidly than a cation exchange membrane such as Nafion. In fact, in a solution of HCl, the Cu species presents in the form of negatively charged complexes such as $CuCl_3^-$, $CuCl_3^{2-}$, $CuCl_4^{2-}$. Thus, an anion exchange membrane can permeate these anions easily. In addition, an anion exchange membrane such as TMA, which allows the movement of chloride ions from the cathode to the anode, shows high resistivity compared to a cation exchange membrane such as Nafion.

The second part of the thesis focused on modifying the Nafion membranes, NRE212, N115 and N117, by *in situ* chemical polymerization with aniline compound using different oxidizing agents: hydrogen peroxide, $FeCl_3$ and ammonium persulfate (APS) solution. Although N115-PANI APS 24 h c and N117-PANI APS 24 h c showed very high selectivity, testing these membranes in the full cell Cu-Cl electrolyzer showed very high resistivity. As an alternative, we tried to test N115-PANI $FeCl_3$ 24 h c and N117-PANI $FeCl_3$ 24 h c as they showed significant Cu reduction accompanied by their conductivity reduction. The electrochemical investigation by the full cell Cu-Cl electrolyzer showed an excellent performance of these membranes compared to the pristine Nafion ones.

Faradic current efficiency is another technique employed to evaluate the membranes in the Cu-Cl electrolyzer by collecting and measuring the produced hydrogen at the cathode side. A large rate of Cu crossover leads to poor current efficiency. We found that the current efficiency of N115 was 79.3 % on the first day but dropped to 18.3 % on the third day, whereas both N115/Ppy and N117- PANI $FeCl_3$ 24 h c displayed superiority and consistency in the hydrogen production.

Electrochemical methods have been used to monitor the Cu species in both the anolyte and catholyte using the same ultramicroelectrode (UME). For example, UME cyclic voltammetry was used to support the Faradic current efficiency results. It was used to speciate the Cu(I) and Cu(II) in the anolyte solution after passing a fixed current for a specific time in the Cu-Cl electrolyzer. In the beginning, the wt % of Cu(I) was 100 %. According to Faraday's law, 28 % of Cu(I) should be oxidized to Cu(II) by 6 h of using a fixed current of 0.5 A, which means that, *ca*. 72 % of Cu(I) should remain in the anolyte solution. By the end of the test, we found that the anolyte of the N115 membrane had Cu(I) of 74.8 and 91.9 % for d1 and d3, respectively.

These results showed that the efficiency of the cell to oxidize Cu(I) to Cu(II) was reduced from d1 to d3. To the contrary, both N115/Ppy and N117- PANI $FeCl_3$ 24 h c showed a consistent efficiency of oxidizing Cu(I) to Cu(II). The anolyte of the N115/Ppy membrane had Cu(I) of 72 and 73 % for d1 and d3, respectively and for N117- PANI $FeCl_3$ 24 h c membrane, the Cu(I) concentration was 73 and 71 % for d1 and d3, respectively. Therefore, UME CV can be used to examine the performance of the membranes in the CuCl/HCl electrolyzer by analyzing the % of Cu(I) and Cu(II) in the anolyte.

In another electrochemical experiment, we have been able to determine the concentration of Cu in the catholyte using differential pulse anodic stripping voltammetry (DPASV) technique. This technique is valuable for tracing any Cu crossover through the membrane as it can quantify a very tiny amount of Cu in the range of ppm. DPASV can replace AAS, as it is more facile and handy in any electrochemistry lab. Furthermore, the results can be used to evaluate the membrane efficiency as a large concentration of Cu in the catholyte means high crossover which leads to low efficiency.

We conclude that, *in situ* polymerization of Nafion membranes is an efficient way to reduce the rate of Cu transport through the membrane. Because of the physical electrostatic interaction between the positively charged polymer and negatively charged sulfonated groups in the membrane, the pore size shrunk. This prevents the copper species to permeate from the anode to the cathode while allow the smaller size protons to permeate. We were able to determine the copper permeation by an *ex situ* experiment which correlates very well with the *in situ* measurements. However, composite membranes are resistive and consequently there is a substantial IR drop when these composites are used, which resulted in lower voltage efficiency. In fact, high conductivity and low Cu permeability are required for an optimum Cu-Cl

electrolyzer membrane, which leads us to a challenge of making a more conductive but less Cu permeable membrane.

Future work could be based on implementing UME in the catholyte and anolyte containers and performing a continuous monitoring of the Cu species. Monitoring can also be implemented to a larger final stage of a Cu-Cl/HCl electrolyzer system for online monitoring. Furthermore, future work could study the tolerable level of Cu in the catholyte prior to start plating the cathode. Cu in the catholyte also has a clear relation with the efficiency and these electrochemical kinetics merit further investigation.

Future work should test the PANI composite membranes, such as N115-PANI APS 24 h c and N117-PANI APS 24 h c that had high resistivity but showed very low Cu permeability with a high concentration of anolyte and hydrochloric acid as a catholyte. Under such conditions, we might see a higher current response.

Future research could also focus on modifying the Nafion membranes with other promising organic compounds that efficiently reduce methanol crossover in DMFC. As we have proved, modified membranes that efficiently able to reduce the methanol crossover would also be able to reduce the Cu crossover.

Future work could also include testing all these promising modified membranes at temperatures higher than 25 °C. Temperatures up to 80 °C are considered as viable for the Cu-Cl cycle [28, 109]. Testing the membranes at such high temperatures would give us the opportunity to evaluate if the trends observed at lower temperatures are predictive of their high temperature performance. Moreover, the durability of the Ppy and PANI composites at higher temperatures should be studied in order to determine their stability periods at such high temperatures.

Future research might also consider focusing on using more characterization techniques such as solid state nuclear magnetic resonance (SSNMR) to examine the porosity of the membranes and to evaluate different protons connectivity and functionality inside the membrane. Such a technique would allow better understanding of the changes that occur to modified membranes.

References

[1] R.J. Press, Introduction to hydrogen technology, John Wiley, Hoboken, NJ, 2009.

[2] B.C.R. Ewan, R.W.K. Allen, A figure of merit assessment of the routes to hydrogen, International Journal of Hydrogen Energy, 30 (2005) 809-819.

[3] J.D. Holladay, J. Hu, D.L. King, Y. Wang, An overview of hydrogen production technologies, Catalysis Today, 139 (2009) 244-260.

[4] A. Steinfeld, Solar thermochemical production of hydrogen—a review, Solar Energy, 78 (2005) 603-615.

[5] G.F. Naterer, I. Dincer, C. Zamfirescu, Water Electrolysis, in, Springer London, London, 2013, pp. 99-152.

[6] J. Russell, L. Nuttall, A. Fickett, Hydrogen generation by solid polymer electrolyte water electrolysis, American Chemical Society Division of Fuel Chemistry Preprints, 18 (1973) 24e40.

[7] M. Carmo, D.L. Fritz, J. Mergel, D. Stolten, A comprehensive review on PEM water electrolysis, International Journal of Hydrogen Energy, 38 (2013) 4901-4934.

[8] S.A. Sherif, Handbook of Hydrogen Energy, CRC Press, 2013.

[9] M.A. Lewis, J.G. Masin, P.A. O'Hare, Evaluation of alternative thermochemical cycles, Part I: The methodology, International Journal of Hydrogen Energy, 34 (2009) 4115-4124.

[10] S. Ranganathan, E.B. Easton, High performance ceramic carbon electrode-based anodes for use in the Cu–Cl thermochemical cycle for hydrogen production, International Journal of Hydrogen Energy, 35 (2010) 1001-1007.

[11] S. Aghahosseini, I. Dincer, G.F. Naterer, Linear sweep voltammetry measurements and factorial design model of hydrogen production by HCl/CuCl electrolysis, International Journal of Hydrogen Energy, 38 (2013) 12704-12717.

[12] V.N. Balashov, R.S. Schatz, E. Chalkova, N.N. Akinfiev, M.V. Fedkin, S.N. Lvov, CuCl Electrolysis for Hydrogen Production in the Cu-Cl Thermochemical Cycle, Journal of the Electrochemical Society, 158 (2011) B266-B275.

[13] G. Naterer, S. Suppiah, L. Stolberg, M. Lewis, Z. Wang, I. Dincer, M. Rosen, K. Gabriel, E. Secnik, E. Easton, Progress of international hydrogen production network for the thermochemical Cu―Cl cycle, International journal of hydrogen energy, 38 (2013) 740-759.

[14] D.M. Hall, E.G. LaRow, R.S. Schatz, J.R. Beck, S.N. Lvov, Electrochemical Kinetics of CuCl(aq)/HCl(aq) Electrolyzer for Hydrogen Production via a Cu-Cl Thermochemical Cycle, Journal of the Electrochemical Society, 162 (2014) F108-F114.

[15] L.C.B.G.E.B.R.T.T.C.B.E.R.B.A.V.B.E.H.T.H. B. W. McQuillan, A. Lewandowski, HIGH EFFICIENCY GENERATION OF HYDROGEN FUELS USING SOLAR THERMAL-CHEMICAL SPLITTING OF WATER (SOLAR THERMO-CHEMICAL SPLITTING FOR H2) (2002).

[16] K. Schultz, L. Brown, G. Besenbruch, C. Hamilton, Production of hydrogen by nuclear energy: the enabling technology for the hydrogen economy, in: America's Nuclear Energy Symp., ANES, 2002, pp. 16-18.

[17] C. Acar, I. Dincer, Comparative assessment of hydrogen production methods from renewable and non-renewable sources, International Journal of Hydrogen Energy, 39 (2014) 1.

[18] L.C. Brown, G.E. Besenbruch, R. Lentsch, K.R. Schultz, J. Funk, P. Pickard, A. Marshall, S. Showalter, High efficiency generation of hydrogen fuels using nuclear power, GA-A24285, Rev, 1 (2003).

[19] L.C.B.G.E.B.C.J.H. K. R. Schultz, PRODUCTION OF HYDROGEN BY NUCLEAR ENERGY: THE ENABLING TECHNOLOGY FOR THE HYDROGEN ECONOMY, American Nuclear Symposium, Miami, Florida, (2002).

[20] M. Sakurai, H. Nakajima, R. Amir, K. Onuki, S. Shimizu, Experimental study on side-reaction occurrence condition in the iodine–sulfur thermochemical hydrogen production process, International Journal of Hydrogen Energy, 25 (2000) 613-619.

[21] K.R. Schultz, L.C. Brown, G.E. Besenbruch, C.J. Hamilton, Production of hydrogen by nuclear energy: the enabling technology for the hydrogen economy, in: America's Nuclear Energy Symp., ANES, pp. 16-18.

[22] P.W.T.E.R.G. Lu, R.L. Ammon, "Recent developments in the technology of sulphur dioxide depolarized electrolysis.", Journal of Applied Electrochemistry, 11.3 (1981) 347-355.

[23] T.R. Garrick, A. Gulledge, J.A. Staser, B. Benicewicz, J.W. Weidner, Polybenzimidazole Membranes for Hydrogen Production in the Hybrid Sulfur Electrolyzer, ECS Transactions, 61 (2014) 11-17.

[24] L. García, D. González, C. García, L. García, C. Brayner, Efficiency of the sulfur-iodine thermochemical water splitting process for hydrogen production based on ADS (accelerator driven system), Energy, 57 (2013) 469-477.

[25] J.A. Staser, M.B. Gorensek, J.W. Weidner, Quantifying Individual Potential Contributions of the Hybrid Sulfur Electrolyzer, Journal of the Electrochemical Society, 157 (2010) B952.

[26] M.A. Lewis, J.G. Masin, The evaluation of alternative thermochemical cycles – Part II: The down-selection process, International Journal of Hydrogen Energy, 34 (2009) 4125-4135.

[27] M.A. Lewis, M.S. Ferrandon, D.F. Tatterson, P. Mathias, Evaluation of alternative thermochemical cycles – Part III further development of the Cu–Cl cycle, International Journal of Hydrogen Energy, 34 (2009) 4136-4145.

[28] G.F. Naterer, E. Secnik, E.B. Easton, S.N. Lvov, V. Papangelakis, A. Odukoya, S. Suppiah, L. Stolberg, M. Lewis, S. Ahmed, Z. Wang, M.A. Rosen, I. Dincer, K. Gabriel, Progress of international program on hydrogen production with the copper–chlorine cycle, International Journal of Hydrogen Energy, 39 (2014) 2431.

[29] G.F. Naterer, E.B. Easton, I. Pioro, S. Lvov, J. Jiang, J. Mostaghimi, B.M. Ikeda, G. Rizvi, L. Lu, A. Odukoya, P. Spekkens, S. Suppiah, M. Fowler, J. Avsec, L. Stolberg, M. Lewis, Z. Wang, I. Dincer, M.A. Rosen, K. Gabriel, E. Secnik, Progress of international hydrogen production network for the thermochemical Cu–Cl cycle, International Journal of Hydrogen Energy, 38 (2012) 740.

[30] G. Naterer, B.M. Ikeda, M.H. Kaye, L. Lu, I. Pioro, P. Spekkens, P. Tremaine, J. Mostaghimi, J. Avsec, J. Jiang, S. Suppiah, M. Lewis, K. Gabriel, I. Dincer, M.A. Rosen, M. Fowler, G. Rizvi, E.B. Easton, Recent Canadian advances in nuclear-based hydrogen production and the thermochemical Cu–Cl cycle, International Journal of Hydrogen Energy, 34 (2009) 2901-2917.

[31] G.F. Naterer, P. Spekkens, S.N. Lvov, M. Fowler, P. Tremaine, J. Mostaghimi, E.B. Easton, L. Trevani, G. Rizvi, B.M. Ikeda, M.H. Kaye, S. Suppiah, L. Lu, I. Pioro, W.R. Smith, E. Secnik, J. Jiang, J. Avsec, L. Stolberg, M. Lewis, Z. Wang, V. Daggupati, K. Gabriel, I. Dincer, M.A. Rosen, Canada's program on nuclear hydrogen production and the thermochemical Cu–Cl cycle, International Journal of Hydrogen Energy, 35 (2010) 10905-10926.

[32] S.J. Peighambardoust, S. Rowshanzamir, M. Amjadi, Review of the proton exchange membranes for fuel cell applications, International Journal of Hydrogen Energy, 35 (2010) 9349-9384.

[33] a.d.S.A.C.a.T.R.R.b. S. Slade, F.C. Walsh, Ionic Conductivity of an Extruded Nafion 1100 EW Series of Membranes, Journal of The Electrochemical Society, 149 (2002) A1556-A1564.

[34] K.A. Mauritz, R.B. Moore, State of understanding of Nafion, Chemical Reviews, 104 (2004) 4535-4585.

[35] A.K. Sahu, S. Pitchumani, P. Sridhar, A.K. Shukla, Nafion and modified-Nafion membranes for polymer electrolyte fuel cells: An overview, Bulletin of Materials Science, 32 (2009) 285-294.

[36] F. Lufrano, G. Squadrito, A. Patti, E. Passalacqua, Sulfonated polysulfone as promising membranes for polymer electrolyte fuel cells, Journal of Applied Polymer Science, 77 (2000) 1250-1256.

[37] G. Shashidhara, K.N. Kumar, Proton conductivity of sPEEK membranes, Polymer-Plastics Technology and Engineering, 49 (2010) 796-806.

[38] Proton Conductivity of SPEEK Membranes, Polymer-Plastics Technology and Engineering, 49 (2010) 796-806.

[39] C. Marestin, G. Gebel, O. Diat, R. Mercier, Sulfonated Polyimides, in, Springer Berlin Heidelberg, Berlin, Heidelberg, 2008, pp. 185-258.

[40] M.A. Hickner, H. Ghassemi, Y.S. Kim, B.R. Einsla, J.E. McGrath, Alternative polymer systems for proton exchange membranes (PEMs), Chemical Reviews, 104 (2004) 4587-4611.

[41] G.F. Naterer, S. Suppiah, L. Stolberg, M. Lewis, Z. Wang, I. Dincer, M.A. Rosen, K. Gabriel, E. Secnik, E.B. Easton, I. Pioro, S. Lvov, J. Jiang, J. Mostaghimi, B.M. Ikeda, G. Rizvi, L. Lu, A. Odukoya, P. Spekkens, M. Fowler, J. Avsec, Progress of international hydrogen production network for the thermochemical Cu–Cl cycle, in, Elsevier, 2013, pp. 740-759.

[42] N.W. Deluca, Y.A. Elabd, Polymer electrolyte membranes for the direct methanol fuel cell: A review, Journal of Polymer Science, Part B: Polymer Physics, 44 (2006) 2201-2225.

[43] X. Yuan, X.-L. Ding, C.-Y. Wang, Z.-F. Ma, Use of polypyrrole in catalysts for low temperature fuel cells, Energy & Environmental Science, 6 (2013) 1105-1124.

[44] E.B. Easton, B.L. Langsdorf, J.A. Hughes, J. Sultan, Z.G. Qi, A. Kaufman, P.G. Pickup, Characteristics of polypyrrole/Nafion composite membranes in a direct methanol fuel cell, Journal of the Electrochemical Society, 150 (2003) C735-C739.

[45] B.L. Langsdorf, J. Sultan, P.G. Pickup, Partitioning and polymerization of pyrrole into perfluorosulfonate (Nafion) membranes under neutral conditions, Journal of Physical Chemistry B, 107 (2003) 8412-8415.

[46] B.L. Langsdorf, B.J. MacLean, J.E. Halfyard, J.A. Hughes, P.G. Pickup, Partitioning and polymerization of pyrrole into perfluorosulfonic acid (Nafion) membranes, Journal of Physical Chemistry B, 107 (2003) 2480-2484.

[47] V. Neburchilov, J. Martin, H. Wang, J. Zhang, A review of polymer electrolyte membranes for direct methanol fuel cells, Journal of Power Sources, 169 (2007) 221-238.

[48] F. Xu, C. Innocent, B. Bonnet, D.J. Jones, J. Rozière, Chemical modification of perfluorosulfonated membranes with pyrrole for fuel cell application: Preparation, characterisation and methanol transport, Fuel Cells, 5 (2005) 398-405.

[49] N. Jia, M.C. Lefebvre, J. Halfyard, Z. Qi, P.G. Pickup, Modification of Nafion proton exchange membranes to reduce methanol crossover in PEM fuel cells, Electrochemical and Solid-State Letters, 3 (2000) 529-531.

[50] A. Bhattacharya, A. De, Conducting composites of polypyrrole and polyaniline a review, Progress in Solid State Chemistry, 24 (1996) 141-181.

[51] M.K. Ram, G. Mascetti, S. Paddeu, E. Maccioni, C. Nicolini, Optical, structural and fluorescence microscopic studies on reduced form of polyaniline: The leucoemeraldine base, Synthetic Metals, 89 (1997) 63-69.

[52] S. Bhadra, N.K. Singha, D. Khastgir, Electrochemical synthesis of polyaniline and its comparison with chemically synthesized polyaniline, Journal of Applied Polymer Science, 104 (2007) 1900-1904.

[53] M.C. De Jesus, Y. Fu, R.A. Weiss, Conductive polymer blends prepared by in situ polymerization of pyrrole: A review, Polymer Engineering and Science, 37 (1997) 1936-1943.

[54] Y. Ding, A. Buyle Padias, H.K. Hall, Chemical trapping experiments support a cation-radical mechanism for the oxidative polymerization of aniline, Journal of Polymer Science Part A: Polymer Chemistry, 37 (1999) 2569-2579.

[55] A. Malinauskas, Chemical deposition of conducting polymers, Polymer, 42 (2001) 3957-3972.

[56] J. Zhu, R.R. Sattler, A. Garsuch, O. Yepez, P.G. Pickup, Optimisation of polypyrrole/Nafion composite membranes for direct methanol fuel cells, Electrochimica Acta, 51 (2006) 4052-4060.

[57] S. Moravcová, Z. Cílová, K. Bouzek, Preparation of a Novel Composite Material Based on a Nafion® Membrane and Polypyrrole for Potential Application in a PEM Fuel Cell, in, Kluwer Academic Publishers, Dordrecht, 2005, pp. 991-997.

[58] A. Sungpet, Reduction of alcohol permeation through Nafion ® by polypyrrole, Journal of Membrane Science, 226 (2003) 131-134.

[59] J. Stejskal, M. Trchová, Aniline oligomers versus polyaniline, Polymer International, 61 (2012) 240-251.

[60] S. Tan, V. Viau, D. Cugnod, D. Bélanger, Chemical modification of a sulfonated membrane with a cationic polyaniline layer to improve its permselectivity, Electrochemical and Solid-State Letters, 5 (2002) E55-E58.

[61] S. Tan, A. Laforgue, D. Bélanger, Characterization of a Cation-Exchange/Polyaniline Composite Membrane, Langmuir, 19 (2003) 744-751.

[62] S. Tan, J.H. Tieu, D. Bélanger, Chemical polymerization of aniline on a poly(styrene sulfonic acid) membrane: Controlling the polymerization site using different oxidants, The journal of physical chemistry.B, 109 (2005) 14085-14092.

[63] S. Tan, D. Bélanger, Characterization and transport properties of Nafion/polyaniline composite membranes, The journal of physical chemistry.B, 109 (2005) 23480-23490.

[64] J. Yang, P.K. Shen, J. Varcoe, Z. Wei, Nafion/polyaniline composite membranes specifically designed to allow proton exchange membrane fuel cells operation at low humidity, Journal of Power Sources, 189 (2009) 1016-1019.

[65] N. Mokhtarian, M. Ghasemi, W.R. Wan Daud, M. Ismail, G. Najafpour, J. Alam, Improvement of microbial fuel cell performance by using nafion polyaniline composite membranes as a separator, Journal of Fuel Cell Science and Technology, 10 (2013).

[66] V.K. Shahi, Highly charged proton-exchange membrane: Sulfonated poly(ether sulfone)-silica polyelectrolyte composite membranes for fuel cells, Solid State Ionics, 177 (2007) 3395-3404.

[67] H. Lin, C. Zhao, W. Ma, H. Li, H. Na, Layer-by-layer self-assembly of in situ polymerized polypyrrole on sulfonated poly(arylene ether ketone) membrane with extremely low methanol crossover, International Journal of Hydrogen Energy, 34 (2009) 9795-9801.

[68] D.H. Jung, S.Y. Cho, D.H. Peck, D.R. Shin, J.S. Kim, Performance evaluation of a Nafion/silicon oxide hybrid membrane for direct methanol fuel cell, Journal of Power Sources, 106 (2002) 173-177.

[69] P. Dimitrova, K.A. Friedrich, U. Stimming, B. Vogt, Modified Nafion®-based membranes for use in direct methanol fuel cells, Solid State Ionics, 150 (2002) 115-122.

[70] S.P. Nunes, B. Ruffmann, E. Rikowski, S. Vetter, K. Richau, Inorganic modification of proton conductive polymer membranes for direct methanol fuel cells, Journal of Membrane Science, 203 (2002) 215-225.

[71] Y.-H. Su, B. Liu, Y.-L. Liu, Y.-M. Sun, J.-Y. Lai, D.-M. Wang, Y. Gao, M.D. Guiver, Proton exchange membranes modified with sulfonated silica nanoparticles for direct methanol fuel cells, Journal of Membrane Science, 296 (2007) 21-28.

[72] X. Ren, T.E. Springer, T.A. Zawodzinski, S. Gottesfeld, Methanol Transport Through Nation Membranes. Electro-osmotic Drag Effects on Potential Step Measurements, Journal of the Electrochemical Society, 147 (2000) 466.

[73] R.S. Schatz, S. Kim, S. Khurana, M.V. Fedkin, S.N. Lvov, High efficiency CuCl electrolyzer for Cu-Cl thermochemical cycle, ECS Transactions, 50 (2012) 153-164.

[74] Y. Xiao-Zi, Electrochemical impedance spectroscopy in PEM fuel cells: fundamentals and applications, Springer Verlag, DE, 2010.

[75] C.H. Lee, H.B. Park, Y.M. Lee, R.D. Lee, Importance of Proton Conductivity Measurement in Polymer Electrolyte Membrane for Fuel Cell Application, Industrial & Engineering Chemistry Research, 44 (2005) 7617-7626.

[76] Q.M. Huang, H.L. Huang, Y.J. Huang, Q.L. Zhang, W.S. Li, J.L. Luo, Methanol permeability and proton conductivity of Nafion membranes modified electrochemically with polyaniline, Journal of Power Sources, 184 (2008) 338-343.

[77] T. Soboleva, Z. Xie, Z. Shi, E. Tsang, T. Navessin, S. Holdcroft, Investigation of the through-plane impedance technique for evaluation of anisotropy of proton conducting polymer membranes, Journal of Electroanalytical Chemistry, 622 (2008) 145-152.

[78] N.E. De Almeida, E.B. Easton, Nafion/ sulfonated silica composite membranes for PEM fuel cells, in, 2010, pp. 29-38.

[79] B.G. Choi, H. Park, H.S. Im, Y.J. Kim, W.H. Hong, Influence of oxidation state of polyaniline on physicochemical and transport properties of Nafion/polyaniline composite membrane for DMFC, Journal of Membrane Science, 324 (2008) 102-110.

[80] B. Schwenzer, S. Kim, M. Vijayakumar, Z. Yang, J. Liu, Correlation of structural differences between Nafion/polyaniline and Nafion/polypyrrole composite membranes and observed transport properties, Journal of Membrane Science, 372 (2011) 11-19.

[81] C.H. Wang, L.C. Chen, C.C. Chen, K.H. Chen, C.P. Chen, H.C. Hsu, H.Y. Du, J.Y. Hwang, H.C. Shih, J. Stejskal, Low methanol-permeable polyaniline/Nafion composite membrane for direct methanol fuel cells, Journal of Power Sources, 190 (2009) 279-284.

[82] K.M. Yarrow, N.E. De Almeida, E.B. Easton, The impact of pre-swelling on the conductivity and stability of Nafion/sulfonated silica composite membranes, Journal of Thermal Analysis and Calorimetry, (2013) 1-8.

[83] S.-E. Nam, S.-O. Kim, Y. Kang, J.W. Lee, K.-H. Lee, Preparation of Nafion/sulfonated poly(phenylsilsesquioxane) nanocomposite as high temperature proton exchange membranes, Journal of Membrane Science, 322 (2008) 466-474.

[84] T.J. Peckham, J. Schmeisser, S. Holdcroft, Relationships of Acid and water content to proton transport in statistically sulfonated proton exchange membranes: variation of water content via control of relative humidity, The journal of physical chemistry.B, 112 (2008) 2848-2858.

[85] V. Tricoli, F. Nannetti, Zeolite–Nafion composites as ion conducting membrane materials, Electrochimica Acta, 48 (2003) 2625-2633.

[86] J. Wootthikanokkhan, N. Seeponkai, Methanol permeability and properties of DMFC membranes based on sulfonated PEEK/PVDF blends, Journal of Applied Polymer Science, 102 (2006) 5941-5947.

[87] P. Edge, T. University of Ontario Institute of, The production and characterization of ceramic carbon electrode materials for CuCl-HCl electrolysis, in, UOIT, Oshawa, Ont, 2013.

[88] M.A. Chougule, Synthesis and Characterization of Polypyrrole (PPy) Thin Films, Soft Nanoscience Letters, 1 (2011) 6-10.

[89] B. Tian, G. Zerbi, Lattice dynamics and vibrational spectra of polypyrrole, The Journal of chemical physics, 92 (1990) 3886-3891.

[90] J.D.T. Hallinan, Y.A. Elabd, Diffusion of water in Nafion using time-resolved Fourier transform infrared-attenuated total reflectance spectroscopy, The journal of physical chemistry.B, 113 (2009) 4257-4266.

[91] M. Lopez, Exchange rates and water content of a cation exchange membrane in aprotic solvents, Analytical Chemistry, 48 (1976) 1120-1124.

[92] M. Ludvigsson, J. Lindgren, J. Tegenfeldt, FTIR study of water in cast Nafion films, Electrochimica Acta, 45 (2000) 2267-2271.

[93] M. Ammam, E.B. Easton, Advanced NOx gas sensing based on novel hybrid organic-inorganic semiconducting nanomaterial formed between pyrrole and Dawson type polyoxoanion [P2Mo18O62]6, Journal of Materials Chemistry, 21 (2011) 7886-7891.

[94] C. Schmidt, T. Glück, G. Schmidt-Naake, Modification of Nafion Membranes by Impregnation with Ionic Liquids, Chemical Engineering & Technology, 31 (2008) 13-22.

[95] V. Compañ, E. Riande, F.J. Fernandez-Carretero, N.P. Berezina, A.A.R. Sytcheva, Influence of polyaniline intercalations on the conductivity and permselectivity of perfluorinated cation-exchange membranes, Journal of Membrane Science, 318 (2008) 255-263.

[96] M.P. Rodgers, Z. Shi, S. Holdcroft, Transport properties of composite membranes containing silicon dioxide and Nafion, Journal of Membrane Science, 325 (2008) 346-356.

[97] J.H. Kim, S.K. Kim, K. Nam, D.W. Kim, Composite proton conducting membranes based on Nafion and sulfonated SiO2 nanoparticles, Journal of Membrane Science, 415 (2012) 696-701.

[98] Y.A. Elabd, E. Napadensky, J.M. Sloan, D.M. Crawford, C.W. Walker, Triblock copolymer ionomer membranes: Part I. Methanol and proton transport, Journal of Membrane Science, 217 (2003) 227-242.

[99] G. Schwitzgebel, F. Endres, The determination of the apparent diffusion coefficient of HCl in Nafion ®-117 and polypyrrole + Nafion ®-117 by simple potential measurements, Journal of Electroanalytical Chemistry, 386 (1995) 11-16.

[100] V. Tricoli, N. Carretta, M. Bartolozzi, Comparative investigation of proton and methanol transport in fluorinated ionomeric membranes, Journal of the Electrochemical Society, 147 (2000) 1286-1290.

[101] Q. Duan, H. Wang, J. Benziger, Transport of liquid water through Nafion membranes, Journal of Membrane Science, 392 (2012) 88-94.

[102] T. Matsuura, S.M.J. Naidi, Polymer membranes for fuel cells, in, Springer Verlag, New York, 2009.

[103] H. Pei, L. Hong, J.Y. Lee, Effects of polyaniline chain structures on proton conduction in a PEM host matrix, Journal of Membrane Science, 307 (2008) 126-135.

[104] L.J. Pan, L. Pu, Y. Shi, T. Sun, R. Zhang, Y.O. Zheng, Hydrothermal Synthesis of Polyaniline Mesostructures, in, 2006, pp. 1279-1288.

[105] I.Y. Sapurina, M.E. Kompan, V.V. Malyshkin, V.V. Rosanov, J. Stejskal, Properties of proton-conducting nafion-type membranes with nanometer-thick polyaniline surface layers, Russian Journal of Electrochemistry, 45 (2009) 697-706.

[106] S.H. de Almeida, Y. Kawano, Thermal Behavior of Nafion Membranes, Journal of Thermal Analysis and Calorimetry, 58 (1999) 569-577.

[107] R.K. Nagarale, G.S. Gohil, V.K. Shahi, R. Rangarajan, Organic-Inorganic Hybrid Membrane: Thermally Stable Cation-Exchange Membrane Prepared by the Sol-Gel Method, Macromolecules, 37 (2004) 10023-10030.

[108] D.M. Hall, N.N. Akinfiev, E.G. Larow, R.S. Schatz, S.N. Lvov, Thermodynamics and Efficiency of a CuCl(aq)/HCl(aq) Electrolyzer, ELECTROCHIMICA ACTA, 143 (2014) 70-82.

[109] S. Khurana, D.M. Hall, R.S. Schatz, M.V. Fedkin, S.N. Lvov, State-of-health of a CuCl electrolyzer during a 168-h test, INTERNATIONAL JOURNAL OF HYDROGEN ENERGY, 40 (2015) 62-69.